

Philipp Bayer — Tim Bleul — Janina Bucher — Steffen BüBecker
Ralph Falk — Christoph Fischer — Julia Flanjak
Jan Freudenberg — Jan Gotthardt — Maximilian Heeg
Leonie Kastner — Jonas Kiefer — Dustin Klinger
Alexandra Nothnagel — Daniela Paunescu — Clemens Scherer
Tina Schmidt — Christian Stoy — Hans Urban
Benjamin Wallisch — Miriam Wiestler

International Science Academy
San Francisco 2007

dkfz.

Heidelberger
Life-Science Lab

Participants of the San Francisco Academy 2007:

Philipp Bayer, *Rheinstetten*
Tim Bleul, *Hockenheim*
Janina Bucher, *Ketsch*
Steffen Büßcker, *Neckargemünd*
Ralph Falk, *Baden-Baden*
Christoph Fischer, *Heidelberg*
Julia Flanjak, *Mannheim*
Jan Freudenberg, *Schifferstadt*
Jan Gotthardt, *Hockenheim*
Maximilian Heeg, *Heidelberg/Freiburg*
Leonie Kastner, *Wiesbaden/Heidelberg*
Jonas Kiefer, *Nußloch*
Dustin Klinger, *Salem*
Alexandra Nothnagel, *Frankfurt am Main*
Daniela Paunescu, *Landau*
Clemens Scherer, *Karlsruhe*
Tina Schmidt, *Kornwestheim/München*
Christian Stoy, *Sinsheim/Heidelberg*
Hans Urban, *Heidelberg*
Benjamin Wallisch, *Burladingen*
Miriam Wiestler, *Heidelberg*

Production Editors:

Christian Stoy, Anna-Lynn Wegener

ISA San Francisco Contact:

Christoph H. Fischer – e-Mail: chf@me.com
Christian Stoy – e-Mail: christian.stoy@urz.uni-heidelberg.de

Heidelberger Life-Science Lab
International Science Academy San Francisco
Im Neuenheimer Feld 581
D-69120 Heidelberg
<http://www.life-science-lab.org>



The academy participants on Berkeley Campus



The Wemmer Lab in the summer of 2007

Foreword

The Heidelberger Life-Science Lab is a remarkable program that places enthusiastic and dedicated German high school (Gymnasium) students in Universities in different parts of the world to learn more about how scientific research is done, and at the same time to foster international cooperation. The third “International Science Academy” brought some of these students to the Bay Area in California in the summer of 2007, which was an excellent experience for all involved, continuing a strong tradition started in 2003.

The Life-Science Lab did an exceptional job of organizing the visits for students, not only coordinating all of the formalities for the visit, but also arranging for social gatherings and sightseeing to make the program a real pleasure for the highly motivated students participating. The organizers are to be congratulated for a wonderfully smooth operation, making it easy for everyone who participates in the program, and assuring thereby that it can continue.

Of course at the heart of this kind of program is the group of students who participate. It was wonderful to see the enthusiasm with which they approached the whole program! This talented group selected laboratories doing interesting scientific work, made the contacts to initiate the labs’ participation in the program, and then took on challenging research projects. They worked hard to prepare for their time in the labs, and also when here to generate results. The quality of results produced has been excellent, most impressive given the short time in which everything gets done.

As important as the science, however, is the spirit of international cooperation which is established. The spirit of these students leaves no doubt that they will be the future ambassadors of science to not only advance the scientific knowledge base for mankind, but also see that it serves the world communities in the best ways possible. It has been a pleasure to play a role in this program (albeit a very small one), and hope that many more students can benefit from it.

David Wemmer

Professor

Department of Chemistry

University of California, Berkeley



Preface

The extraordinary experience of the 2007 International Science Academy in San Francisco stood at the end of a turbulent journey for all participants. After two years of intensive preparation and many ups and downs, 19 students of the *Heidelberg Life-Science Lab* realized their own version of the “American Dream” – and the four weeks of fascinating science between July 22nd and August 18th presented in this pack, were well worth the trouble and hard work.

For the third time since 2003, laboratories at the Universities of Berkeley and Stanford opened their doors and welcomed a group of German high-school graduates for the unique chance to experience the academic environment of a different culture, which broadened the horizons of all involved and often led to new and lasting friendships.

Yet, the experience at the International Science Academy in San Francisco goes beyond those four weeks by the Bay. The participants faced a steep and stony learning curve, which at times appeared obstructed and insurmountable. Even prior to boarding their planes, the participants had already gone through an arduous 2 year stint of preparation. At first, the students faced the task of finding professors at Berkeley and Stanford, who were willing to host motivated and dedicated students, and although this proved to be the most challenging task of the project, everyone managed to find a lab willing to take them on for this experience. But there was still more work to be done. Housing needed to be arranged, flights to be booked, insurances to be activated and many other small and seemingly negligible details needed to be dealt with, which later on turned out to be crucial. Thankfully, the experiences of planning and managing the previous two academies in 2003 and 2005 proved invaluable in this process. Still, every International Science Academy is a challenge in its own with new and unforeseen issues, but fortunately all obstacles were overcome, mostly due to the perseverance and strong belief in their own abilities of the people involved.

As in the previous years, the project’s financing turned out to be the most insistent challenge and the costs had to once again be carried by the participants themselves and their families.

Retrospectively, the project was a great success and it was worth both the enormous effort and the financial investment. It managed to reach and surpass its successful predecessors and proved an unforgettable experience for all involved. The students were able to find internships in a kaleidoscope of interest areas: from cell and molecular biology, developmental biology, biochemistry, structural biology; to medical sciences, including gene therapy and stem cell research; to chemistry, seismology and mathematics.

The following pages offer you the opportunity to read in more detail about the academy participants’ fascinating projects, actual work and achievements, as well as their personal impressions from this life-altering experience. We hope that some of their enthusiasm will rub off on you and you will be able to feel the same passion and excitement of discovery that our participants felt during this academy.

Acknowledgements

We would like to extend our gratitude to Anna-Lynn Wegener, who was a great help in proof-reading the participants’ articles, all the mentors and staff of the Heidelberg Life-Science Lab, especially Dr. Thomas Schutz, Dr. Katrin Platzer, and Hannah Novatschkova, as well as the Alumni Association of the Heidelberg Life-Science Lab.

Christoph Fischer and Christian Stoy
Student Mentors and Coordinators of the SFA 2007



Golden Gate Bridge

University of California at Berkeley

The University: The campus of UC Berkeley is ideally located right in the middle of town on a westward slope overlooking San Francisco Bay with beautiful sunsets over the Golden Gate Bridge. The often European-style buildings are widely spaced between lush-green lawns and recreation areas where students often sit and chat under the Californian sun. The tallest building on campus, and a landmark clearly visible from San Francisco, is the Campanile (1914), built after the original in Venice.



Seal of UC Berkeley

The university was founded in 1868, and the present campus inaugurated in 1873, with an enrollment of 191 students. Today, roughly 35,000 students are enrolled in some 40 academic programs, with around 2000 active instructional faculty. At the undergraduate level, there is a highly competitive 21.5% admissions rate. About 900 doctoral degrees are conferred each year, of which roughly 10% are in biology. The library provides 10 million print volumes, one of the finest research collections in the United States.



The Campanile

Nobel Laureates: Throughout the years 18 Nobel Prizes have been awarded to Berkeley faculty members – presently there are seven active Nobel Laureates among the faculty. Ernest O. Lawrence, who developed the first cyclotron, was awarded the Nobel Prize in 1939 – today his name is commemorated in the Lawrence Berkeley National Laboratory.

Geography and Safety: The particular combination of soft rolling hills with the soft rolling waves of the picturesque San Francisco Bay and its passage to the Pacific, spanned by the architectural masterpiece of the Golden Gate Bridge, marks a breathtaking geographical setting, particularly as viewed from the upper Berkeley campus, and particularly from the Campanile. Some think that the Bay Area is not the most secure place, not only in geographical terms. Prudence and appropriate safety are mandatory in everyday life (as in any big city, after all it's

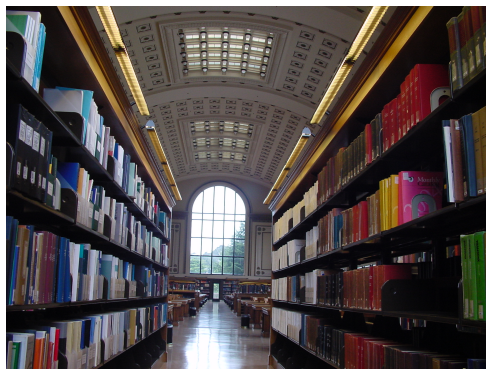
a 3-million metropolis) – but it is also true that the Hayward fault runs right underneath the Berkeley stadium. Fortunately, there was no damage done to the campus by the big earthquake of 1989, which took down part of the Oakland Bay Bridge. Earthquake drills and emergency training programs are commonplace to California... and an essential part of all lab safety instructions... so, watch yourself, and you'll be alright... you're 'living on the faultline'.



The University Library

Tuition: And now, how 'bout finances? Well, at an average nonresident tuition of about \$27,000 per annum, it ranks close to private universities; however, resident tuition (taxpayers) is considerably less, at around \$7,000 – and most students in need receive financial aid, on the average covering at least half of their tuition. So, while German universities are still partly non-tuition and tax-financed, American universities are partly so, but the fact that students have to pay their own fare, means that American universities are more customer-oriented and try to offer according services.

Leisure: In order to relax from studying, the Berkeley hills are attractive for hiking and jogging under *non-native* huge eucalyptus and palm trees (beware of the *native* poison oak) – blue jays and squirrels abound, but luckily there are no mountain lions or bears (and very few rattlers, if any!). The Berkeley Botanical Gardens is an oasis of peace and contemplation – and, of course, a nursery for many native Californian and exotic plants. The Bay Area's got everything from music to the arts, how 'bout a symphony concert at Hertz Hall, or a visit to the Museum of Paleontology, Natural History, Anthropology, or Modern Art – or a “Golden Bears” basketball game. . . or if you just feel like sitting down for a good meal, there are plenty of excellent ethnic restaurants (how 'bout Ethiopian), . . . or healthy, organic American food!



Inside the library

Our San Francisco Academy has been very fortunate to be hosted by the friendly and generous Berkeley faculty – it has been an exciting experience for each one of us to meet you and your staff.

<http://www.berkeley.edu>

Theodor C. H. Cole

Stanford University

In 1876, former California Governor Leland Stanford purchased 650 acres for a country home and began the development of his famous Palo Alto Stock Farm for trotting horses. He later bought adjoining properties to bring his farm to more than 8,000 acres, land that became the Stanford campus.

On October 1st, 1891, Stanford University opened its doors after six years of planning and building. Jane and Leland Stanford established the university in memory of their only child, Leland jr., who died of typhoid fever at the age of 15. Within weeks of his 1884 death, the Stanfords determined that, because they no longer could do anything for their own child, they would use their wealth to do something for other people's children. "The children of California shall be our children." Leland Stanford devoted to the university the fortune he had amassed, first by supplying provisions to the mining for California gold and later as one of the "Big Four", whose Central Pacific Railroad laid tracks eastward to meet the Union Pacific and complete the transcontinental railway. They settled on creating a great university, one that, from the outset, was untraditional: co-educational, in a time when most were all-male; non-denominational, when most were associated with a religious organization; avowedly practical, producing "cultured and useful citizens" when most were concerned only with the former. Jane and Leland Stanford determined that the character of the Main Quadrangle and the Palm Drive main entrance would reflect a grand, formal style: California Mission-inspired buildings of local sandstone and red-tiled roofs surround a cloistered quadrangle, the so-called Main Quad, with Memorial Church as its focal point.



Hoover Tower

A Teaching and Research University



Seal of Stanford University

Presently, there are approximately 7000 undergraduate and 8000 graduate students inscribed, instructed by about 1800 faculty. With an approximate 8 to 1 student-to-faculty ratio, Stanford emphasizes close interaction with faculty. Of the seven schools at Stanford, three award undergraduate degrees: Humanities and Sciences, Earth Sciences, and Engineering. Working under the supervision of faculty, undergraduates may join laboratory teams on campus, research a topic through Stanford's extensive library or travel to field sites around the world to complete an independent project. Study opportunities are offered in overseas to participate in internships and research projects. Approximately 90 percent of undergraduates receive their degree within five

years. A Stanford student needs a budget of \$48,900 a year (tuition \$34,800 plus costs for room and board, books etc.). In order to allow admittance to qualified students without regard to their ability to pay, 77 percent of them get financial aid by the university. 95 percent of undergraduates live on campus as do 54 percent of graduate students and 30 percent of faculty members. The housing system for students consists of residence halls with traditional dormitories, apartments, suites and residences. Faculty and staff live in owner-occupied housing units or in rental units on the campus.

Graduate students can pursue postbaccalaureate degrees in seven schools: Business, Earth Sciences, Education, Engineering, Humanities and Sciences, Law and Medicine. Exchange programs with the universities at Berkeley and San Francisco complement the courses.



Memorial Auditorium

Stanford researchers have contributed to many developments over the years, 29 of Stanford faculty have been awarded the Nobel Prize since the university's founding. Among the living Nobel laureates are:

- Arthur Kornberg, Nobel Prize in Physiology or Medicine, for the discovery of the mechanisms in the biological synthesis of RNA and DNA
- Paul Berg, Nobel Prize in Chemistry, for his research on recombinant DNA
- three physicists at the Stanford Linear Accelerator Center (SLAC) were honored for their work they conducted at SLAC on elementary particles
- three professors in the Department of Physics
- and eight are faculty in economics or business

The Stanford Medical Center

The Stanford Medical Center includes the Stanford School of Medicine, Stanford Hospital & Clinics and the Lucile Packard Children's Hospital.

The Stanford Medical Center is well known for its breakthrough technologies and treatments, including the first synthesis of biologically active DNA in a test tube, the first construction of a recombinant DNA molecule containing DNA from two different species, discovery of immune response genes and development of the microarray technology that allows researchers to see at once which genes of the thousands present in a cell are switched "on."

We are grateful for this third International Science Academy, made possible by the kind support and welcoming acceptance of our hosting professors and their staff at Stanford. Our young eager students have enjoyed and absorbed every bit of it, and have learned for life!

<http://www.stanford.edu>

Monika Gessat

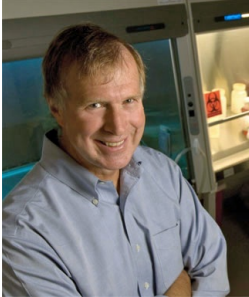
The Hosting Professors

Michael F. Clarke

Professor

Stanford Institute for Stem Cell Biology and Regenerative Medicine

Stanford University School of Medicine



Dr. Clarke maintains a laboratory focused on two areas of research: i) the control of self-renewal of normal stem cells and their malignant counterparts; and ii) the identification and characterization of cancer stem cells. A central issue in stem cell biology is to understand the mechanisms that regulate self-renewal of hematopoietic stem cells, which are required for hematopoiesis to persist for the lifetime of the animal.

<http://med.stanford.edu/profiles/Michael.Clarke/>

Douglas S. Dreger

Assistant Professor

Department of Earth and Planetary Science

University of California, Berkeley



Research includes use of waveform data to investigate seismic source, wave propagation, and Earth structure problems including geophysical inverse problems.

Additionally, research is conducted to develop robust automated procedures to analyze earthquakes as they occur and to report strong shaking levels on a local and regional scale.

Current research is focussed on nuclear event discrimination using regional distance moment tensors, investigating anomalous seismic radiation of Mammoth Lakes, CA, events, the development of a regional distance methodology to rapidly determine near-source strong ground motion shaking levels, and investigation of 3D crustal structure effects on ground motions in the greater San Francisco bay area.

<http://seismo.berkeley.edu/~dreger/>

David G. Drubin

Associate Director

Department of Molecular and Cell Biology

University of California, Berkeley



Cells consist of many discrete compartments designated for specific functions. The combined research laboratory of David Drubin and Georjana Barnes is addressing how specific cellular processes are performed in distinct sub-cellular localities, and the dynamics and regulation of these processes. The biological problems under investigation include actin cytoskeleton dynamics and actin mediation of endocytosis, Golgi trafficking, and viral budding.

Also being investigated are fundamental mechanisms of chromosome segregation, with a particular emphasis on the kinetochore, the structure that attaches chromosomes to the mitotic spindle.

http://mcb.berkeley.edu/labs/drubin_barnes/

Marcus W. Feldman

Professor

Department of Biological Science

Stanford University



Professor Feldman's research group uses applied mathematics and computer modelling to simulate and analyze the process of evolution, which by its very nature is statistical. It focuses on four general areas of interest. First is the evolution of complex genetic systems that can undergo both natural selection and recombination. Second, the evolution of learning is being examined as one interface between modern methods in artificial intelligence and models of biological processes, including communication. Third, the interaction of biological and cultural evolution is being investigated. The fourth area concerns mathematical and statistical analysis of molecular evolution, particularly microsatellite polymorphism.

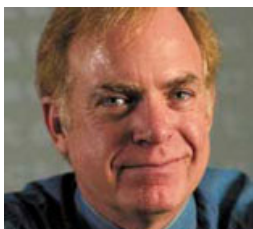
<http://www-evo.stanford.edu/index.html>

John G. Flannery

Professor

Department of Molecular and Cell Biology

University of California, Berkeley



Retinal degeneration and blindness result from the loss of rod and cone photoreceptors due to mutations in these cells or in their closely interacting and supportive retinal pigment epithelium (RPE), from environmental or poorly defined age-related factors, or the actions of other retinal neurons, glia or vascular elements.

One of the major goals of our laboratory is to develop therapeutic approaches that will slow or prevent the loss of rods, cones, RPE and other cells in retinal degenerations.

<http://mcb.berkeley.edu/labs/flannery/>

Mark A. Kay

Professor

Departments of Pediatrics and Genetics

Director, Program in Human Gene Therapy

Stanford University School of Medicine

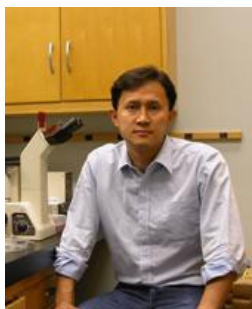


The goals of my laboratory are to establish the scientific principles and develop the technologies needed for achieving persistent and therapeutic levels of gene expression in vivo. While our ultimate aim is to use gene transfer to treat human disease, we plan to address basic biological questions that will be important for rational design of vectors for gene therapy applications. Towards this goal, we are working on developing new non-viral and viral vectors for gene transfer and establishing the cellular and molecular mechanisms involved in gene transduction in animals.

<http://www.med.stanford.edu/kaylab/>

Seung-Wuk Lee

Assistant Professor
Department of Bioengineering
University of California, Berkeley



A fundamental challenge in nanoscience is to accomplish two “complementary” goals simultaneously: One is synthesis of high performance functional materials on nanometer scale and the other is their assembly into well-defined structures which can surpass current lithographic capabilities. To achieve these goals, our research group is developing novel basic building blocks which store blueprint information about both their specific functions and the direction of their self-assembly structures using “evolutionary peptides” conjugated to programmable structural motifs.

<http://leelab.berkeley.edu/>

Jeffrey R. Long

Associate Professor
Department of Chemistry
University of California, Berkeley



When a correlation between the chemical structure and a physical property of a material is postulated, measurements on compounds exhibiting a range of structural variations are required to establish its validity and, ultimately, to optimize performance for an application. Yet the controlled modification of inorganic structures remains, in many instances, an open challenge. Our research is directed toward developing general strategies for the synthesis of inorganic clusters and solids.

<http://alchemy.cchem.berkeley.edu/>

Marcin M. Majda

Professor
Department of Chemistry
University of California, Berkeley



Research in our group addresses a variety of problems concerned with the structural and dynamic properties of molecular assemblies at solid and liquid interfaces. One of the long-term goals is design of protein and DNA micro-array sensors. The fundamental problems of current interest include behavior of antibody-antigen equilibria in a field of small mechanical forces, mobility of amphiphiles at the air/water interface, dynamic properties of the aqueous liquid-vapor interface, and electron tunneling across monolayer films. Our interest is devoted to and divided between biophysical/bioanalytical as well as interfacial chemistry areas.

<http://www.cchem.berkeley.edu/mmmgrp/>

Nipam Patel

Professor

Department of Integrative Biology

University of California, Berkeley



Patel Lab's research can be divided into five main categories: 1. the role of homeotic (Hox) genes in the evolution of body morphology – 2. the evolution of segmentation mechanisms during early development – 3. the evolution of the central nervous system of arthropods – 4. the analysis of regulatory changes in genes during evolution – 5. the development of misexpression systems to manipulate organisms not amenable to standard genetic approaches.

<http://www.patellab.org/>

Suzanne R. Pfeffer

Professor

Department of Biochemistry

Stanford University School of Medicine



A major goal of our research is to understand the molecular basis of receptor trafficking in mammalian cells. We would like to understand how cells localize receptors to specific subcellular compartments and how receptors move from one compartment to another. To study these processes, we have reconstituted the vesicular transport of mannose 6-phosphate receptors (MPRs) from late endosomes to the trans-Golgi network (TGN) in the test tube and have shown that this process requires the Rab9 GTPase.

<http://biochemistry.stanford.edu/research/pfeffer.html>

Kristin Scott

Assistant Professor

Department of Molecular and Cell Biology

University of California, Berkeley



We study taste perception in the fruit fly, *Drosophila melanogaster*, to examine how sensory information is processed by the brain. We use a combination of molecular, genetic, electrophysiological and behavioral approaches to study taste circuits. Our aims are to understand how different tastes are distinguished by the brain and how taste perception is modified by experience.

<http://mcb.berkeley.edu/labs/scott/>

David E. Wemmer

Professor

Department of Chemistry

University of California, Berkeley



Our work is aimed at understanding the structure, dynamics, and function of biological molecules. Our primary tool of investigation is nuclear magnetic resonance (NMR) spectroscopy, particularly multidimensional techniques.

For a majority of the ongoing studies we take advantage of isotope enrichment with ^{15}N and ^{13}C with 3D and 4D NMR experiments. Studies have focused on proteins involved in regulation of genetic expression, but also on unusual DNA structures, a variety of cofactors, peptides, and unnatural biopolymers.

<http://www.cchem.berkeley.edu/wemmer/Home.html>

Table of Contents

Berkeley

Tim Bleul and Jonas Kiefer

Taste Perception in *Drosophila melanogaster*

Laboratory of Kristin Scott

Department of Bioengineering, University of California at Berkeley 1

Janina Bucher

Synthesis of (001) hydroxyapatite surfaces on various substrates

Laboratory of Prof. Seung-Wuk Lee

Department of Bioengineering, University of California at Berkeley 5

Steffen Bübecker

Identification of morphogen expression patterns within imaginal discs and comparative investigations to *Drosophila* and the butterfly *Junonia*

Laboratory of Nipam H. Patel

Department of Molecular and Cell Biology, Department of Integrative Biology, University of California at Berkeley 11

Ralph Falk and Julia Flanjak

Wave Analysis and Seismic Moment Tensor of the Oakland event from 20th July 2007

Laboratory of Douglas S. Dreger

Department of Earth and Planetary Science, University of California at Berkeley 17

Jan Freudenberg

Effect of Small Forces on Adhesion of Micro-Spheres to a Surface Treated with Protein Adlayers and Reduction of Non-Specific Binding

Laboratory of Marcin Majda

Department of Chemistry, University of California at Berkeley 23

Jan Gotthardt

Synthesis and characterization of metal-oxo and metal-cyanide cluster magnets

Laboratory of Jeffrey R. Long

Department of Chemistry, University of California at Berkeley 29

Maximilian Heeg

ASE1 is a microtubule stabilizing MAP

Laboratory of David Drubin

Department of Molecular and Cell Biology, University of California at Berkeley 35

Alexandra Nothnagel and Benjamin WallischNMR Investigation of the Involvement of Mn²⁺ in the Activation of DR2356

Laboratory of David E. Wemmer

Department of Chemistry, University of California at Berkeley 41

Clemens Scherer

Development of hSSTR2 Promoter to Target ON Retinal Ganglion Cells via Adeno-Associated Viral Vectors

Laboratory of John G. Flannery

Helen Wills Neuroscience Institute, Department of Molecular and Cell Biology, University of California at Berkeley 51

Hans Urban

Influence and moderating roll of lipids in endocytosis

Laboratory of David Drubin

Department of Molecular and Cell Biology, University of California at Berkeley 57

Stanford**Philipp Bayer and Daniela Paunescu**

Structural Similarities of Small Hairpin RNA Structure to the Inverted Terminal Repeat T-shape correlate with unsteadiness in packaging of Adeno-Associated Virus vectors for RNA interference gene therapy

Laboratory of Mark Kay

Department of Pediatrics and Genetics, Stanford University School of Medicine 61

Leonie Kastner and Dustin Klinger

The Rab9 Effector GCC185 Interacts With Several Other Rab Family Proteins

Laboratory of Suzanne R. Pfeffer

Department of Biochemistry, Stanford University School of Medicine 67

Tina Schmidt

Invasion of a two-deme population by an imprinting allele

Laboratory of Marcus W. Feldman

Department of Biological Science, Stanford University 73

Miriam Wiestler

The role of Bmi-1 in maintaining self-renewal of cancer stem cells

Laboratory of Michael F. Clarke

Institute for Stem Cell Biology and Regenerative Medicine, Stanford University School of Medicine 83

The Academy Participants 89

Taste perception in *Drosophila melanogaster* – ppk23 ion channel is involved in salt perception

Tim Bleul and Jonas Kiefer

Laboratory of Kristin Scott

Department of Molecular and Cell Biology

University of California at Berkeley

Introduction

The ability to recognize and respond to chemosensory information is crucial for all animals and they have therefore developed specialized mechanisms for chemosensory detection. The gustatory system in *Drosophila melanogaster* is primarily involved in feeding behavior and enables them to detect nutritious foods and avoid toxic substances. In insects, taste neurons also initiate innate sexual and reproductive responses. Taste neurons are broadly distributed on the fly's body surface and they recognize taste stimuli such as sugars, salts, acids, alcohols and noxious chemicals. A recent study has shown that *Drosophila* flies are able to recognize carbon dioxide. Despite differences in terms of gustatory anatomy and taste-receptor families, gustatory systems share a basic organization that is different from other sensory systems. Recent studies with model organisms have examined the logic of taste coding in the periphery (Wang et al., 2004) and identified candidate taste receptors (Scott et al., 2001).

The robust behavioral responses and the relative simplicity of the fruit fly brain, along with the molecular, genetic and functional approaches available in *Drosophila*, makes the gustatory system of *Drosophila melanogaster* an excellent system to study taste responses. The sensory bristles for taste recognition are located on the pro-

boscis, internal mouthpart organs, legs, wings and ovipositor. Each bristle is innervated by 2-4 gustatory neurons and a single mechanosensory neuron. 68 gustatory receptor genes have been identified providing molecular markers that are used to examine taste recognition. Taste receptors mediating sweet (Gr5a) and bitter (Gr66a) taste perception have already been identified but it is still unknown which receptors mediate salty perception.

Our project shows the Scott lab's assumption on the ppk23 receptor being involved in salt perception is very likely to be right. In a feeding assay we examined the behavioral responses of *W118* flies, *Pexcision* flies (ppk23 wild-type) and *Piggyback* flies (ppk23 mutants) to different salt concentrations. We were able to show that the avoidance behavior of ppk23 wild-type flies to high concentrations of salt is significantly stronger than the avoidance behavior of ppk23 mutants, in which the ppk23 receptor is not expressed.

Materials and Methods

To examine salt perception and the avoidance or preference behavior mediated by different concentrations, we made a feeding assay with two different diets.

The experiment consisted of three major steps:

At first flies were put on test plates with two different test agar solutions to perform

the feeding assay. Afterwards the solutions were extracted out of the flies. The third step was to analyze the extract under the spectrophotometer.

Before starting the assay male flies were separated against females as it is known that males and females show different behavioral responses. For one trial about 40 flies of each gender were used. The flies were then placed on a sucrose agar (100 mM Sucrose, 1% agar) to clean their stomach as their regular food interferes with the spectrophotometer readings. Afterwards the flies were put into vials with half size Kim wipe soaked with 1.5 ml dH₂O for 24 hours for starvation. Then the flies were introduced in test plates (72-well micro plate) for 4 hours with the choice between red and blue solutions. Different trials were made with different salt concentrations in the blue dye. The red dye only contained 5 mM Sucrose and 1% agar while the blue dye additionally contained different salt concentrations. Trials were made with salt concentrations of 25 mM, 50 mM and 500 mM in the blue agar solution. To make sure the experiment works and to show that the flies do not feel more attracted to one of the two solutions right from the start we made control trials with no salt in both the blue and the red agar solution suspecting that the absorbance in the spectrophotometer would be equal on both 499 nm (blue) and 630 nm (red). Each trial was made with five sets of flies to have enough data to give reliable results. The test plates were put in the -20° C refrigerator overnight after the feeding assay. Then the red and blue agar were extracted out of the flies stomachs and the extract was analyzed with the spectrophotometer. For the extraction 30 flies were collected and 100 µl PBS (Phosphate Buffered Saline pH 7.2) was added. After the flies were smashed mechanically 500 µl PBS was added and the tubes were put in the centrifuge (15 min, 14,000 rpm). Then 500 µl of the supernatant was transferred to a new tube and 500 µl of n-heptane was added.

After shaking the tubes they were put in the centrifuge again (15 min, 14,000 rpm). 450 µl of the lower phase (PBS phase) were then transferred into a plastic cuvette for the final spectrophotometer readings. The absorbance was measured at 499 nm (for blue) and at 630 nm (for red).

Afterwards the absorbance of the red dye was divided by the absorbance of the blue dye. A result bigger than 1 would indicate that the flies preferred the red dye to the blue dye, a result of 1 that the flies did not care about the salt and a result smaller than 1 that the flies preferred the blue dye over the red one.

In our experiment three different fly strains were used. For each trial 5 sets of *W118* flies, 5 sets of *Pexcision* flies with the normal *ppk23* gene and 5 sets of *Piggyback* flies in which the *ppk23* ion channel is not expressed due to an hypomorphism were used. The Scott Lab has produced the *Piggyback* flies by inserting a long DNA strain into the *ppk23* gene. The expression of a Diphtheria toxin in the specific taste cells would not be useful as we wanted to examine the function of the ion channel and not the function of the whole taste cells in which the *ppk23* gene is expressed.

Results

Fig. 1 shows our results of the different behavioral responses towards different salt concentrations. In our control experiment with no salt in both the red and the blue dye we saw a slight preference of the flies towards the red dye. During our experiments we also realized that we extracted the red pigments out of the eyes of the *Piggyback* flies. The *Piggyback* flies were the only flies with red eyes we used in our experiments. But as we always used the ratio between the results of the experiments with salt in the blue dye and our control experiment these deviations do not affect our results. In our experiments with 25 mM NaCl and 50 mM NaCl in the blue dye we were

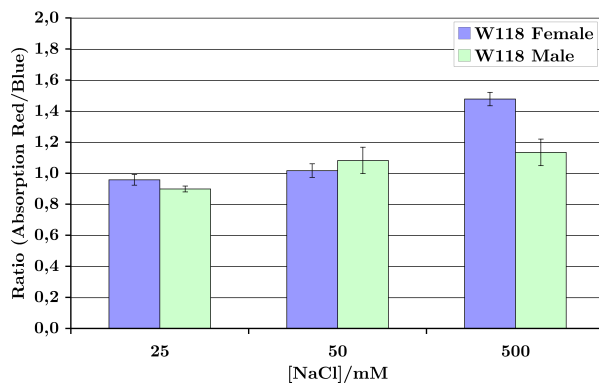
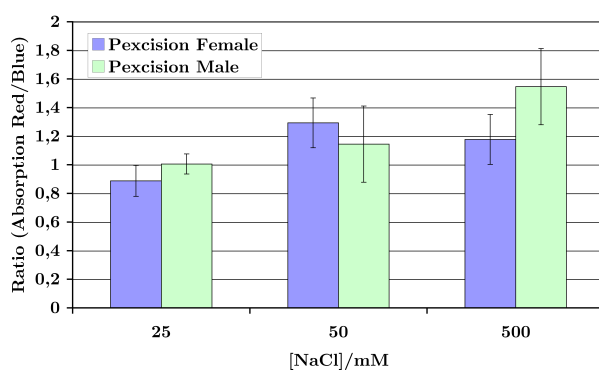
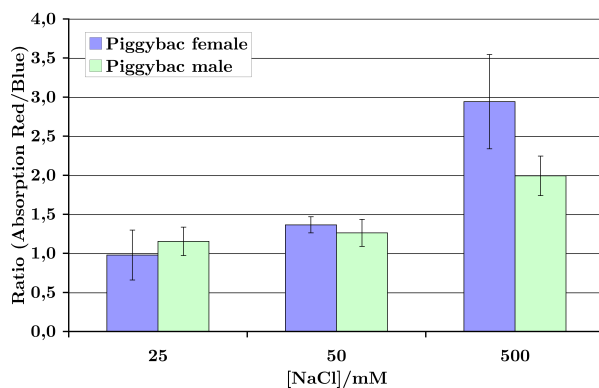
(a) Salt perception in *W118* flies(b) Salt perception in *ppk23* mutant flies(c) Salt perception in *ppk23* wild-type flies

Fig. 1. The three graphs list the 3 trials for each fly type with salt concentrations of 25, 50 and 500 mM. The abscissa (x -axis) lists the salt concentrations and the ordinate (y -axis) lists the ratio of the red versus the blue dye. Values above 1 illustrate avoiding behavior, values under 1 preference behavior. For each fly type, concentration and gender the experiment was run 5 times to get meaningful results.

not able to obtain clear results. It seems like the flies show a slight preference towards 25 mM NaCl and a slight avoidance behavior towards 50 mM NaCl. The Chi-Test, however, showed that our results at 25 mM and 50 mM are not significant. We can see a clear avoidance behavior towards a concentration of 500 mM NaCl. This avoidance behavior varies depending on the different fly strains we used. The *ppk23* wild-type flies show the strongest avoidance behavior towards 500 mM NaCl while the avoidance behavior is significantly less strong at the *ppk23* mutants as expected. Also the *W118* flies show a clear avoidance behavior towards 500 mM NaCl. As anticipated there seem to be slight differences between the behavioral responses of males and females. However, we were not able to identify any regularity in the differences between males and females.

Discussion

We expected a different behavioral response between the *ppk23* wild type and the *ppk23* mutants as the *ppk23* ion channel is not expressed in the *ppk23* mutants due to a hypomorphism. As expected the *ppk23* wild type flies showed a stronger avoidance behavior than the *ppk23* mutants. The Chi-Test shows that the differences are significant and our results therefore proof that the *ppk23* ion channel is involved in salt perception as suspected by the Scott lab. Identifying behavioral responses to low concentrations of salt is known to be very difficult. As we were not able to do more than five trials with each fly strain we were not able to obtain clear results at 25 mM and 50 mM salt.

Personal Impressions

We would like to thank Kristin Scott and the members of the Scott Lab for hosting us three weeks in the laboratory. We enjoyed our stay in the Scott Lab very much and are thankful for the opportunity to experience world-class research and the possibility to get insight into the daily routine of the work done in a laboratory. Moreover, we want to

thank all the members of the lab for helping us when we had questions or problems. We especially liked to organize our own work-timetable and run the project on our own. Our experiment gave us the possibility to really get involved in fundamental science and we are proud that we have been able to gain some significant results. The atmosphere in the lab and during the common lab-lunches, especially at the Pizza-Thursdays was always friendly and warm. The members of the Scott lab made our stay in Berkeley a wonderful experience which we will never forget.

References

- Wang Z, Singhvi A, Kong P, Scott K (2004) Taste representations in the *Drosophila* brain. *Cell* 117:981-991
- Scott K, Brady R Jr., Cravchik A, Morozov P, Rzhetsky A, Zuker C, Alex R (2001) A chemosensory gene family encoding candidate gustatory and olfactory receptors in *Drosophila*. *Cell* 104:661-673
- Scott K (2005) Taste Recognition: Food for Thought *Neuron* 48(3):455-464

Synthesis of (001) hydroxyapatite surfaces on various substrates

Janina Bucher

Laboratory of Seung-Wuk Lee
Department of Bioengineering
University of California at Berkeley

Abstract

Hydroxyapatite (HAP), the major inorganic component of bone, is used as a simpler model system for the study of bone formation. Understanding how the crystal grows is essential for the treatment of bone deficiency diseases such as osteoporosis. We tried to synthesize HAP crystals with a parallel alignment in the c -axis direction on iron, glass or silicon surfaces. This orientation leads to a crystal layer that only displays the top (001) surfaces of the crystal, so that crystal growth can be studied exclusively on these surfaces.

Before synthesis, the different substrate surfaces were modified, freeing them not only from any impurities but also coupling amino groups onto the glass and silicon surfaces, which are thought to be good nucleation points for crystal growth. On these modified substrates, HAP crystals were grown out of a solution with varying reaction parameters.

Scanning electron microscope observation shows that crystal growth occurred, but not in the desired direction. However, the different arrays suggest that the crystals grow best when the substrate is modified for a medium period of time and the reaction is run for a long time.

Introduction

The study of bone, how it forms, how it maintains itself, how it dissolves, is of crucial importance for the development of new

treatments for bone deficiency diseases such as osteoporosis.

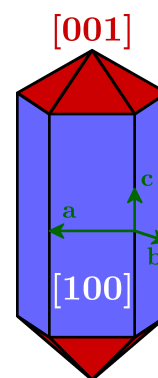


Fig.1. Schematic model of a HAP crystal showing the three coordination axes of the hexagonal crystal (green), the side surfaces (blue) and the desired (001) surfaces at the top and bottom (red).

Since bone itself is a very complex structure made up of organic molecules, such as collagen or other peptides as well as inorganic crystals, simpler model systems are employed for the study purpose, one of which is hydroxyapatite (HAP), the major inorganic component of bone.

HAP ($\text{Ca}_5(\text{PO}_4)_3(\text{OH})$) consists of Ca^{2+} , PO_4^{3-} and OH^- ions. The crystal has a hexagonal shape, so there are distinct surfaces. Most important is the difference between those on the sides of the crystals and those on top and bottom (fig. 1).

The latter ones are highly interesting since it is known that the crystal preferably grows in the longitudinal direction and therefore crystal growth is mainly carried

out on these (001) surfaces. In order to study the mechanisms behind as well as the impacts on this growth it is necessary to get a HAP sample that only displays these surfaces so that influences from the side surfaces of the crystal can be excluded.

Therefore we tried to synthesize HAP crystals with a parallel alignment and *c*-axis orientation. These syntheses were carried out on three different substrates whose surfaces were modified in advance in order to improve their ability to act as a nucleation point for HAP.

Materials and Methods

Chemicals

All chemicals used were from Sigma Aldrich except for the NaH_2PO_4 , which was obtained from Fluka.

Surface Modification

The first sample, an iron plate, was put in 1 M HCl for different times (2, 5 and 10 min respectively) in order to remove any impurities such as oxidized spots. Afterwards, it was thoroughly washed with water.

The glass and silicon surfaces were treated with γ -APTS (gamma-aminopropyltriethoxysilane) in order to couple amino-groups onto their surfaces (see fig. 2 for the complete reaction)

Therefore every sample was first washed in a highly acidic solution of H_2O_2 (30 %) and H_2SO_4 in a ratio of 1:4.

Afterwards, they were washed in two successive rounds, first with water and second with ethanol and then they were dried under argon. Next, they were kept in a solution containing 5 % of γ -ATPS in ethanol for different modification times (1 h, 2 h, 1 day, 3 days and 1 week respectively).

This step was followed by another round of washing with ethanol and drying under argon before the samples were kept in a drying chamber at $> 100^\circ\text{C}$ for 15 min.

Crystal synthesis

Haifeng Chen et al. were able to synthesize fluoroapatite crystals out of a growth solution [1] containing Ca^{2+} , PO_4^{3-} and F^- ions.

In order to get HAP, the solution was altered and the F^- ions were substituted by OH^- ions.

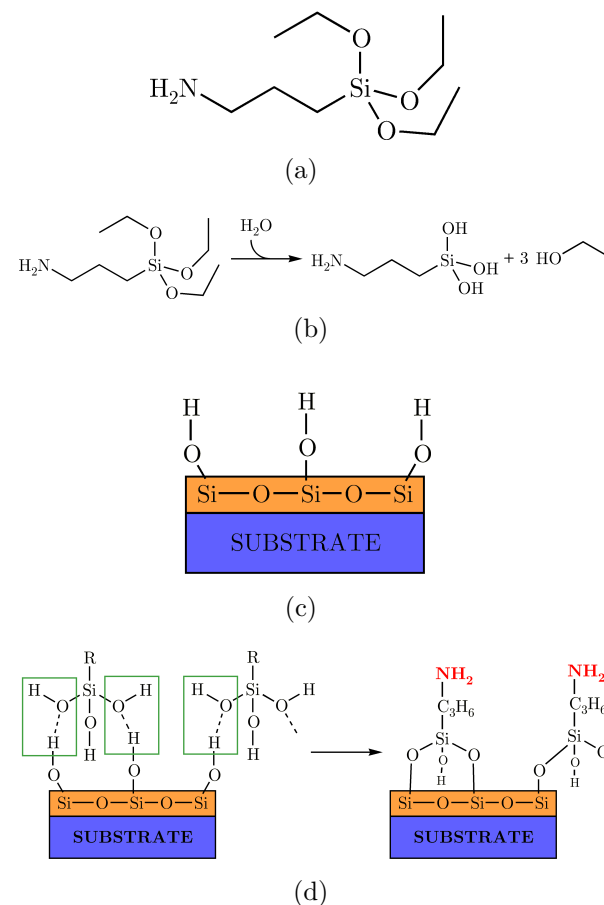


Fig. 2. Surface modification with APTS. (a) structural formula of γ -APTS (b) hydrolysis of γ -APTS. The reaction with the water present in ethanol splits the ester bonds, releases ethanol from the molecule and leaves hydroxyl groups behind (c) Schematic view of a glass or silicon surface. In both cases, there are thin layers of SiO_2 on the surface whereby hydroxyl groups are coupled to the silicon atoms (d) Reaction of SiO_2 with hydrolysed γ -APTS. Hydrogen bonds between the respective hydroxyl groups finally lead to a release of water, which leaves the γ -APTS rest covalently coupled to the substrate surface.

All concentrations were maintained so that the growth solution contained 0.25 mol

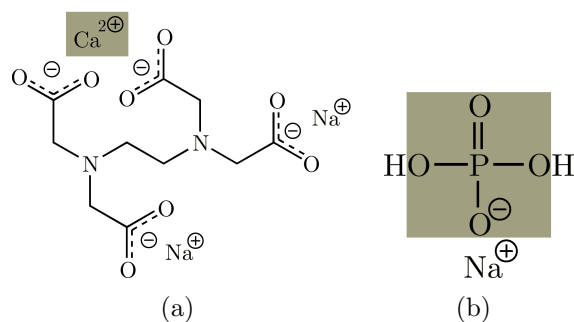


Fig. 3. Structural formulae of (a) EDTA-Ca-Na₂, which was used as a source of Ca²⁺ ions and of (b) NaH₂PO₄, which was used as a source of PO₄³⁻ ions

EDTA-Ca-Na₂ (ethylenediamine tetraacetic acid calcium disodium salt) and 0.15 mol NaH₂PO₄. Its pH was adjusted to 9. 2.34 g EDTA-Ca-Na₂ and 517.5 mg NaH₂PO₄ were put in a falcon tube in the solid state. The chemicals then were solved in 20 ml water and the pH was adjusted using 1 M NaOH. Finally, water was added up to a total volume of 25 ml. In one array, EDTA-Ca-Na₂ was substituted by CaCl₂ as a source of Ca²⁺ ions. In order to maintain the same Ca²⁺ concentration, 693.4 mg of CaCl₂ were added to the solution instead of EDTA-Ca-Na₂.

For the synthesis, this growth solution was poured into a teflon chamber and one or even up to three different substrates were added respectively.

After closing with its teflon lid, the chamber was put in an autoclave reactor in which it was kept in a heated silicon oil bath for the respective reaction time at the respective temperature (see table 1).

When the reaction time was over, the autoclave reactor was taken out and cooled down by keeping it at room temperature.

After opening the reactor and the teflon chamber, the substrate was taken out with tweezers, washed with water and stored in a petri dish in a desiccator at room temperature.

The growth solution was filtered and the teflon chamber as well as the supernatant

in the filter paper were washed with water. The latter then was dried under vacuum at room temperature.

Observation

The crystals grown on the various substrates were finally observed using an atomic force microscope (AFM; Asylum Research, MFP3D) and a scanning electron microscope (SEM)

Results

Table 1(a)–(c) present an overview of all arrays that have been carried out during the 3 weeks of the project.

The three different arrays are sorted by the kind of substrate they were grown on and arranged according to increasing modification time.

The tables contain a qualitative judgement of the thickness of the crystal layer. Thin refers to a sample where the respective substrate was still visible through the crystal layer whereas a thick crystal layer completely covered the substrate in white.

None of the samples shows the desired alignment and orientation. Instead, crystal growth took place in different directions yielding bulks of single HAP crystals, which together formed a pattern that looks similar to blossoms (see fig 4)

Fig. 4(a) can be regarded representative of all other HAP synthesis samples that have been observed. The only samples that look different are sample 5 grown on glass and the array carried out with CaCl₂, which are both also shown in fig 4.

Although the desired orientation could not be achieved, the results allow some suggestions about the influences on crystal growth.

Regarding the syntheses carried out on the iron plate, no proportional relationship could be observed between the modification time and crystal growth, which was assessed by judging the thickness of the crystal layer qualitatively.

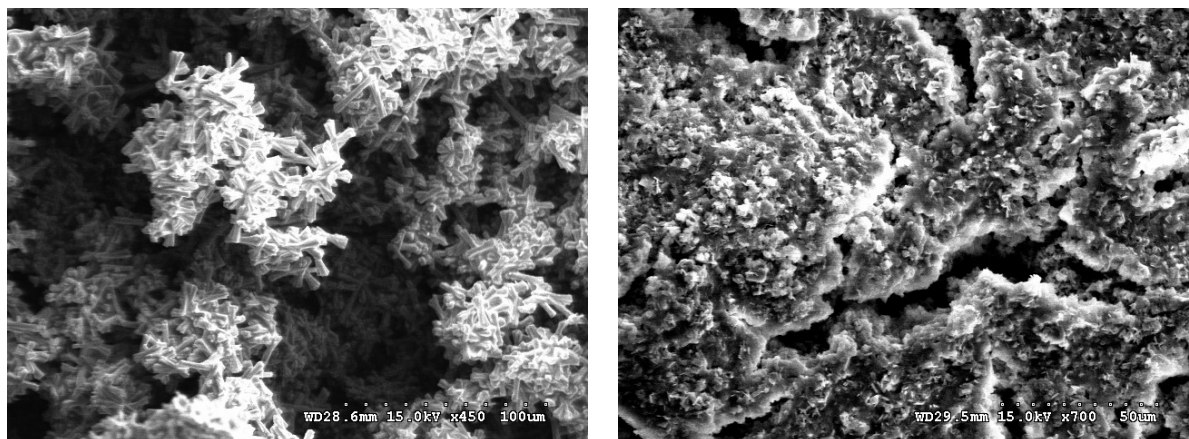
Table 1. Overview of the different HAP synthesis arrays. The arrays are sorted by the kind of substrate and arranged according to increasing modification time. Modification time refers to the period of time during which the respective substrates were kept in the respective modification solution. Reaction time refers to how long the autoclave reactor was kept in the oilbath. Thickness refers to a qualitative judgement of the crystal layer whereby thin refers to a layer under which the substrate was still visible and thick to a layer which completely covered it. Crystal growth refers to the orientation and alignment of the synthesized crystals, stating whether the desired shape has been achieved or not.

(a) iron plate						
#	modification time	reaction time	temperature [° C]	pH	thickness	crystal growth
1	2 min	16 h 45 min	100	9.10	thin	no orientation
2	2 min	17 h	120	9.00	thick	no orientation
3	5 min	2 d 17 h	120	9.00	almost nothing	not observed
4	30 min	3 h	150	9.01	thin	not observed
5	30 min	1 d	120	9.00	thin	no orientation
6	2 min	1 d, CaCl ₂	120	9.20	thin	no orientation
(b) glass						
#	modification time	reaction time	temperature [° C]	pH	thickness	crystal growth
1	1 h	1 d	120	9.02	almost nothing	no orientation
2	2 h	2 d 17.5 h	120	9.00	nothing	no orientation
3	1 d	3 h	150	9.01	almost nothing	not observed
4	1 d	2 d	120	9.00	thick	no orientation
5	3 d	16 h 45 min	100	9.10	almost nothing	no orientation
(c) silicon						
#	modification time	reaction time	temperature [° C]	pH	thickness	crystal growth
1	1 h	4 h	155	9.03	thick	no orientation
2	1 d	3 h	150	9.01	thin	no orientation
3	1 d	22.5 h	120	9.03	thick	no orientation
4	3 d	16 h 45 min	100	9.10	thin	no orientation

These findings are similar to the crystals grown on glass and silicon surfaces. For them, an interdependence between the modification and reaction time was found since crystal growth was best with a medium modification and a long reaction time.

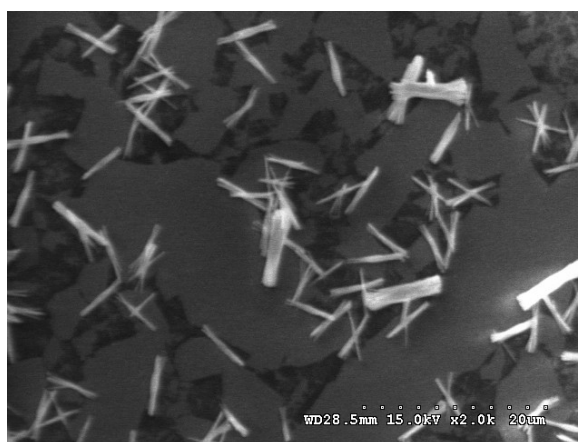
Furthermore, silicon seems to be the best substrate since crystal growth was good in 50% (2 out of 4 samples yielded a thick

crystal layer) compared to 17% (1 out of 6) for iron and 20% (1 out of 5) for glass. Since 80% (4 out of 5) of the glass samples yielded nearly no crystals, glass nevertheless appears to be worse than iron where the remaining 83% (5 out of 6) of the samples were at least covered with a thin crystal layer.

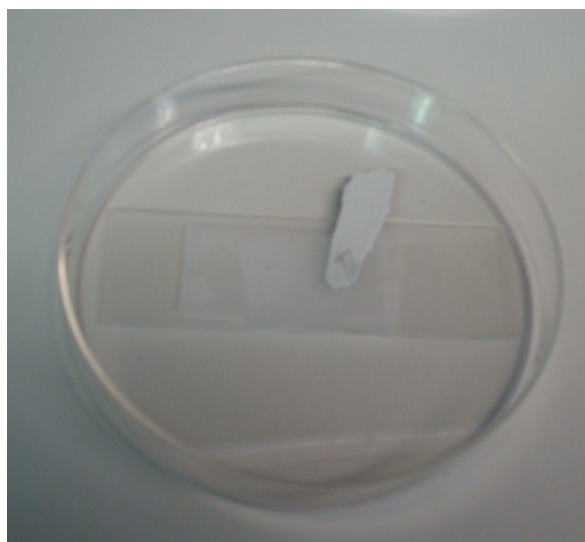


(a)

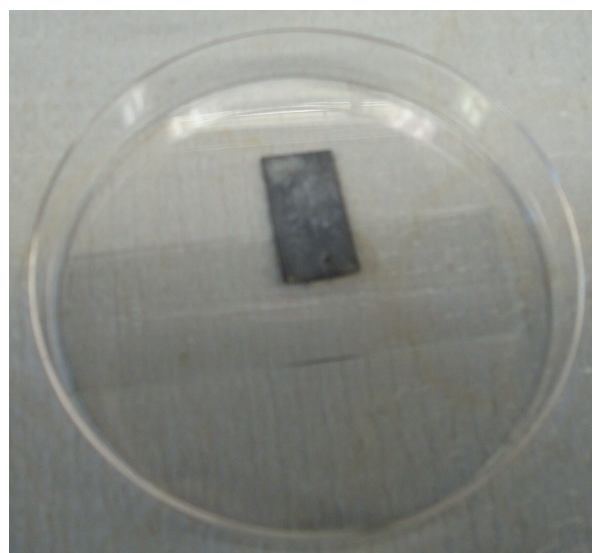
(b)



(c)



(d)



(e)

Fig. 4. SEM image of HAP crystals grown on (a) iron plate (sample 2, modified for 2 min, reaction time 17 h), (b) iron plate with CaCl_2 (sample 6, modified for 2 min, reaction time 1 day), (c) glass (sample 5, modified for 3 days, reaction time over night), (d) picture of a thick crystal layer (sample 3 grown on silicon, modified for 1 day, reaction time 22.5 h) and (e) picture of a thin crystal layer (sample 6 grown on iron with CaCl_2 , modified for 2 min, reaction time 1 day)

Furthermore, it was shown that crystals can also grow out of a solution which contains CaCl_2 as a source of Ca^{2+} ions instead of EDTA-Ca- Na_2 . However, the SEM image shows a different crystal structure than in all other arrays.

Discussion

All the statements made about the influences on crystal growth have to be handled with care since not all possible combinations of modification and reaction time on the different samples could be covered within the three weeks.

However, the results suggest that crystal growth works best when the substrate is not modified for too long and the reaction not carried out for too short.

Therefore, a really long reaction time, such as one week or longer, will maybe improve not only crystal growth but also the orientation of the crystals in the desired c -axis direction.

With regard to the crystals grown out of the solution containing CaCl_2 , this result must be treated very carefully since it is not yet proven that the grown crystal really is hydroxyapatite. Therefore, an analysis of the filtered rest of the solution is still necessary.

Since there are no reports about earlier experiments trying to synthesize the specific HAP crystals in that way, further investigation will be necessary to strengthen the findings about the influences on crystal growth. Regarding the ability of the dif-

ferent substrates as a nucleation point for crystal growth, our findings differ from other groups that found iron to be a better substrate than silicon. But this could be due to the low number of arrays that were carried out on each sample during the three weeks of the project, so that no real statistical statement is possible.

Nevertheless, our findings may help to improve the outcome of further experiments of HAP (001) surface synthesis and therefore finally reveal the best connection between the different parameters, which yields the desired crystal orientation.

Acknowledgements

My sincere appreciation is expressed to Prof. Seung-Wuk Lee for making this internship possible, for his trust and his friendly support whenever I needed help.

Furthermore, I would like to thank all members of the Lee-Group, especially Dr. Woo-Jae Chung, who introduced me to the field of crystal research and Dr. Ki-Young Kwon, who always managed to spread a relaxed atmosphere. I am also indebted to all the members of the lab as well as to the summer intern students, who integrated me so kindly in their group and made me feel so welcome.

All of them showed me how wonderful and exciting research can be, an invaluable experience for my choice to study chemistry.

References

- [1] Haifeng Chen, Zhiyong Tang, Jun Liu, Kai Sun, Sywe-Ren Chang, Mathilde C. Peters, John F. Mansfield, Agata Czajka-Jakubowska, and Brian H. Clarkson. Acellular Synthesis of a Human Enamel-like Microstructure. *Advanced Materials* 2006, 18

Identification of morphogen expression patterns within imaginal discs and comparative investigations to *Drosophila* and the butterfly *Junonia*

Steffen Bückecker

Laboratory of Nipam H. Patel
Department of Integrative Biology
University of California at Berkeley

The research on which the following report bases was affected by some minor successes in the staining procedure. Further, the project had to be done in a very short span of time as a developmental biological research. However, it is possible here to present results and interesting exposures because of a tight schedule and Mike Perry's all-embracing support.

Introduction

In most arthropods body appendages develop from the embryonic epithelium and are functional after hatching. The insect legs and wings, which have not only a locomotory purpose, but have a feeding and mating function as well, give fundamental opportunities and are essential to survive.

The epidermal limb structures of adult thoracic segments of *Drosophila* and *Junonia* derive from specialized precursors known as imaginal discs. The cell clusters emerge in the embryonic ectoderm after germ band elongation occurred at stage 10 in fruit flies. Meanwhile, the cells are set aside while most of the ecto-, meso- and endodermal tissue differentiates. At 10 hours (about stage 13) of embryonic development small clusters composed of 3–5 cells are separated from the leg primordia in the second (T2) and third (T3) thoracic segment. Moving dorsally, they differ in the expression of the morphogen *Vestigial*

(*Vg*), whereas the leg discs express *Distal-less* (*Dll*; Williams et al. 1991, Cohen and Simcox 1993). Both homeodomain transcription factors are markers of the common imaginal disc at stage 10–13. Moreover, limb primordia are allocated by a small stripe of *Decapentaplegic* (*dpp*)-expressing cells on the anterior-posterior axis at both sides of the embryo body and *Wingless* (*wg*)-originating domains, which are ventrally structured in rows collateral with the parasegmentation boundaries.

Several investigations carried out on the allocation of genes, that primarily affect the pattern formation within the early imaginal primordium, have shown a series of expression mechanisms (Cohen and Simcox 1993, Hayashi 1996, Hayashi and Goto 1999). The structure of the patterns of *wg*, *dpp* and *Dll* which had been derived from the response to antibody signals and cRNA-localization (by *in situ* hybridization) both in the three leg discs and in the wing disc lying in T2 as well as in the haltere disc that is located in T3 is well known.

In this report the expression signals of *wg*, *dll* and the segment-polarity gene *engrailed* (*en*) is investigated and it is tried to describe the cell arrangement of the morphogen-containing cells. The observations give some evidence of what happens within the precursor cells of leg and wing discs in stage 10–13 *Drosophila* embryos. Moreover, we com-

pared the same signals in butterfly embryos of the species *Junonia coenia*.

Materials and Methods

Fly stocks

For the wg-immunostaining a *wg-lacZ* fly strain was used as it is described in Perimon et al. 1991 (*en-lacZ*). A cross of two different mutant alleles, *slit*⁻*wg*⁺ and *slit*⁺*wg*⁻ balanced with a CyO chromosome and an enhancer detector for β -Galactosidase inserted at the *wg* locus, were recovered for *wg* mutant embryos. Produced by crossing them, the phenotypes are identifiable by their midline structure. In *slit*⁻ embryos many developing muscles are formed near and at the dorsal midline, stretching across it. Wild-type flies were used in any other histochemical stains.

Histochemical analyses

The *en* single-staining was performed with a primary mouse antibody for *en* 4D9 and a secondary goat anti-mouse IgG (conjugated to HRP, 1:20 dilution for primary and 1:600 dilution for secondary in PT+NGS). For black HRP reaction nickel was added to the DAB solution (see usual HRP reaction protocol). The fluorescent *wg*-sample was treated with chicken anti- β -Galactosidase and a commercial Alexa Fluor rabbit anti-chicken 555 IgG (1:1500 and 1:500). The *Dll* single-staining was set up with rabbit anti-*Dll* and goat anti-rabbit with a 1:100 and 1:600 dilution. For *Dll/wg* double staining the *Dll*-labeled embryos were subjected to a staining for *wg* with an HRP-conjugated secondary antibody but without adding nickel. Thus, *lacZ*-tagged flies were taken for the *Dll*-stain. A primary antibody chicken anti β -Galactosidase and a secondary mouse anti-chicken were used (1:1500 and 1:300 diluted). In fig. 4 the *Drosophila* embryo was dissected by opening the dorsal side and folding ventrally. Finally, it was prepared with PBS, or PBS/50% glycerol or even higher for storage.

To visualize *Dll* and *wg* activity in *Junonia* a double-labeling for both proteins and an *in situ* hybridization for *wg* (see *in situ* Hybridization) as well as two histochemical stains for *Dll* were done. Rabbit anti-*Dll* was diluted 1:100, whereas goat anti-rabbit was diluted 1:600, followed by brown HRP reaction. Most HRP signals became visible after 5–10 minutes. The fluorescent *wg*-label has to be kept dark, otherwise the signal gets weak. Every stain was observed by a Zeiss Lumar V12 and photographed by a Zeiss Axiophot microscope.

In situ Hybridization

In situ Hybridization was performed with digoxigenine-marked *wg*-RNA probe and detected with the standard procedure as described previously by Tautz and Pfeifle (1989). RNA was diluted 1:100 and the anti-digoxigenine (DIG) was diluted 1:300.

Results

Dll expression identifies the early thoracic limb primordia

Dll expression occurs mainly in the central cells of the primordium (together with the zinc-finger transcription factor *Buttonhead*, *btd*). The homeobox gene is responsible for the later distal leg morphology, as it is characterized by tarsus and tibia. Thus, it is used as a molecular marker for early limb structures in insect embryos. The histochemical staining shows that the three circular discs have an equal size and are located at the same level related to the thickness of the thorax directly behind the head. These observations suggest that the imaginal discs have a relatively wide extension in consideration of the fact that an additional domain expressing *Escargot* (*esg*) and not *Dll* surrounds the center. Moreover, the first disc does not differ, though some cells will leave the two posterior discs when germ band retraction begins.

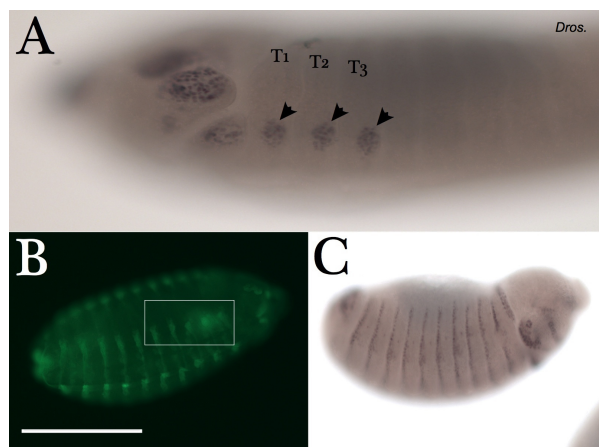


Fig. 1. Picture (A) shows the HRP signal for Distal-less and picture (B) and (C) below show the signals for the two segment-polarity genes *Wingless* and *Engrailed*. Both play an important role during the determination of the parasegment boundaries and contribute to the cell orientation within each of the parasegments. (A) *Dll* is expressed in the center of every primordial disc (arrows). The expression domain is surrounded by a slight stripe of *Escargot* (*esg*) expressing cells (Hayashi 1996) which is not detected here. The stage 11 embryo bears additional *Dll* signals in head regions. The exposure is blurred lengthwise. (B) Fluorescent image (wave length 555 nm) with a dorsal view sideways through the embryo. The signal arises in response to β -Galactosidase activity in this stage 11–12 mutant. The signals in T1-3 stop abruptly, whereas the ones in the following segments continue for 10–20 μ m. The framed part accords to fig. 2. (C) An older stage 13 embryo. The *Engrailed*-protein is the antigen for the used mouse antibody which will then be detected by the secondary antibody. The signal extends almost over the whole embryo body and a gap of the stripe in the first thoracic segment is noticeable. It is assumed that *Engrailed* is expressed in the posterior part of the imaginal disc. Bar: 80 μ m (A), 150 μ m (B,C)

***Dll* domain affects the run of ventral *wg* stripes and the coexpression within the imaginal disc**

To examine *wg* distribution especially in T1-3 the *wg*-secreting cells express β -Galactosidase enzyme under control of the

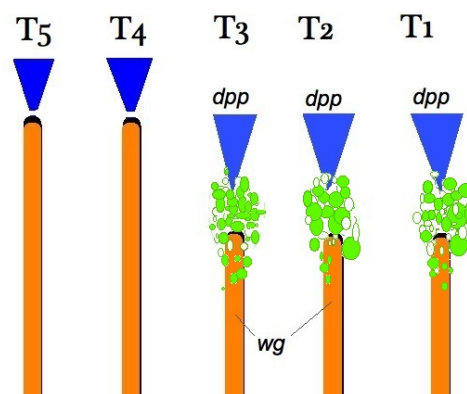


Fig. 2. A model of the arrangement of morphogen expressing cells at the lateral thorax. The *wg*-stripes come up from the embryo's venter. In T1-3 they extend into the *Dll*-expressing cells (green), which are restricted by a *dpp*-gradient. There are cells expressing both *wg* and *Dll* and there are cells expressing only *Dll* (see fig. 4). The stripes in T4 and 5 show the relationship between *wg* expression domains influenced by *Dll* and those without *Dll* contact.

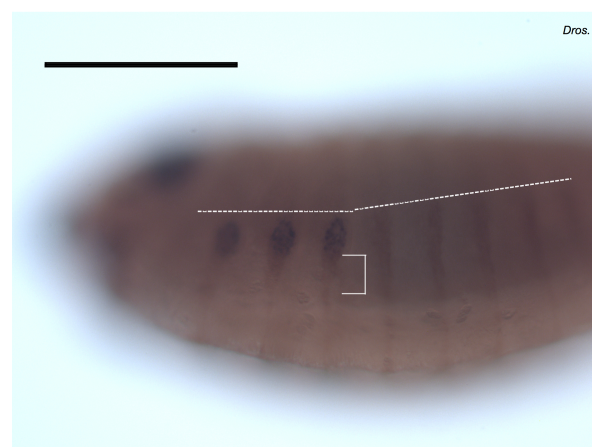


Fig. 3. Left side of a stage 11 embryo. It has been stained twice: brown for *wg* expression and black for *Dll* expression. The bracket marks an area where *wg* expression is broadened slightly and reaches up to the imaginal disc allocated by *Dll* signals. It seems that the *wg* stripes stop earlier in T1-3 (white line). Bar: 90 μ m.

wg enhancer that has been inserted into the *hox* gene in *lacZ* fly strains. As shown in fig. 3, the observations indicate that *wg* is

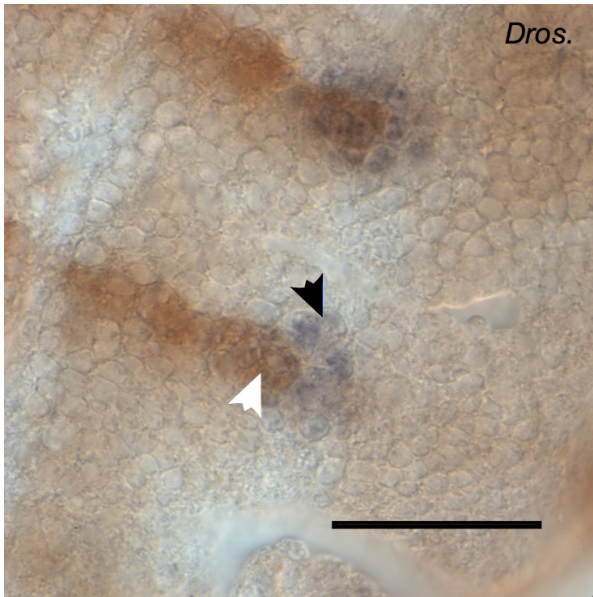


Fig. 4. Dissected embryo displayed to show the partial overlapping of *Dll* expressing cells (purple, black arrow) and the *wg* expressing cells (brown, white arrow). Bar: 35 μ m.

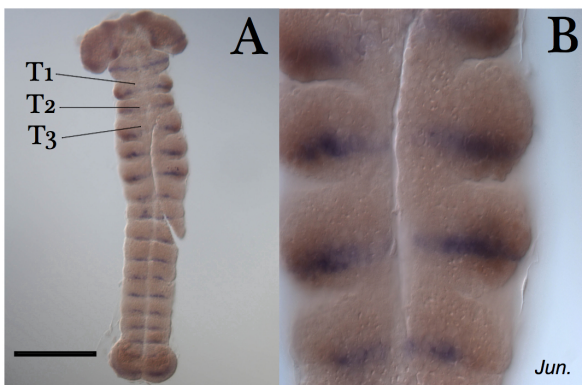


Fig. 5. (A) Dissected preparation of a *Junonia* embryo double-labeled to visualize both *wg* (purple) mRNAs by *in situ* hybridization and *Dll* (brown) expression patterns by histochemical staining. *wg* signals can also be found at the posterior end of each parasegment and *Dll* appears in some abdominal domains as well. (B) View at the central section of the butterfly embryo in (A) with higher magnification. Note, that most of the cells with only *Dll* expression are arranged anteriorly from the *wg* expression zone. The bulge on each segment are precursor structures of the larval prolegs. Bar: 300 μ m (A), 75 μ m (B).

influenced by the presence of Dll. Based on the information the picture gives, we cre-

ated the graph in fig. 2. Dpp represses *Dll* dorsally and EGFR does it ventrally (Estella et. al 2003). The circular expression of *esg* determines the Dll domain as well. Thus, *Dll* expression is restricted to the middle of the imaginal disc. As such, *Dll* expression may control a mechanism involved in patterning *wg* expression in the concerned parasegments. In the segments without discs *wg* stripes stretch until reaching the diffusible dpp (not labeled in any pictures here). Controversely, when the *wg* stripes approach the Dll domain, they broaden and strike. The detail in fig. 4 confirms that the *wg* stripe does not pass the primordium completely, but rather stops. Dll-secreting cells seem likely to be arranged dorsally from the stripe without any *wg* expression. Thus, the *wg* stripe pattern may stop earlier in primordia bearing segments as it stops in segments without primordia.

Limb primordia in the Buckeye butterfly *Junonia coenia*

Leg discs of *wg* and Dll double-stained embryos produced structures characteristic of the ventral thoracic body part. Like in *Drosophila*, *wg* stripes run from the ventral midline up to the Dll positional signal and get weaker. Contrary to our expectations the Dll circle is more extended and localized more anteriorly as it was observed in *Drosophila*. The stripes are rather short and constantly expressed in each segment. Dll appears in five prolegs, whereas *wg* is to find in the prolegs as well as in the following still coalesced-looking segments.

Discussion

What is the evolutionary background behind the similarly located and structured primordial discs?

The fact that the observed expression patterns in all imaginal discs are very similar to each other raises the possibility that their evolutionary origin is similar or even equal as well. The equal sizes confirm the idea

of three pairs of wings in some extinct insects. The distribution of wg^- , Dll^- and en -expressing cells is almost analog in every embryo of the entire dyed stock (further experimentation could investigate the gap of the en stripe in fig. 1C and the five Dll domains in fig. 5A. What causes the growth of wings and halteres that does not occur in T1? The answer seems to reside in the *Vestigial* (Vg) activity as it is mentioned in García-Bellido (2003). The *Vestigial* gene is selectively required for wing-cell proliferation and when it is expressed, wing tissue emerges. In combination with Boekhoff-Falk's results (2005) showing that cells which will adopt leg imaginal identity by coexpression of Dll and esg proteins, the differentiation seems logical.

Furthermore, in suitable stainings one could detect how the expression patterns of these morphogenous substances differ in the primordia of T2 and T3 in *Drosophila*. The halteres are degenerated ancient appendages which has been used to navigate during flight as a second wing pair, comparable to butterflies' hind wings.

Butterfly wing development

In some way butterflies preserved the complete mechanism to develop fully functional flight appendages. In comparison to *Drosophila*, morphogen transcription ways in T3 result in the growth of hind wings. However, the regulation mechanism during the stages which has been observed is identical. The patterns suggest a late developmental as well as an evolutionary divergency of the flight organs. Tissue transplantation could give further evidence. In different stages cells from a donor *Junonia* embryo expressing wing growth relevant proteins could be put into host *Drosophila* exoderm in T3. One injected cell can contribute to either an imaginal disc or to the larval hypoderm. The cell adapts its expression products to its fate and this determines the expression pattern. Monitoring the fate of the clonal progeny of the injected cells gives

information whether divergency occurred or not and if so, in which extend it occurred.

A fundamental improvement of histochemical stains is offered by the DAPI method. By a strongly binding DAPI stain, nuclei can be visualized well and it can relate background tissue to stained tissue structures which contributes to a clearer result and an easier analysis.

Acknowledgements

Special thanks go to the Graduate student Mike Perry for his help within this three weeks and to Nipam Patel who made that research opportunity possible in the first place.

I would also like to thank YaJen Cheng, Crystal Chaw, Christina Grande, Kristen Koenig, Danielle Liubicich, Melinda Modrell, Julia Serano, Meredith Protas, Annalisa VanHook, Jay Rehm, Paul Liu, Ron Parchem and Mario Vargas-Vila for their helpfulness and for a friendly working atmosphere in the Patel Lab.

At this point, I would finally like to thank the ISA 2007 administration for the long-standing attendance to accomplish the academy.

References

- [1] Boekhoff-Falk G and Bolinger RA (2005) Distal-less Functions in Subdividing the *Drosophila* Thoracic Limb Primordium. *Developmental Dynamics* 232:801-816
- [2] Estella C, Rieckhof G, Calleja M and Morata G (2003) The role of buttonhead and Sp1 in the development of the ventral imaginal discs of *Drosophila*. *Development* 130:5929-5941
- [3] García-Bellido A. and Baena-López LA (2003) Genetic requirements of vestigial in the regulation of *Drosophila* wing development. *Development* 130:197-208
- [4] Hayashi S, Fuse N and Hirose S (1996) Determination of wing cell fate by the escargot and snail genes in *Drosophila*. *Development* 122:1059-1067
- [5] Hayashi S and Goto S (1999) Proximal to distal cell communication in the *Drosophila* leg provides a basis for an intercalary mechanism of limb patterning. *Development* 126:3407-3413
- [6] Perrimon N, Noll E, McCall K and Brand A (1991) Generating Lineage-Specific Markers to Study *Drosophila* Development. *Developmental Genetics* 12:238-252

[7] Simcox AA, Cohen B and Cohen SM (1993) Allocation of the thoracic imaginal primordia in the *Drosophila* embryo. *Development* 117:597-608

[8] Williams JA, Bell JB and Carroll SB (1991) Control of *Drosophila* wing and haltere development by the nuclear vestigial gene product. *Genes and Development* 5:2481-2495

Wave Analysis and Seismic Moment Tensor of the Oakland event from 20th July 2007

Ralph Falk and Julia Flanjak
 Laboratory of Douglas S. Dreger
 Department of Earth and Planetary Science
 University of California at Berkeley

Introduction

On July 20, 2007 an earthquake of magnitude 4.2 occurred north of Oakland below the Hayward fault. Hayward fault is a geological fault parallel to the San Andreas fault expanding through the foothills of the eastern Bay Area. It is known for causing significantly destructive earthquakes and for being more active and thus more feared than the San Andreas fault.

The epicenter of the quake was located near Oakland, but the ground motion was very strong only at the region of Berkeley. This effect is being caused by special ground structures.

This study examines the seismograms of the July 20 event at Berkeley (BRK) and all stations around, especially the ones north and south of it. Unfortunately the aftershocks could not be studied since the magnitude range was below the noise level.



Fig. 1. Map of Hayward Fault and the surrounding area

There are already several techniques available to look at earthquakes, to com-

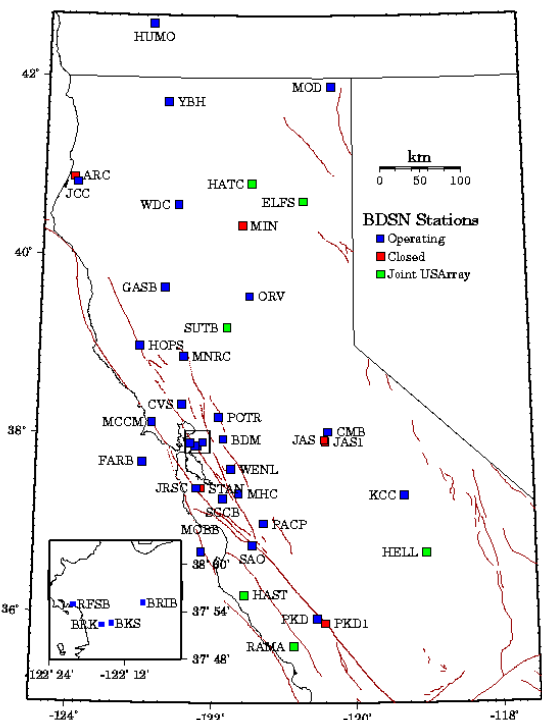


Fig. 2. Map of the Berkeley Digital Seismic Network (BDSN) with the most important stations.

pare them and to study the events in the underground. One of them is working with Seismic Analysis Code (SAC).

Each earth ground motion in Northern California is recorded by about 20 broadband, high dynamic range, digital stations that consist of collocated weak motion velocity, strong motion acceleration sensors and GPS. These instruments provide on-scale recording of earth ground motions. Thus, they record everything from background noise up to magnitude 8 earth-

quakes. All recorded data is being sent to the Northern California Earthquake Data Center (NCEDC) and provided in near-realtime (~ 28 s delay) to the worldwide research community.

Epicentral information on each earthquake on the northern or the southern hemisphere regardless of whether it was huge or small can be obtained on the NCEDC homepage. There it is possible to find exact information on the location of the earthquake, the magnitude, the time and depth. The corresponding data can be downloaded from the BDSN server for further study.

Methods

Using “Hummingbird Connectivity 10”, “Exceed” and the “SSH Secure Shell Client” we started collecting as much information as possible on the earthquake of 20th July 2007 near Oakland.

Instrument Response

First we looked at the main shock (location: 37.8040 N, 122.1930 W; depth 5.33; time: 2007/07/20 11:42 22.36 GMT). After downloading all files of this time and location from all stations of the BDSN server the instrument response had to be filtered out first. Therefore we took an ASCII file especially made for each station and component to remove the instrument response of each station. The response file contains a gain constant, zeros and poles that describe the response.

Here follows an exemplary general calculation for a simple pendulum seismometer. The output $U(t)$ of the seismometer is related to the input acceleration $\ddot{z}(t)$ by the indicator equation, where A is the gain, γ is the damping factor, and ω_0 is the resonance frequency of the instrument.

$$\ddot{U}(t) + 2\gamma\omega_0\dot{U}(t) + \omega_0^2U(t) = A\ddot{z}(t)$$

By taking the Fourier transform of the indicator equation a 2nd order polynomial equation is found relating the instrument

output acceleration spectrum $U(\omega)$ to the input acceleration spectrum $\ddot{z}(\omega)$.

$$[(i\omega)^2 + 2\gamma\omega_0(i\omega) + \omega_0^2] U(\omega) = A\ddot{z}(\omega)$$

Solving for $U(\omega)$ results in a response function that can be characterized by a gain constant A , the product of zeros (there are no zeros in this case), and the product of poles, which are equal to $-\gamma\omega_0 \pm i\omega_0\sqrt{1-\gamma^2}$.

$$U(\omega) = \frac{A\ddot{z}(\omega)}{(i\omega)^2 + 2\gamma\omega_0(i\omega) + \omega_0^2}$$

$$= \frac{A\ddot{z}(\omega) \prod(i\omega - \text{zeros}_j)}{\prod(i\omega - \text{poles}_j)} = I(\omega)\ddot{z}(\omega)$$

Ground acceleration may be found from

$$\ddot{z}(\omega) = \frac{U(\omega)}{I(\omega)}$$

SAC Filters

Filtering the data resulted in comparable files since the unique part of each station had been eliminated. The next important step was to have a look at each station to find out if there is any noise visible on the seismogram. This was done by hand, filtering out any small shakings not fitting to the seismograms of other stations. SAC has a variety of filters that may be used. We focused only on the Butterworth Filter (BWF). This filter offers three possibilities of filtering: high pass, low pass and band pass. High pass (hp) allows filtering below a certain frequency. Low pass (lp) filters above a certain frequency. The third filter is a mixture out of the first two, filtering above and below two certain frequencies. By increasing the number of poles in the filter, more irrelevant data could be filtered out.

Moment Tensor

For the moment tensor analysis it was important to find out how far away from each station the epicenter had been located. Using a macro we obtained the distance, the Green’s functions for this distance and all

depths at a distance between 5 and 39 km. With the already noise-filtered data and these Green's functions we could now compare our data with the theory.

The data obtained by cross-correlation were aligned by using zero-offset. The code gives the variance reduction (VR) for each station as well as collective variance reduction. By variations of the automatically calculated zero-offset value we aligned the data to the theory. We also strived for a VR of 100 for each station by testing different but similar distances between epicenter and station and different depths by using other Green's functions.

With the now aligned data we had to find out if there were any stations given by the code that did not fit. On the first glance the output of the code seems to be homogeneous. However, when excluding three stations out of six, we saw how the remaining stations work together. Sometimes in case of only three stations we observed the VR of one station decreasing enormously and found the waveform of the data did not fit to the waveform of the theory any more. In such cases the station had to be exchanged for another one.

Results

Rapidly we found out that after the main shock at 11:42 GMT, 03:42 local time, there had been four aftershocks. The first one 11:47 GMT, the second one at 19:53 GMT, the third one at 00:48 GMT (July 21, 2007) and the last one at 20:44 GMT. Only the third one was huge enough (Mw 2.74) to be over the background noise level.

With this information we collected the data from the BDSN Server. Filtering the data resulted in the waveforms shown in fig. 4

With the data of six recording stations we did a full moment tensor analysis.

To see if all stations were fitting the theory we tested each constellation of three out of six stations. By excluding three different

Terms and abbreviations

Strike: fault direction relative to North in degrees between 0 to 360, counted clockwise

Rake: the direction of the slip with respect to the strike, measured anticlockwise from the horizontal, upward being positive; between -180 and $+180$ degrees

Dip: the dipping angel of the fault, measured from the horizontal; between 0 and 90 degrees

Mo: Seismic Moment

Mw: Magnitude, how strong the shaking has been pointed out in a logarithmic scale

DC: Double Couple, how well the number of data is fitting to the theory (in %)

CLVD: "Non Double Couple", the part not fitting to the theory (in %)

Variance: Deviation of the model from the data. Lowest value indicates the best solution

Variance Reduction: largest value indicates the best solution

Beachball diagram: Projection on the fault plane and auxiliary plane onto a focal-sphere equatorial plane. Different fault types are visible. Dark regions indicate compressional P-wave motions.

```
catalog = NCSN
start_time = 2007/07/20,11:42:00
end_time = 2007/07/25,01:00:00
minimum_magnitude = 1.0
maximum_magnitude = 10
event_type = E
delta = 0 km to 0.9 km from (37.8040, -122.1930)
```

Date	Time	Lat	Lon	Depth	Mag	Magt	Nst	Gap	Clo	RMS	SRC	Event ID
2007/07/20	11:42:22.36	37.8040	-122.1930	5.33	4.20	Mw	146	16	3	0.16	NCSN	40199209
2007/07/20	11:47:32.12	37.8068	-122.1910	4.47	1.04	Md	25	60	3	0.07	NCSN	40199210
2007/07/20	19:54:15.66	37.8017	-122.1855	4.32	1.20	Md	19	97	2	0.08	NCSN	71050296
2007/07/21	00:48:55.32	37.8097	-122.1997	5.80	2.74	Md	103	28	4	0.17	NCSN	51184315
2007/07/21	20:44:26.57	37.7988	-122.1902	3.93	1.29	Md	22	58	2	0.08	NCSN	51184333

Fig. 3. NCEDC with search parameters and output: Date and time, latitude, longitude and depth and magnitude of the earthquake

stations each time we found out whether one station did not fit and replaced it by another one. With these six stations we did the same again to find out the best result and the lowest standard deviation.

We further tried to fit the *zcor* better. First the code works with *zcor* = 0 to perform a cross-correlation to find the optimal zero offset. Starting with this value we slightly varied it to see if the VR for the particular station is increasing. However, in most cases the best value was the one re-

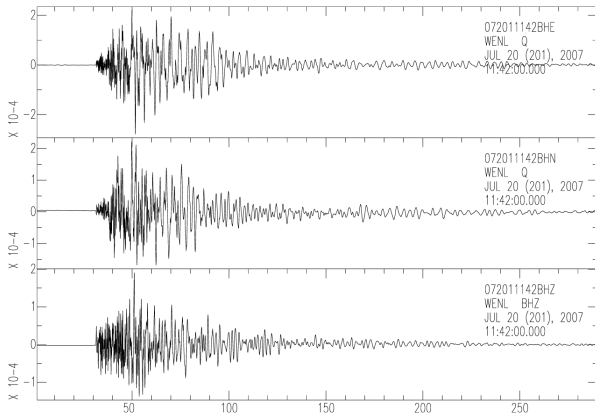


Fig. 4. Waveform of the Oakland event (E, N, Z). Three component waveforms of the Oakland event at 11:42 GMT. Five minute broadband velocity record by the WENL station, located southeast of the event.

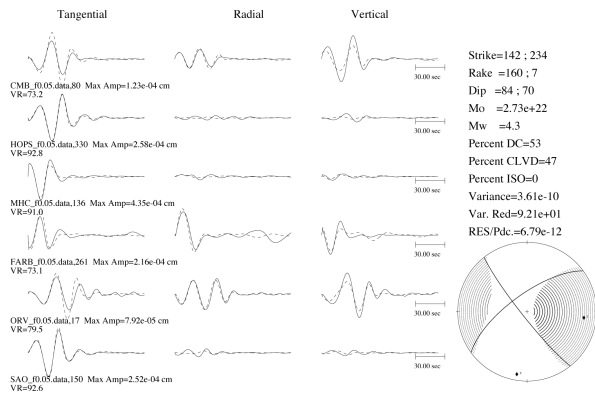


Fig. 5. Best result with three stations (CMB, FARB and ORV). The other three stations are shown but not taken into consideration. The best result means that it is the result most similar to the result of all six stations.

turned by the code.

In the end we obtained a result with a Var. Red. of 8.76 which is very good for an earthquake of this magnitude.

Discussion

On this earthquake we noticed some interesting facts. The first one is the real damage around Oakland and Berkeley. Judging from the epicenter and the magnitude one would expect an elliptic field of big damage. (Theoretically it should be a circle but due to the landscape it becomes an ellipse.) However, this was different on July 20. The

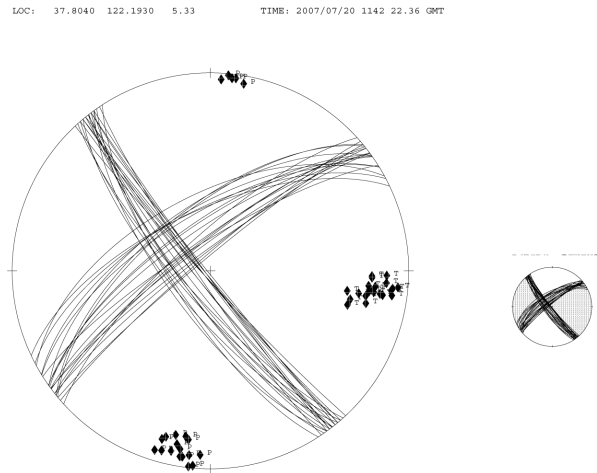


Fig. 6. Beachball diagrams for all combinations of three out of six stations. It can be clearly seen that there is no deviation bigger than $\pm 10^\circ$ from the average.

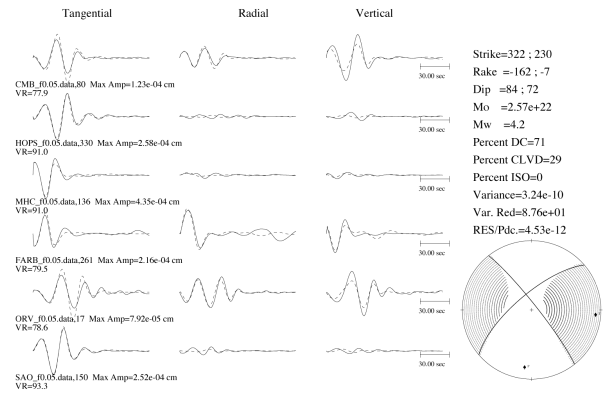


Fig. 7. Six station Moment Tensor. Each horizontal shows the entire data of one station (3 waveforms, name of the data file, max. amplitude, Variance Reduction (VR)). The vertical rows show the tree parts of each wave form separated. The right hand side shows additional information (Strike, Rake, Dip, Mo, Mw, DC, CLVD, Variance, Var. Red, RES/Pdc.). Inlay: beach ball diagram.

epicenter was located at Oakland but south of it there had been no damage. Instead damage north of Oakland, around Berkeley, had been much stronger as it is typical for this magnitude.

These results suggest only one possibility. The waveforms must result in a type of Doppler effect. This means that some earthquake waves (α) took the direct way from the epicenter to a certain point A. Another

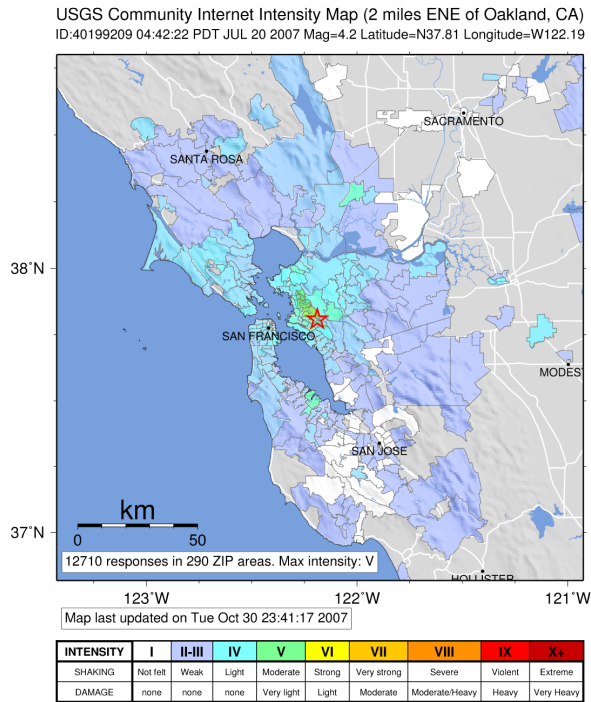


Fig. 8. People who noticed the earthquake

wave (β) took a longer way and is reflected from other ground structures. They arrive at the same time at A because β is much faster than α . This is possible due to the different structures in the soil. If now both arrive at the same time at A they superimpose. Overlay of two up or two down motions at the same point results in stronger shaking as in the northern part of the epicenter. Overlay of an up and a down motion as in the southern part results in weaker or no shaking.

This earthquake shows that not only the magnitude is important to find out how big the damage in populated areas could be. Disadvantageous ground structures can result in bigger damage than it would be expected from the magnitude.

Based on this data Douglas Dreger and his postdocs, especially Ahyi Kim, are working on a complete 3D-Model of the earth structure of the Bay Area. With this model it will be possible to test which areas are mainly in danger of Doppler waves.

With this realization it would be possible to give better risk analyses for all areas where the ground structure is well known. This would increase the possibility of predictions of the damage in certain areas. Thus, it should be possible to save lives with special steps before an earthquake, e. g. by making houses in affected areas more resistant.

Acknowledgements

I thank all members of the Berkeley Seismo Lab, especially Douglas Dreger who took me in to his research group and made this internship possible. He impressed me not only with his huge knowledge and his talent to pass it to others, but also with all his small, genius programs which helped me out in each seemingly hopeless situation. He is a great mentor who has always the right words to lead a young high school student to his biggest experience ever since.

I thank Ahyi Kim for her helping hand with all my small and big problems. Each time she talked about her personal research she gave me the feeling of being part in a really big thing that does not only produce data, but also will help to save lives.

Furthermore I thank the whole BSL staff which integrated me in their team and made me feel very welcome.

For the great BBQ I thank Peggy Hellweg. This out-of-lab event showed me an interesting view on the best seismologists and what life really is about in the Bay Area.

References

- [1] Mark Panning, Douglas Dreger, and Hrvoje Tkalčić (May 1, 2001) Near-source velocity structure and isotropic moment tensor: a case study of the Lang Valley Caldera. *Geophysical Research Letters*, Vol. 28, No. 9, pages 1815–1818
- [2] Douglas Dreger and Brian Savage (August 1999) Aftershock of the 1952 Kern County, California, Earthquake Sequence. *Bulletin of the Seismological Society of America*, 89, 4, pp. 1094–1108
- [3] M. L. Jost and R. B. Herrmann (April–June, 1989) A Student's Guide to and Review of Moment Tensors. *Seismological Research Letters*, Volume 60, No. 2

Effect of Small Forces on Adhesion of Micro-Spheres to a Surface Treated with Protein Adlayers and Reduction of Non-Specific Binding

Jan Freudenberg
Laboratory of Marcin Majda
Department of Chemistry
University of California at Berkeley

Abstract

The effect of small forces on the adhesion of micro-spheres to a surface treated with protein adlayers was examined. This work was part of a large investigation testing properties of a protein micro-sensor prototype. In the past problems concerning adhesion of the micro-spheres to the sensor surface occurred which could be related to non-specific binding.

The goal was to reduce non-specific binding by adding a further treatment step to the construction of the protein adlayers on the sensor. Octylamine was used in an attempt to prevent the aldehyde-groups of the surface from reacting with Avidin.

To observe the micro-spheres under the influence of different forces, an optical microscope and a massively parallel magnetic tweezers apparatus were used. The number of micro-beads was estimated by counting them on photographs. These were taken after having reached an equilibrium of all forces and compared to runs without the extra treatment.

The results, however, showed that the treatment with octylamine was not effective in preventing non-specific binding, the number of beads left on the sensor surface could not be reduced by this additional step.

Introduction

Sensors nowadays play a very important role, not only in daily life (e. g. a thermometer) but also in science. They are used to detect and to analyze, to qualify and quantify various substances, mixtures, molecules etc.

In Professor Majda's group, Christopher F. Monson is trying to develop a protein micro-sensor. It should be very simple, require little training, be easy to interpret and to maintain, perhaps even be portable and/or reagentless and nevertheless provide quantitative and highly sensitive data in very short time – real time, if possible. The aim is to detect whether a certain strand of DNA or antigen is present in a solution with the help of this biosensor. In case of DNA it breaks up an already existing tether consisting of two single DNA strands and then replaces one of the strands by the strand in the sample, which has a higher affinity for the remaining strand. This reaction takes place in a tiny space so that the confinement effect assists the exchange of strands and traps bound analyte molecules. Its integrative and competitive nature as well as the transferability of the basic mechanism from DNA to proteins are major advantages for this kind of sensor.

The first step towards the creation of this protein micro-sensor is to conduct force experiments. The experimental set-up con-

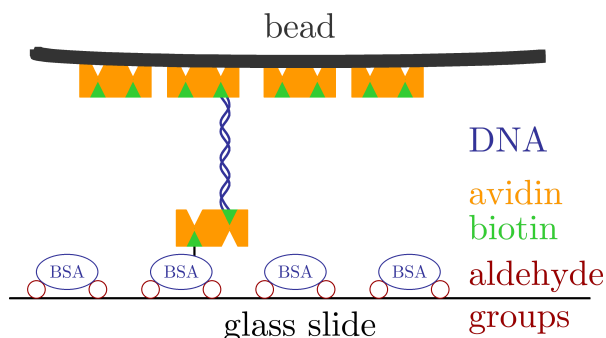


Fig. 1. Outline of the sensor

sists of a well, which is neither treated nor marked. It is placed onto a treated and marked surface, in this case a glass slide. Inside, the well is filled with an aqueous solution and magnetic micro-spheres, which are bound by tethers of DNA to the treated slide. The device is then turned over and magnets are placed under it in various distances. That way, at different forces, different amounts of micro-spheres will be released. However, at 950 pN, which is a force where all micro-beads should be released, some of them still remain at the surface of the treated slide. One possibility could be that these are cases of non-specific binding, in which aldehyde groups of the glass slide react with avidin and form a strong covalent bond.

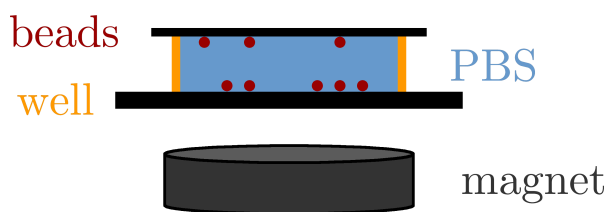


Fig. 2. Outline of the experimental setup

In this study it was tried to reduce these assumed cases of non-specific binding by adding another treatment step to the preparation of the protein adlayers and thus to find out, whether the possible reaction between the aldehyde groups and avidin is responsible for this phenomenon.

Materials and Methods

The series of experiments were performed using an upright optical microscope with a

built-in camera and a photo editor as well as a parallel magnetic tweezers apparatus.

The built-together device observed under the microscope can be described as follows (see fig. 1): BSA (bovine serum albumin) and BBSA (biotinylated BSA) had been bound via aldehyde-groups onto the glass slide. The biotin itself is bound to avidin on one side. On the other side of the avidin molecule biotinylated single-stranded DNA is bound and hybridizes with another DNA strand, which is bound to another molecule of avidin stuck to one of the magnetic microspheres. This way, the tethers are formed.

To prevent cases of non-specific binding between the aldehyde groups and avidin an extra treatment step using octylamine was introduced. Octylamine should react with the left-over aldehyde groups so that they are no longer available for other non-specific reactions.

In order to assemble the device and to prepare the glass slides with the microspheres the following steps were undertaken: The surface, which had been treated with 1,3-diaminopropyltriethoxysilane and glutaraldehyde in order to fix aldehyde groups on it, was cut into several smaller pieces roughly the same size (ca. 1.5 cm × 2 cm). Tiny rectangles were carved into each slide marking the observation area for the microscope. The slides were rinsed with water to free them of small fragments of glass that could be left on them and then dried with air. On top of the rectangles an aqueous solution of 33 µl of BSA and BBSA (100:1) was applied. The slides were then stored over night in an hour glass covered with wet filter paper at 4° C.

One half of the glass slide was then rinsed again, dried and then treated with an aqueous solution of octylamine and stored at 4° C again. The other set of slides were left as they were. After 1.5 h, all slides were rinsed again, dried, then treated with 5.8 µl of avidin-solution (940 µg/ml BSA, 75 µg/ml avidin, 0.1 M NaHCO₃ and 0.2 M NaCl) which was set up on the surface so it cov-

ered the rectangles carved into the slides, and kept at 4° C again.

Two hours later, after rinsing and drying them, the slides were treated with 5.8 μ l of an aqueous solution of single-stranded, biotinylated DNA and then stored again at 4° C.

After another two hours, a well consisting of a plastic ring with an approximate diameter of 6 mm glued to a glass slide, was filled with phosphate buffered saline (0.23 M NaCl, 0.1 M phosphate). Small magnetic micro-spheres which consist of a polymer mix with iron oxide particles suspended in it and which are about 5.91 μ m in diameter had been treated with avidin and biotinylated DNA. 10 μ l of them were taken out of their solution, the micro-spheres were fixated with a magnet in the pipet so that the aqueous solution could be drained away. The micro-spheres were then put into the phosphate buffered saline in the well under which a second magnet had been placed. That way it could be made sure that the micro-spheres all stay in the well while withdrawing the pipet. The treated small glass slides were then placed onto the wells, the marked, treated surface facing the liquid inside the well. A third glass slide was then placed on top of the small treated slide. The whole device was turned upside-down and then secured with rubber bands. That way the single-stranded DNA can hybridize and form tethers. No force is exerted on these because the micro-spheres rest on the surface of the small glass slide.

The device was then placed onto the observation dish of the microscope this way, and a corner of the scratched rectangle was thoroughly photographed. Then the device was turned upside-down so that gravity can strain the tethers with a force of about 0.1 pN. Before photographing the same corner over and over again, the device is put to rest for 10 min so that equilibrium is established.

Five magnets were placed under the device in 5 mm distance to increase the force

to 950 pN. Again, after 10 min, the corner was photographed several times.

With the help of imaging software the single images were assembled to create a full picture of the corner. Then, the images at different forces were overlayed and another layer with a marked area was projected onto these. The visible micro-spheres in this area were then counted by hand.

Results

In the following, three different runs of this procedure were conducted: two with the untreated slides and another one with the octylamine-treated one. In each run three sets of photographs were taken, each set at a different force starting with no force at all, then gravity, achieved (about 0.1 pN) by turning the device around, and at last 950 pN by using five magnets at a distance of 5 mm.

To make sure equilibrium is reached, the device was put to rest for 10 min at every step before photographs were taken. One set of photos consists of about 20 images of one corner of the rectangle. These images were then digitally overlayed, the three sets of one run arranged so that they were exactly on top of each other and an area of exactly the same size was then drawn onto them for each of the sets. The micro-spheres visible as black, round dots were then marked in the photographs and counted by hand.

In the first untreated run which was conducted as a control, when no force was applied to the tethers and the micro-spheres, 798 micro-spheres (100 %) were found in the marked area. After turning the device around and putting it to rest for 10 minutes, 540 micro-spheres (67.67 %) were left on the slide, meaning 258 tethers were broken by gravity. After applying a force of 950 pN to the microspheres, 160 spheres (20.05 % or 29.63 % in relation to the 2nd image) could still be found in equilibrium on the first slide.

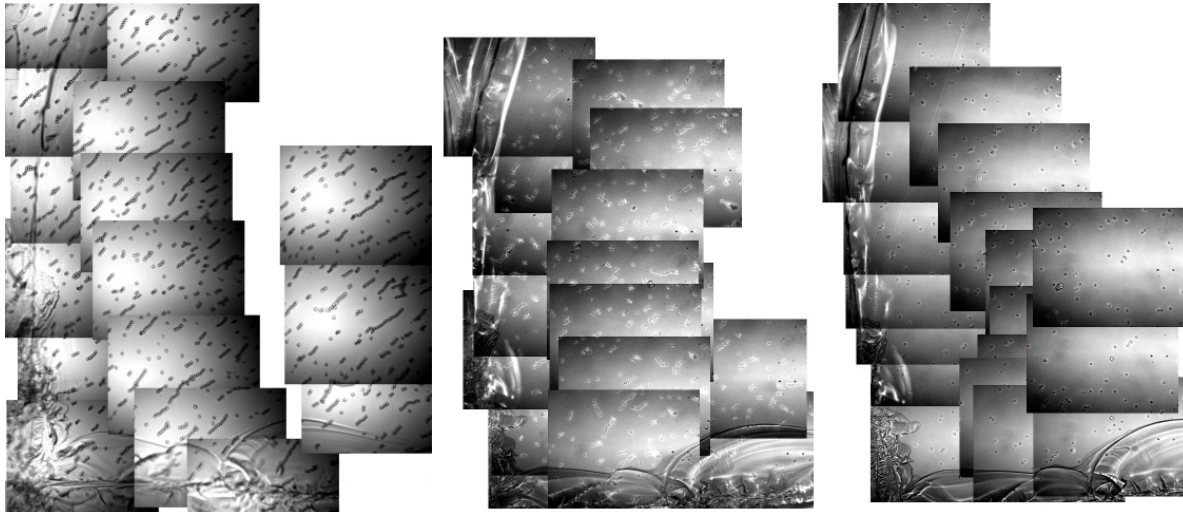


Fig. 3. Run 1, images at no force, gravity and 950 pN (left to right)

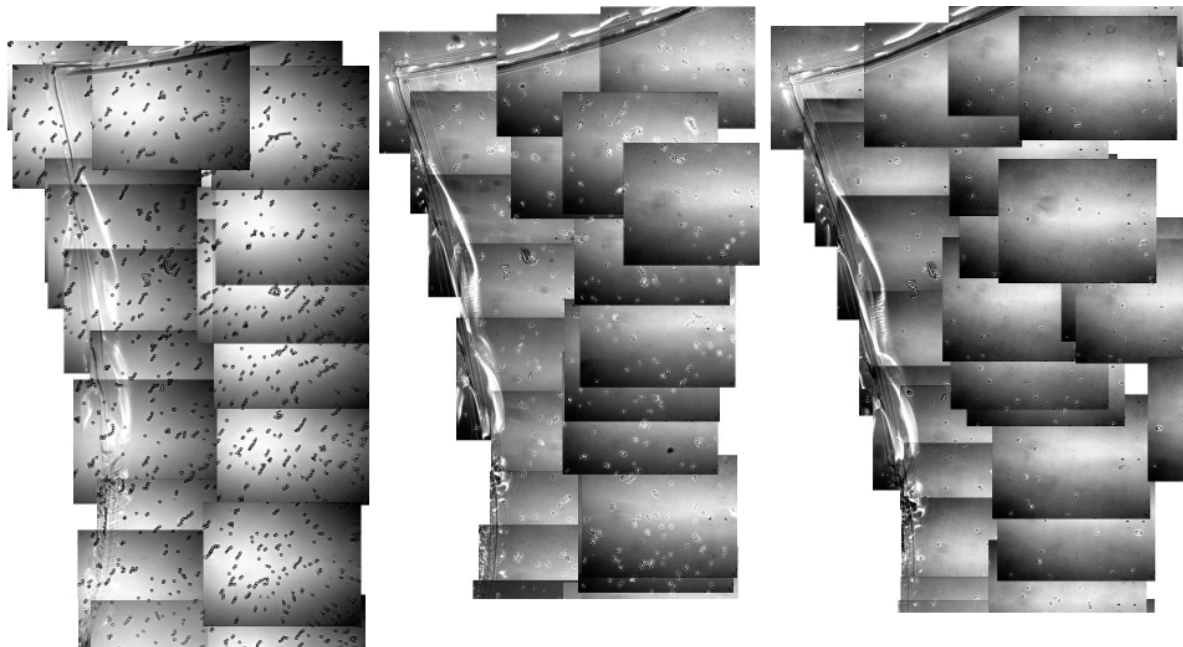


Fig. 4. Run 2, images at no force, gravity and 950 pN (left to right)

In the second untreated run at the beginning there were 660 micro-spheres (100 %) to be found on the marked surface. After applying gravity to them 332 (50.3 %) were still visible so 328 micro-spheres did go off. In the next image 96 micro-spheres (14.55 % or 28.98 % in relation to the 2nd image) were to be seen, making a difference of 236 micro-spheres.

In the third run, which was the one with

the treated device, only 205 micro-spheres (100 %) were visible in the marked area. After applying gravity 159 (77.56 %) were still left, which makes a difference of 46 micro-spheres. In the third image, after having applied 950 pN and waited for the equilibrium, 68 micro-spheres (33.17 % or 42.77 % in relation to the 2nd image) were left on the surface of the treated glass slide, so 91 went off in the meantime.

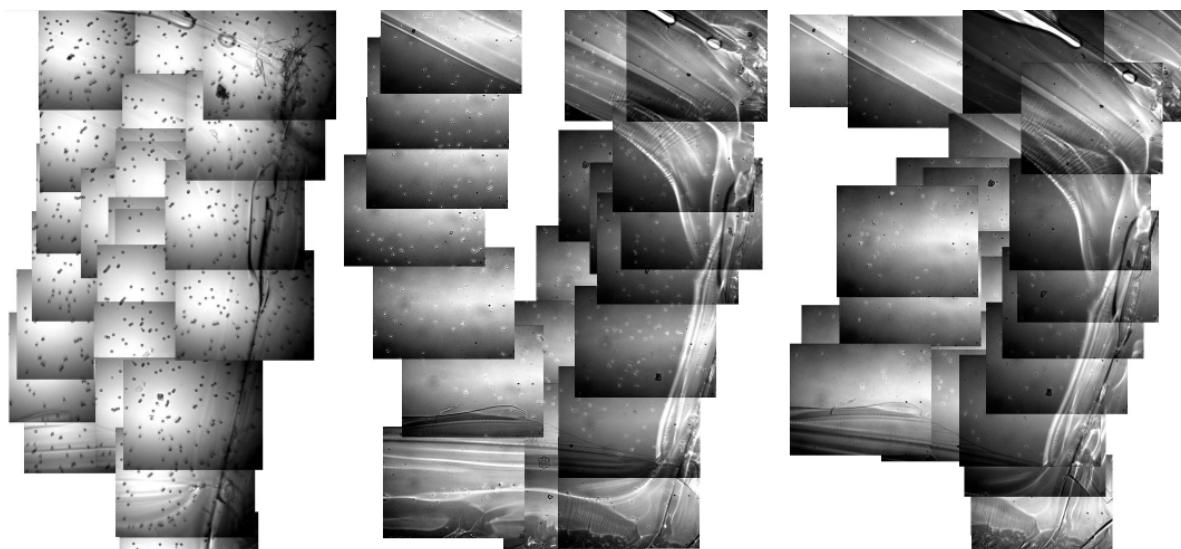


Fig. 5. Run 3, images at no force, gravity and 950 pN (left to right)

Discussion

As can be seen from table 1 and figure 6 a slight increase instead of a decrease in the amount of micro-spheres left on the glass slide can be observed. This was exactly the opposite of what we expected. In comparison to the first and second run the percentage of micro-spheres rose from 20.05 % (relating to total amount) or 29.63 % (relating to influence of gravity) in the first run respectively 14.55 % (relating to total amount) or 28.98 % (relating to influence of gravity) in the second to 33.17 % (relating to total amount) or 42.77 % (relating to influence of gravity). That means, that the total number of micro-spheres in percentages has increased by about 10 % to 15 %. If the second image is related to the third and thus the influence of gravity and 950 pN between the amine-treated and the blank slide are compared it seems as if less microspheres went off on the amine-treated slide (difference of about 14 %). But what exactly does that mean?

One possible answer is that the treatment with amine was insufficient and not all aldehyde groups reacted with the amine-group of octylamine in a nucleophilic addition. Thus, not enough bonds have been estab-

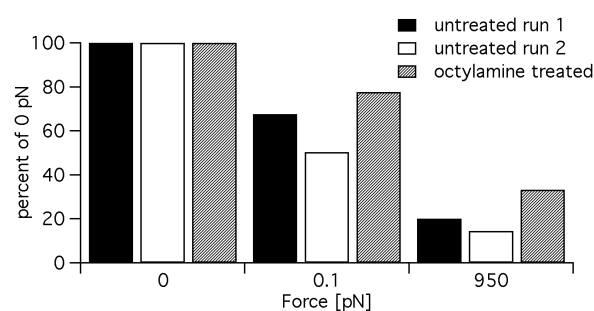


Fig. 6. Number of Beads at different forces

Table 1. Number of Beads at different forces

Run	F [pN]	# Beads	% I	% II
1	0	798	100	–
1	0.1	540	67.67	100
1	950	160	20.05	29.63
2	0	660	100	–
2	0.1	332	50.3	100
2	950	96	14.55	28.92
3	0	205	100	–
3	0.1	159	77.56	100
3	950	68	33.17	42.77

lished in order to prevent the aldehyde groups from reacting non-specifically with avidin. This could be improved by repeating the treatment steps with the aqueous solution of octylamine.

Another possibility could be that there has been a change in covalent bonding and a much stronger covalent bonding might have been established, for the micro-spheres were much more reluctant to come off than in the other runs. This might explain the increased amount of micro-spheres still connected via tethers to the glass slide.

A bubble, which had been trapped in the device in the third run, did not greatly affect the resolution of the microscope for not all of the rectangle had been covered by it. So it was possible to photograph a corner that was unoccupied. However, the effect of the bubble would merely have been that it would have knocked more micro-spheres off the surface. Apparently, this had not been the case.

To conclude, the results of these experiments suggest that the treatment with octy-

lamine is not effective in preventing non-specific binding. A different approach has to be chosen in order to reduce adhesion of the beads to the surface of the sensor.

Acknowledgements

I want to thank Professor Majda for generously hosting me in his laboratory and for patiently answering all my questions. Furthermore I'd like to thank Chris Monson, who let me do this small part of his vast project as well as Eric Carlson, who introduced me to the lab and let me work on his project for the first two weeks. Special thanks to Christoph Fischer and Christian Stoy, who, as our mentors, accompanied and supervised us in California.

References

- [1] Monson, C.F.; Majda, M. Ion Diffusion in Channels Containing Random Arrays of Micro-Spheres: An Electrochemical Time-of-Flight Method. *Anal. Chem.*, submitted July 2007

Synthesis and characterization of metal-oxo and metal-cyanide cluster magnets

Jan Gotthardt

Laboratory of Jeffrey R. Long

Department of Chemistry, University of California at Berkeley

Introduction

Molecules possessing a high-spin ground state S and axial anisotropy caused by a negative zero-field splitting D are generally referred to as single-molecule magnets. These single-molecule magnets exhibit magnetic bistability, i.e. there are two stable magnetic ground states. Due to the existence of an energy barrier $U = S^2|D|$ for integer values of S ($U = (S^2 - \frac{1}{4})|D|$ for half-integer values of S) for converting “spin up” to “spin down” in the ground state, the hope of one day being able to store one bit of information in a single molecule as the direction of magnetisation was raised [1].

Research is now directed towards the development of new single-molecule magnets possessing a higher spin reversal barrier U which would be a benefit to the temperature and duration of potential data storage.

$[\text{Mn}_{12}\text{O}_{12}(\text{CH}_3\text{CO}_2)_{16}(\text{H}_2\text{O})_4]$ (fig. 1) was the first single-molecule magnet discovered, with $S = 10$ and $D = -0.5 \text{ cm}^{-1}$ and therefore a spin reversal barrier of 50 cm^{-1} , leading to magnetic blocking at temperatures below 4 K. Since then much of this research was directed towards transition metal-oxo clusters. The problem with oxygen as a bridging ligand is, that it can bridge anywhere from two to six metal centers, with a wide range of M-O-M angles and therefore controlling the structure of new metal clusters is difficult. The advantage of cyanide as a bridging ligand is its preference for just binding two metal centers and it can be expected that products of solution assembly reactions will contain linear M'-CN-

M moieties [1]. The experimentally measured anisotropy is governed by the single-ion anisotropy of each consistent metal ion and the overall distribution of electrons in the molecule, which is influenced by the molecule's geometry. Controlling the structure of new metal clusters is important for predicting and controlling magnetic properties. As the anisotropy in a single molecule magnet is much more difficult to predict or control than the spin S , current research is interested in understanding anisotropy arising from the zero-field splitting [2].

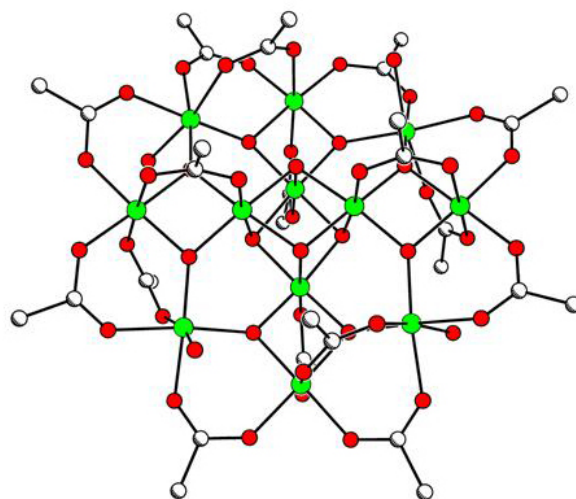


Fig. 1. $[\text{Mn}_{12}\text{O}_{12}(\text{CH}_3\text{CO}_2)_{16}(\text{H}_2\text{O})_4]$ – Mn (green), O (red), C (white); H atoms are omitted for clarity

Materials and Methods

Synthesis of $[\text{Mn}_{12}\text{O}_{12}(\text{CH}_3\text{CO}_2)_{16}(\text{H}_2\text{O})_4] \cdot \text{CH}_3\text{CO}_2\text{H} \cdot 4\text{H}_2\text{O}$ (1)

4.03 g (25.3 mmol) of potassium permanganate (KMnO_4) were weighed in a glass jar, after being crushed with a mortar and a pestle. 40 ml of a 60% acetic acid/water solution were added along with a stir bar and the deep purple solution was allowed to stir for 5 h.

16.05 g (65.5 mmol) manganese(II)acetate tetrahydrate ($\text{Mn}(\text{OAc})_2 \cdot 4\text{H}_2\text{O}$) were weighed in a 400 ml beaker and 100 ml of the 60% acetic acid/water solution and a stir bar were added. The pink slurry was stirred until all of the Manganese(II)acetate tetrahydrate had been dissolved (30 min).

Then the viscous potassium permanganate solution was poured into a 500 ml addition funnel and 4 times 10 ml of the 60% acetic acid water solution were used to transfer as much of the solution as possible. The potassium permanganate solution was added drop wise to the manganese(II)acetate tetrahydrate solution. The stir bar was removed and the beaker with the resulting red-brown solution was covered with Parafilm. With a spatula a hole was punched into the top and the beaker was placed on a shelf outside the fume hood to lie undisturbed for 72 h. After three days the solution was filtered through a Büchner funnel with a filter paper under vacuum. The black needle-shaped crystals resting on the filter paper were washed with acetone to get rid of the starting materials, the solvent and the unwanted manganese oxides.

Synthesis of $[\text{Bu}_4\text{N}][\text{TpFe}(\text{CN})_3]$ (block for new cluster-based magnets) (2)

0.811 g of FeCl_3 (5 mmol) were weighed into a three-neck flask under a nitrogen atmosphere and a stir bar was added. 125 ml methanol were filled into a round bottom flask, the flask was closed with a septum and the methanol was degassed with nitro-

gen. Then the methanol was cannulated into the three-neck flask. The black FeCl_3 was stirred and solved and resulted in an orange solution. 1.261 g of KTp (5 mmol) (Tp = Tris(1-pyrazolyl)borate) and 1.628 g of KCN (25 mmol) were weighed into a round bottom flask and solved in 125 ml water. The round bottom flask was closed with a rubber plug and the solution was degassed with nitrogen. The KTp/KCN solution was cannulated into the FeCl_3 solution which turned red. The three-neck flask was put in an oil bath, a reflux condenser was put on top of the three-neck flask, the solution was heated up to 70° C and was stirred over night. (reaction 1)

Then the dark red solution was cooled down to room temperature and filtered through a glass frit. The orange solids resting in the frit are unwanted by-products. The filtered red solution was poured into a round bottom flask which was put into an oil bath. A water cooled condenser was put on top of the round bottom flask and a liquid nitrogen cooled flask was put on the other end of the condenser to collect the solvents. Then the solution was distilled under vacuum. The orange solid ($\text{K}[\text{TpFe}(\text{CN})_3]$) was scratched out of the round bottom flask and weighed ($m = 2.645$ g). 0.3 g of $\text{K}[\text{TpFe}(\text{CN})_3]$ and 1.08 g of $[\text{Bu}_4\text{N}]\text{Cl}$ were solved in 20 ml water and the solution was stirred over night. Then the solution was filtered through a glass frit under vacuum and the orange solid was kept to weigh it ($m([\text{Bu}_4\text{N}][\text{TpFe}(\text{CN})_3]) = 0.05$ g). (reaction 2)

Synthesis of $[\text{Tp}_2(\text{Me}_3\text{tacn})_3\text{Cu}_3\text{Fe}_2(\text{CN})_6](\text{ClO}_4)_4$ (3) (fig. 2)

0.05 g $[\text{Bu}_4\text{N}][\text{TpFe}(\text{CN})_3]$ (0.0848 mmol) were dissolved in 3 ml acetonitrile and 1 ml ethanol in a small glass vial. A stir bar was added and the solution was stirred until completely dissolved. 0.04 g of $[(\text{Me}_3\text{tacn})\text{Cu}(\text{H}_2\text{O})_2](\text{ClO}_4)_2$ (0.0848 mmol; $\text{Me}_3\text{tacn} = \text{N},\text{N}',\text{N}''$ -trimethyl-1,4,7-triazacyclononane) were

dissolved in 2 ml ethanol and 1 ml acetonitrile in a glass vial and stirred. Then the $[(\text{Me}_3\text{tacn})\text{Cu}(\text{H}_2\text{O})_2](\text{ClO}_4)_2$ solution (blue) was slowly pipetted into the $[\text{Bu}_4\text{N}][\text{TpFe}(\text{CN})_3]$ solution (orange). (reaction 3)

The stir bar was removed and the vial with the resulting brown solution was covered with aluminium foil, which was perforated with a needle. Then the vial was put into a closed glass jar filled with 14 ml ethyl ether. The ethyl ether vapor would diffuse into the vial and due to the fact that $[\text{Tp}_2(\text{Me}_3\text{tacn})_3\text{Cu}_3\text{Fe}_2(\text{CN})_6](\text{ClO}_4)_4$ is insoluble in ethyl ether it would slowly crash out as crystals. This method is called vapor diffusion. After the crystals had grown the solution was filtered using a Büchner funnel and filter paper. The remaining dark brown blockshaped crystals were washed with THF to get rid of the solvents and starting materials.

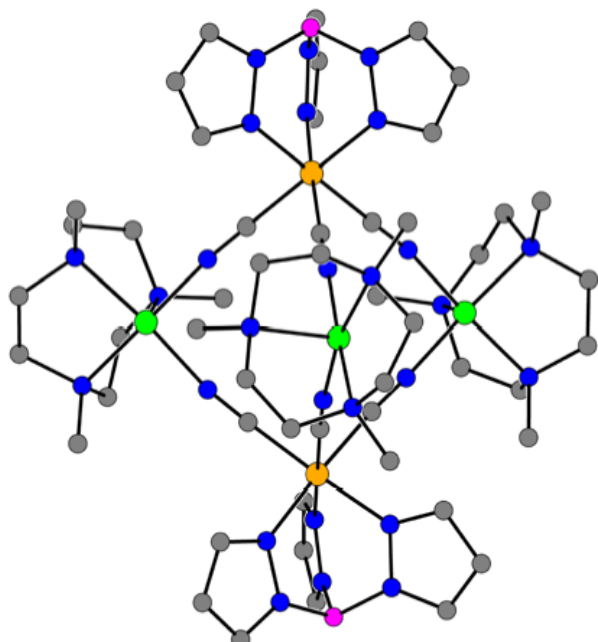


Fig. 2. Structure of the trigonal bipyramidal cluster $[\text{Tp}_2(\text{Me}_3\text{tacn})_3\text{Cu}_3\text{Fe}_2(\text{CN})_6]^{4+}$ – Fe (orange), Cu (green), B (magenta), C (gray), N (blue); H atoms are omitted for clarity

Synthesis of $[\text{Tp}_2(\text{cyclen})_3\text{Ni}_3\text{Fe}_2(\text{CN})_6](\text{BF}_4)_4$ (4) (fig. 3)

0.05 g $[\text{Bu}_4\text{N}][\text{TpFe}(\text{CN})_3]$ (0.0848 mmol) (reaction 2 was started again with the same

quantities to get 0.05 g of product) were dissolved in 3 ml acetonitrile and 1 ml ethanol in a small glass vial. A stir bar was added and the solution was stirred until completely dissolved. 0.033 g $[(\text{cyclen})\text{Ni}](\text{BF}_4)_2$ (cyclen = 1,4,7,10-tetraazacyclododecane) were dissolved in 2 ml of ethanol and 1 ml acetonitrile in a glass vial and a stir bar was added. Then the purple $[(\text{cyclen})\text{Ni}](\text{BF}_4)_2$ solution was slowly pipetted into the orange $[\text{Bu}_4\text{N}][\text{TpFe}(\text{CN})_3]$ solution which was stirred. The stir bar was removed and the vial with the resulting red/brown solution was covered with a piece of perforated aluminium foil. Then a vapor diffusion with ethyl ether was started as in synthesis (3). When the red block-shaped crystals had grown they were filtered and washed as in synthesis (3).

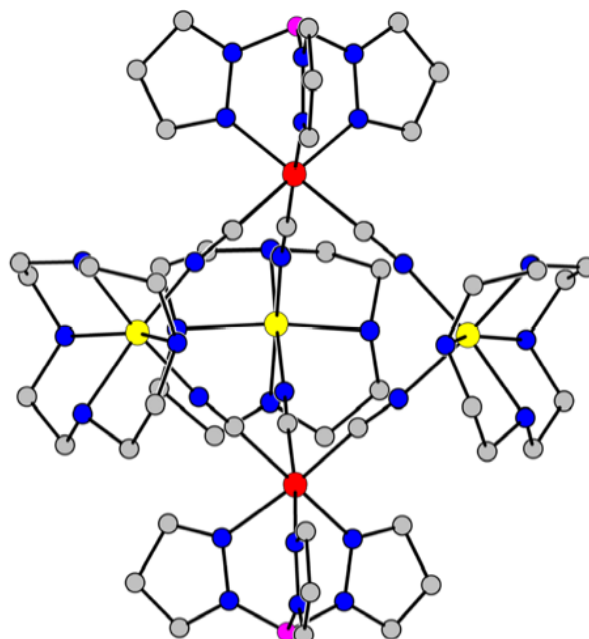


Fig. 3. Structure of the trigonal bipyramidal cluster $[\text{Tp}_2(\text{cyclen})_3\text{Ni}_3\text{Fe}_2(\text{CN})_6]^{4+}$ – Fe (red), Ni (yellow), B (magenta), C (gray), N (blue); H atoms are omitted for clarity

Synthesis of $[\text{Tp}_2(\text{acac})_6\text{Ni}_3\text{Fe}_2(\text{CN})_6](\text{H}_2\text{O})_4$ (5)

0.05 g $[\text{Bu}_4\text{N}][\text{TpFe}(\text{CN})_3]$ (0.0848 mmol) were dissolved in 3 ml acetonitrile and 1 ml ethanol in a small glass vial. A stir bar was added and the solution

was stirred until completely dissolved. 0.0671 g Ni(acac)₂(H₂O)₂ (0.127 mmol; acac = acetylacetonate, pentane-2,4-dione) were solved in 6 ml acetonitrile 2 ml ethanol in a glass vial. A stir bar was added and the solution was stirred until completely dissolved. Then the green Ni(acac)₂(H₂O)₂ solution was pipetted into the orange [Bu₄N][TpFe(CN)₃] solution and the resulting honey brown solution was stirred. To grow crystals a vapor diffusion as in synthesis (3) was started. Because no crystals would grow after 10 days the solution was distilled in a Schlenk flask under vacuum to get rid of the solvents. To get the wet brown solid of the Schlenk flask, 20 ml ethyl ether were added and the flask was put into the sonicator/ultrasonic bath. The resulting green brown slurry was filtered through a Büchner funnel with filter paper and the remaining yellow solid powder was investigated by IR and UV-Vis spectroscopy.

Results and Discussion

The black needle-shaped crystals of synthesis (1) were proved to be [Mn₁₂O₁₂(CH₃CO₂)₁₆(H₂O)₄] · 3 CH₃CO₂H · 4 H₂O by X-ray powder diffraction and IR spectroscopy. The crystals were sent to the Crommie Group in the Department of Physics at Berkeley University. There, they want to find out more about the electron density in the molecule and about its magnetic structure by using scanning tunnelling microscopy.

UV-Vis spectra were taken of the [Tp₂(Me₃tacn)₃Cu₃Fe₂(CN)₆](ClO₄)₄ and [Tp₂(cyclen)₃Ni₃Fe₂(CN)₆](BF₄)₄ complex as well as of the starting materials [Bu₄N][TpFe(CN)₃], [(Me₃tacn)Cu(H₂O)₂](ClO₄)₂ and [(cyclen)Ni](BF₄)₂. With the help of the UV-Vis spectra ϵ , the molar absorptivity or the molar extinction coefficient which is specific for every compound was calculated for each of the absorbance peaks, using Lambert-Beer's law.

The UV-Vis spectra and the calculation

data were sent to Prof. Mihail Atanasov, currently a co-worker in the Comba Group in the Department of Chemistry at Heidelberg University. With the help of the UV-Vis data they want to calculate the magnetic exchange coupling in cyanide bridges. Later they want to compare their theoretically calculated results with the measurements the Long Group has already done with those clusters. The variables J (exchange coupling) and D (zero-field splitting) are of a special interest for them.

The [Tp₂(Me₃tacn)₃Cu₃Fe₂(CN)₆](ClO₄)₄ and [Tp₂(cyclen)₃Ni₃Fe₂(CN)₆](BF₄)₄ complex crystals were sent to Dr. Joris van Slageren an employee in the Physics Department at Stuttgart University. They want to do multi frequency epr (electron paramagnetic resonance) with the clusters to find out more about the electron spin, change of the spin and the anisotropy.

IR and UV-Vis spectra were taken of the yellow solid powder of synthesis (5) and compared to the spectra of the starting materials. It is not quite clear if the yellow solid is just a mixture of the starting materials or a new cluster. But the peak at 2113.54 nm in the IR spectra of [Bu₄N][TpFe(CN)₃] which marks the cyanide bridges is split up into four different peaks in the IR spectra of the yellow solid (fig. 4). This peak splitting might implicate that a new cluster has been built.

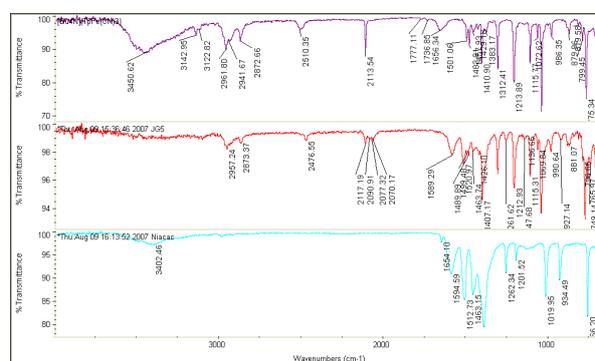


Fig. 4. IR spectra of starting material [Bu₄N][TpFe(CN)₃] (purple graph), yellow solid out of synthesis 5 (red graph), starting material Ni(acac)₂(H₂O)₂ (blue graph)

Acknowledgements

I would like to thank Prof. Jeffrey R. Long for giving me the opportunity to stay in his lab in the first place. I enjoyed these three weeks incredibly. I would like to thank Kathleen M. Bean for helping me with my visa and all the administration stuff. Special thanks to Bart M. Bartlett who supervised me and who not only taught me practical laboratory skills but also supported me with lots of theoretical information. Thanks to Aude Demessence who helped me with the X-ray powder diffractometer, thanks to Danna Freedman, T. David Harris, Navid Soheilnia who outlined their current research to me. Thanks to "Wesker" KinWai Lei who shared his desk with me. And thanks to all of them and everybody else in this great lab for accepting and integrating me in their group and making me feel welcome. I had an absolutely great time. Thanks to my family for supporting me not only financially. Thanks to Christoph Busche, who helped me prepare for this internship.

Personal remarks

I really enjoyed working in the lab of Prof. Jeffrey R. Long. As you can see in my results and discussion part my main work was to synthesise known and new single molecule magnets and to approve the structure of the synthesised crystals by different spectroscopy methods. Due to the short time I spent in this lab I was not able to do any magnetic measurements or any further characterization of the synthesised clusters.

References

- [1] L.M.C. Beltran, J.R. Long, *Acc. Chem. Res.* 2005, 38, 325-334
- [2] B. M. Bartlett, T. D. Harris, M. W. Degroot, J. R. Long, *Z. Anorg. Allg. Chem.* 2007, 633 (13-14), 2380-2385
- [3] C.-F. Wang, J.-L. Zuo, B. M. Bartlett, Y. Song, J.R. Long, X.-Z. You, *J. Am. Chem. Soc.* 2006, 128, 7162-7163

ASE1 is a microtubule stabilizing MAP

Maximilian Heeg

Laboratory of David Drubin

Department of Molecular and Cell Biology, University of California at Berkeley

Abstract

Microtubule stability is essential for the proper function of mitosis. Several microtubule-associated proteins (MAP) involved in microtubule polymerization and depolymerization have been identified, thereunder Ase1. However, the function of these proteins is widely unknown. We created modifications in Ase1 in *Saccharomyces cerevisiae* in order to localize it in different stages during mitosis. We found out, that Ase1 occurs mainly in mid-anaphase and that there is nearly no presence of Ase1 in the beginning and in the end of mitosis. In addition Ase1 is attached to microtubule structures.

Introduction

In eucaryotic mitosis, duplicated sister chromatids are distributed equally between daughter cells. The distributions of sister chromosomes to opposite poles occurs in anaphase, so that each daughter cell receives a complete chromosome set. Anaphase is divided into two stages, anaphase A or early anaphase, where the chromatids abruptly separate and move towards the spindle poles, and anaphase B or late anaphase, where the spindle is extended and the poles are segregated between daughter cells.

During mitosis there are three classes of microtubules: polar microtubules that extend from the centrosome and overlap with polar microtubules from the opposite centrosome, kinetochore microtubules that attach to condensed chromosomes at their centromeres and thus link the chromosomes

to the centrosomes and astral microtubules that extend to the cell periphery. The changes in spindle structure are regulated primarily by proteins that bind along microtubules. These microtubule-associated proteins (MAP) regulate the stability of microtubules including both stabilizing and destabilizing and mediate interactions with other proteins.

Experiments showed that the force required for anaphase pole segregation is generated from the central spindle (pushing mechanism) and by kinesin proteins attached to polar microtubules. In anaphase polar microtubules increase in length whereas the region of overlap between the polar microtubules decreases. The resulting force drives the segregation of the sister centrosomes.

Ase1 is a member of a conserved family of midzone-specific MAPs. A loss of Ase1 results in a specific defect: premature spindle disassembly in mid-anaphase. The degradation of Ase1 thus appears to be required for the normal timing of spindle disassembly.

Materials and Methods

Polymerase Chain Reaction

To amplify DNA a PCR with the following components was used: 35.5 μ l H₂O, 10 μ l 5x HF buffer, 1 μ l 40 mM dNTPs (10 mM each), 1.25 μ l 20 μ M primer 1, 1.25 μ l 20 μ M primer 2, 0.5 μ l DNA, 0.5 μ l PhusionTM polymerase. Steps for the PCR: 1. 98° C for 00:30, 2. 98° C for 00:07, 3. 57° C for 00:20, 4. 72° C for 02:00, repeat steps 2-5 29 times, 6. 72° C for 10:00, 7. 12° C forever. The primers used are shown in table 1 (1 & 2),

Table 1. The primers used for PCR

No.	Name	Sequence (5'-3')
1	Ase1 C-T tagging - forward	GAA AAA ATG AGC AAG TTT CGA AAT TGA ATG GAT TCT CCT TTA CAG ATA TTC GGA TCC CCG GGT TAA TTA A
2	Ase1 C-T tagging - reverse	AGA GAC AAT GTA GCG AAG GCT AGA AAG TGA TGT GAA AAA AAA AAC CGA ATT CGA GCT CGT TAA AAC
3	Ase1 insert/tag identification - forward	GCA CAG CAT ATA TAA ACT TTC CAT GTC GCC
4	Ase1 insert/tag identification - reverse	CCA GAT ACC AAA AGG GCT ATG ATG AAA TCC

the plasmids are described in “Yeast Functional Analysis Report” [1] (pFA6a-3HAKanMX6 and pFA6a-13Myc-kanMX6)

Purification of DNA

The DNA acquired from PCR was purified using QIAquick PCR Purification Kit (50) by Qiagen (Catalog No. 28104) after running on a 1% agarose gel at 100 V. The results have been checked by DNA-sequencing (cp. fig. 1).

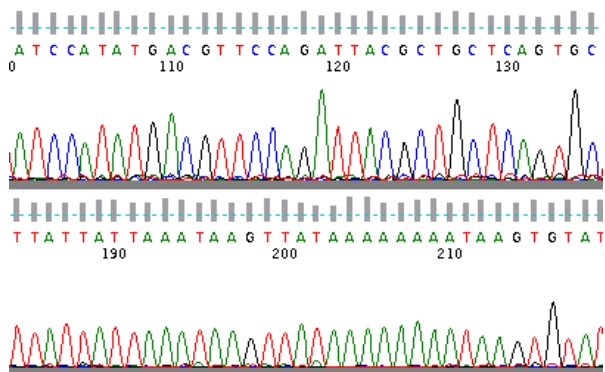


Fig. 1. Excerpt of the sequencing results, validating the successful cloning of the modified proteins. Chromatograph visualized using FinchTV v.1.3.1 by Geospiza, Inc.

Transformation

Yeast cells were inoculated from an o/n culture in 100 ml liquid YPD at $OD_{600} = 0.125$ and were grown to an $OD_{600} = 0.5-0.7$ at 30°C . After spinning at 2500 rpm for 3 min at RT and washing with 10 ml H_2O , the cells

were resuspended in 1 ml H_2O and transferred to a microfuge tube. The cells were pelleted briefly at 3000 rpm for 2 min and all the H_2O was removed. The cells were resuspended in 1.5 ml 1x TE (10 ml 1 M Tris-HCl and 400 μl 0.25 M EDTA in 990 ml ddH_2O) containing 1% LiAc. 10 μl of transforming DNA were mixed with 20 μl herring sperm DNA (reboil before use; 1 mg/ml) and 200 μl yeast suspension were added. 1.2 ml sterile 40% PEG 4000 solution (40% PEG 4000, 1x TE containing 1% LiAc) were added and incubated for 30 min at 30°C and heat shocked for 15 min in a 42°C waterbath. The tubes were spun for 10 sec and, washed with 1 ml H_2O , resuspended in YPD and were distributed on plates and incubated at 30°C .

The next day the yeast cells were transferred to plates with 250 μl G418.

Yeast Genomic DNA prep

To check the transformation, cells were harvested from an overnight culture in YPD, washed with 1 ml H_2O and resuspended in 0.5 ml lysis buffer. 0.5 g of 0.4–0.6 mm acid washed glass beads were added. The tubes were vortexed at maximum speed for 1 min and incubated on ice for 1 min 5 times. After incubation for 10 min at 75°C 200 μl 5 M KOAc and 150 μl NaCl were added and were put on ice for 10 min. The tubes were centrifuged at maximum speed for 10 min, the supernatant was transferred to a fresh tube

and 2 volumes of 95 % EtOH were added. The samples were centrifuged for 15 min and the pellet was washed with 70 % cold EtOH. The pellet was resuspended in 49 μ l TE and 1 μ l 10 mg/ml RNase and was incubated for 30 min at RT. The samples were diluted with 450 μ l H₂O and 1 μ l was used for a PCR as described above but with different primers (3 & 4 in table 1). The PCR was checked with an agarose gel (cp. fig. 2).

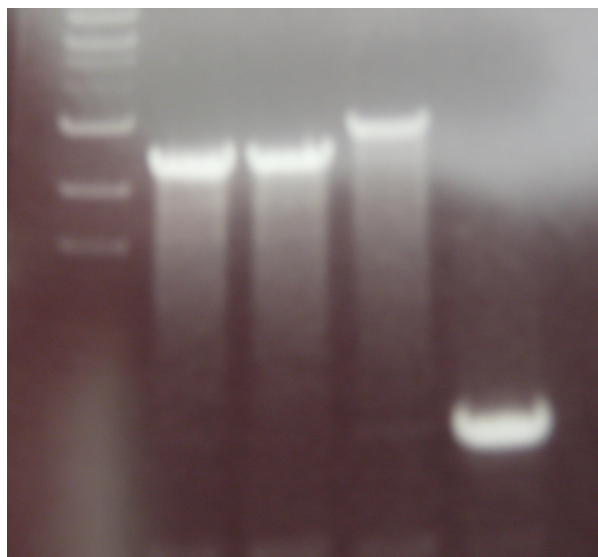


Fig. 2. Results of the Yeast Genomic DNA prep. First lane: DNA ladder. Lanes 2 and 3: samples of the cells with the HA-tag, lanes 4 and 5: samples of the yeast with the Myc-tag. Lanes 2,3 and 4 were proven to be positive.

SDS-PAGE

To check the expression of the modified gene an SDS-PAGE was done. Therefore cells from an overnight cell culture were diluted to a starting OD₆₀₀ of 0.15 in 100 ml YPD and were grown until OD₆₀₀ reached 0.5. The cells were spun down at 2500 rpm for 3 min, the supernatant was removed and the cells were washed in 20 ml cold H₂O. The cultures were resuspended in 300 μ l cold lysis buffer (50 mM Tris-HCl (pH 7.5), 150 mM NaCl, 5 mM EGTA (pH 7.5), 5 mM EDTA (pH 8.0), 1x phosphatase inhibitor cocktail, 1x protease inhibitor IV) and were sonicated for 5 sec. An equal volume of tiny acid washed glass beads was added and the

cells were beaten for 10 min. 5 μ l NP-40 were added and the tubes were spun for 15 sec at 13 000 rpm. The supernatant was transferred to a new tube and was spun again at max speed for 10 min. The supernatant was transferred to a new tube and 0.33 volumes of glycerol was added.

The separating gel was 7.5 % acrylamide/bisacrylamide, the stacking gel 5 %. The gel was run at 150 V until the dye front had entered the buffer chamber at the bottom. The proteins were transferred to a Nitrocellulose membrane with a pore size of 0.45 μ m at 100 V. The membrane was washed with H₂O and 15 ml of Ponceau red was added to verify transfer. When Ponceau red had been removed, the blot was blocked for 1 h at RT with 3 % BSA/TBS-T. The membrane was incubated for 1 h in primary antibody (anti-HA (1:5000) and anti-myc (1:2500)) diluted in 3 % BSA/TBS-T. Then the membrane was washed 5 times with 1x TBS-T and was incubated for 1 h in secondary antibody (α -mouse HRP (1:10000)). The membrane was washed 5 times with 1x TBS-T and the proteins were detected through electrogenerated chemiluminescence as shown in figure 3

Yeast Immunofluorescence

Cells from an overnight culture were diluted to a starting OD₆₀₀ of 0.04 in a total volume of 60 ml and were grown to an OD₆₀₀ of 0.1. Benomy (20 μ g/ml) and hydroxyurea (0.2 M) were added to arrest the cells and the tubes were incubated for 2.5 h at 30° C. The cells were spun down at 2500 rpm for 3 min, washed with 20 ml H₂O and resuspended in 30 ml YPD. Every 30 minutes 1 ml was transferred to a new tube, 0.156 ml formaldehyde were added and incubated at 25° C for 1 h. All cells were washed two times with 2 ml 0.1 M potassium phosphate buffer (pH 7.5) and resuspended in 1 ml potassium phosphate buffer. The cells were spheroblashed by adding 1 μ l BME and 25.5 μ l 1 mg/ml zymolyase to 500 μ l cells. The cells were incubated at 37° C for 35 min,

spun down at 3000 rpm for 3 min and resuspended in 50 μ l 0.1 M potassium phosphate buffer. The 10-well slide was coated with lysine and rinsed with H₂O after 30 sec. 20 μ l cells were placed in each well. After 20 min the excess solution was aspirated off and the cells were air-dried. After rehydrating the cells for 5 min in PBS they were fixed in methanol for 6 min at -20° C and 30 sec in acetone at -20° C. The cells were blocked with PBS + 1 mg/ml BSA for 15 min and were incubated with 20 μ l of the primary antibody (YOL134 (1:200), anti-HA (1:1000) and anti-myc (1:1000) for 45 min in a humid chamber. After washing with PBS-BSA the cells were incubated with the secondary antibody for 45 min with the second antibody (goat anti-rat antibody (1:500) tagged with CFP for YOL134 and anti-mouse (1:500) tagged with FITC for anti-HA and anti-myc) in a humid chamber in the dark. After washing again with PBS-BSA 15 μ l of mounting medium + DAPI were added to each well and sealed with a coverslip.

Fluorescence Microscopy

The fluorescence microscopy was performed by using a microscope (IX81, Olympus) equipped with 100X/NA 1.4 objectives and a camera (ORCA II, Hamamatsu). The wavelength of the light was 433 nm for CFP and 48 nm for the FITC.

Image Analysis

Patch lifetime analysis was done by visually identifying every single appearance and disappearance in the pictures. ImageJ (<http://rsb.info.nih.gov/ij/download.html>) software was used for postprocessing of the single pictures.

Results

Fig. 3 shows the results of the Western Blot. The first lane is the negative control with only one band. The second and third lane were samples with the HA-tagged Ase1. Since these two lanes have a band that does not exist in the negative control and the band has approximately 106 kDa,

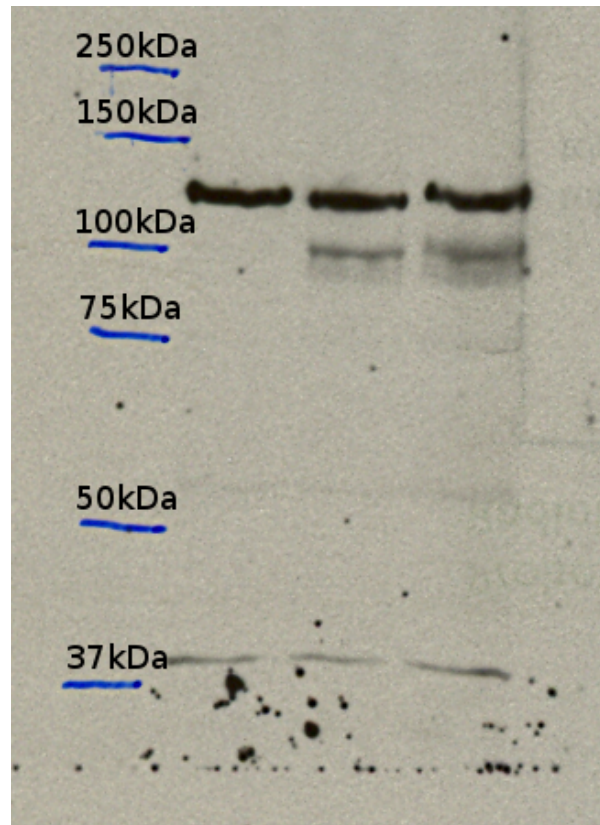


Fig. 3. Results of the Western Blot. Two colonies with a HA-tag were proven to be positive (two rightmost lanes). The very left lane is a negative control.

the two used colonies were proven to express the modified gene.

Hydroxyurea inhibits DNA synthesis and arrests the yeast cells at the beginning of mitosis. The pictures show the cells that have been arrested after 30, 60 and 90 minutes. Both Ase1 and the microtubules have been stained in the cells. After 30 minutes there is nearly no existence of Ase1 but the microtubules were already present. 30 minutes later the presence of Ase1 became observably stronger. The pictures show clearly that Ase1 is only located along the microtubules. Elsewhere Ase1 could not be seen in our studies. After 90 minutes neither microtubule nor Ase1 are visible. The cells have almost segregated and mitosis is finished.

As the pictures show, the concentration of Ase1 is highest after 60 minutes which pro-

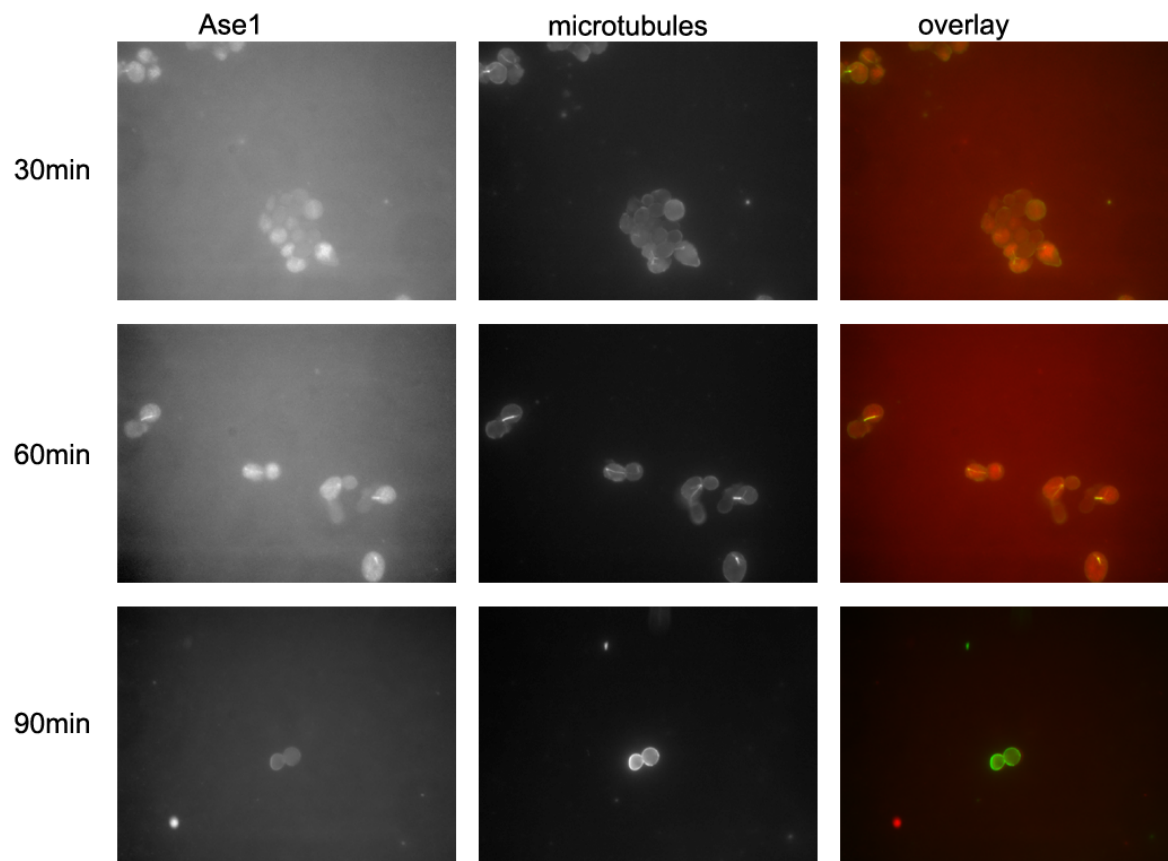


Fig. 4. Occurrence of Ase1 and the microtubules after 30, 60 and 90 minutes. Right column: overlay of microtubules (green) and Ase1 (red).

poses that Ase1 is mainly involved in mid-anaphase, which takes place after approximately 60 minutes. As shown in the picture Ase1 is located all along the microtubules.

Discussion

Since Ase1 is located along the microtubules, this experiment supports the idea of Ase1 being an MAP. As already said, the concentration of Ase1 is highest at mid-anaphase. This suggests, that Ase1 is involved in microtubule stabilization. Thus, it could be explained why there is nearly no presence of Ase1 after 30 minutes, where the mitotic spindle is still growing, and after 90 minutes, where mitosis has finished.

In further experiments the Drubin lab tries to identify proteins Ase1 interacts with to achieve a deeper understanding of the

role of Ase1 in mitosis. Since the sequencing, the genome prep and the Western Blot results proved that the transformation was successful, these cells could be used for further studies. One could try to pull out the Ase1 with hopefully a protein Ase1 binds to using antibodies. Then these proteins could be examined.

An Ase1 knockout should be done to examine the defects that cells get thereof. This would improve the understanding of Ase1 and could give clues for further experiments.

Acknowledgements

My sincere thanks is expressed to David Drubin and Georjana Barnes for giving me the unique chance to work in their lab for four weeks and for supporting me during this time. Special thanks to Ann Marie Faust and Yidi Sun for showing great patience in showing and explaining me everything and answer-

ing all my questions. It was an unforgettable experience and I really enjoyed the time in your lab.

Last but not least I want to thank the whole group of ISA San Francisco 2007 for the time we spent together in the United States.

References

- [1] Mark S. Longtine. Additional modules for versatile and economical pcr-based gene deletion and modification in *Saccharomyces cerevisiae*. *Yeast*, 1998.
- [2] Scott C. Schuyler. The molecular function of Ase1p: evidence for a MAP-dependent midzone-specific spindle matrix. *The Journal of Cell Biology*, 2003
- [3] The Homepage of the Drubin/Barnes Lab, University of California, Berkeley Department of Molecular & Cell Biology, http://mcb.berkeley.edu/labs/drubin_barnes/

NMR Investigation of the Involvement of Mn^{2+} in the Activation of DR2356

Alexandra Nothnagel and Benjamin Wallisch

Laboratory of David E. Wemmer

Department of Chemistry, University of California at Berkeley

Abstract

The bacterium *Deinococcus radiodurans* is known for its remarkably high resistance to radiation and its capability to withstand desiccation for a long time. DR2356, one of its proteins, is a member of the family of the so called Nudix hydrolases that are suggested to play a key role in the maintenance of homeostasis and physiological balance and thus to the bacterium's capability to survive. It was previously tried to solve the structure of the active form of DR2356, but only low activity was achieved in enzyme assays with Mg^{2+} . Recently, Mn^{2+} was stated to be the real cofactor for high activity.

DR2356 was expressed in *E. coli* grown in minimal medium enriched with glucose and ^{15}N -labeled ammonium chloride. Afterwards the cells were sonicated, then the protein was purified using FPLC and SEC and concentrated in order to be able to conduct ^1H - ^{15}N -HSQC experiments on both Bruker 500 MHz DRX and Bruker 800 MHz DRX spectrometers. The NMR spectra were monitored as a function of the concentration of manganese ions in order to determine the location of its binding site.

The 800 MHz assignments proved that manganese interacts and binds to the protein. The 500 MHz titration series with manganese sulfate showed that chemical shift changes accumulate in a certain area of the protein that is now identified as the first manganese binding site of DR2356.

Introduction

Bacteria of the genus *Deinococcus* are among the most radiation-resistant organisms known [9]. In addition to the ability of *Deinococcus radiodurans* to withstand γ -radiation fluxes 200-fold greater than those withstood by *Escherichia coli*, it is 20-fold more resistant to ultraviolet radiation, and it is also remarkably resistant to desiccation [2, 3]. In 1956, *Deinococci* were isolated from meat that had been strongly irradiated with radiation intended to sterilize the meat for packaging and later consumption [1]. Additionally, *D. radiodurans* has been reported to survive long periods of exposure in a desiccator. In these cases dehydration is thought to cause breaks in double-stranded DNA. Survival of *D. radiodurans* may be in large part due to its ability to repair damaged DNA.

An examination of the sequence of the bacterium's genome [12] reveals the existence of a widely distributed family of enzymes called nudix hydrolases, which catabolize substrates that are nucleoside diphosphates linked to some other moiety X. These enzymes share a conserved sequence of amino acids dubbed the nudix box [4]. Substrates for nudix proteins include NTPs, nucleotide sugars, coenzymes and $\text{A}_n\text{P}_n\text{As}$ (diadenosine polyphosphates). As these substrates and their derivatives are potentially toxic to the cell, it has been suggested that nudix hydrolases are cellular surveillance agents participating in physiological homeostasis [4, 13].

The 144-residue nudix hydrolase DR2356

has been shown to hydrolyze the substrate diadenosine tetraphosphate (Ap₄A), which has been observed in high concentrations in bacterial cells experiencing environmental stresses [7], such as a lack of nutrients or high exposure to heat or oxidation. Ap₄A has been found to have pharmacological effects on the cardiovascular and neurological system in humans. It remains unclear exactly what role Ap₄A plays in the overall endurance of *D. radiodurans* in the face of biologically extreme conditions, but it has been shown that DR2356 recognizes Ap₄A as a substrate. The ¹H-, ¹³C-, and ¹⁵N-resonances have been assigned and the structure of the inactive protein has previously been determined [11]. However, the cofactor required to activate the protein could not be found and the common cofactor Mg²⁺ was ineffective. Recently, it has been shown that Mn²⁺ ions, rather than Mg²⁺ ions, are probably the real cofactor for DR2356. Maximum activity in biochemical assays was obtained with 2 mM Mn²⁺. Only 5% of the activity achieved with 2 mM Mn²⁺ is supported by Mg²⁺ ions at 15 mM [6]. Up to now there is only limited information on the effects of the divalent cation Mn²⁺, but it has been reported that *D. radiodurans* can accumulate manganese in large amounts [8] and Mn²⁺ is supposed to fulfill different functions as second messenger and cofactor in *Deinococci*.

Nuclear magnetic resonance is a very important technique for structural analysis of molecules that combines the fields of chemistry, biochemistry, physics, and medicine. NMR is based on the fact that most elements in the periodic table have at least one nuclear isotope that interacts with a magnetic field and resonates at a certain radiofrequency depending on the atom's chemical environment. The shift of the resonant frequency e.g. due to a changing chemical environment is called the chemical shift which is a function of the secondary

and tertiary structure of the protein. In this project, the NMR method of Heteronuclear Single Quantum Coherence (HSQC) was used to measure twodimensional spectra with one axis for ¹H and another for a heteronuclear, most often ¹³C or as in this case ¹⁵N. Therefore the HSQC spectra contain a peak for each unique proton attached to a nitrogen [5].

NMR and especially the HSQC experiment is perfectly suited to study protein-ligand complexes due to the chemical shifts, which are sensitive markers of local structure as mentioned above. For that purpose NMR spectra of a protein are monitored as a function of the concentration of the ligand in order to determine, for instance, the location of a binding site or the effect of binding on the overall structure of a protein. This way it is possible to find a binding interface by comparing the NMR signals of the protein in the absence and presence of the ion based on differences in the chemical shifts between the bound and the unbound states [5].

Materials and Methods

Protein Expression in *E. coli*

Escherichia coli Tuner cells (DE3) with a *pET24a* vector containing the gene for DR2356 and a Kanamycin-resistance was kindly provided by Dr. Libby Holbrook (Lawrence Berkeley National Laboratory). 2 ml of starter cultures including 2 ml LB-medium (25.0 g/l Luria Broth; SigmaAldrich), 100 mg/ml Kanamycin and 20 µl of transformed and Kanamycin-resistant *E. coli* were inoculated into 1 l of minimal growth medium (0.5 g/l NaCl, 3.0 g/l KH₂PO₄, 6.78 g/l Na₂HPO₄, 0.24 g/l MgSO₄, 11.10 mg/l CaCl₂, 0.01 mg/ml Kanamycin, 2 g/l D-Glucose, 10 ml 100x *E. coli* Trace Metals and 10 ml 100x Vitamin Mix (see Tab. 1)) enriched with 1.0 g/l ¹⁵NH₄Cl (pH adjusted to 7.2 with NaOH). These cultures were incubated at 37° C and 225 rpm on a shaker to an OD₆₀₀ of ≈ 0.6

and ≈ 0.8 respectively (first and second expression respectively), at which point they were induced with 1 mM IPTG (Isopropyl- β -D-thiogalactopyranoside). After 4.5 h and 6 h, the first and second preparation of cells were harvested by centrifugation at 5,000 rpm, 4° C for 12 min and 20 min, respectively, and resuspended in 40 ml resuspension buffer (10 mM NaP_i consisting of 0.96 g/l NaH₂PO₄ · H₂O and 0.81 g/l Na₂HPO₄ · 7H₂O; pH to 6.5 with NaOH, 50 mM NaCl, 1 mM EDTA (ethylenediamine tetraacetic acid) and 1 mM DTT (dithiothreitol). Before and after lysing the *E. coli* by sonication for 180 s, 40 μ l PMSF (phenylmethanesulphonyl fluoride) were added.

To check the presence of DR2356, a 30 % SDS-PAGE was run with the samples taken before induction and before lysing the cells.

Purification

The resuspended cells were centrifuged for 25 min at 4° C and 30,000 rpm. The supernatant was dialysed in a Spektra/Por molecularporous membrane tubing (Spektrum) in 2l of resuspension buffer at 4° C overnight. The dialysed solution was filtered and purified by FPLC (Fast Protein Liquid Chromatography) ion-exchange chromatography over a DEAE Sepharose column (Pharmacia) at 1 ml/min with increasing NaCl (from 50 mM to 600 mM) in 200 min. The purified fraction was concentrated by centrifugation in Amicom Ultra (Millipore) tubes at 5,000 rpm and 7° C.

The concentrated solution was purified with size exclusion chromatography (SEC) over a superdex 75 HR/10/30 column (GE Healthcare) at 1 ml/min of resuspension buffer without EDTA and thus buffer-exchanged. The purified fraction was concentrated by centrifugation in Amicom Ultra (Millipore) tubes at 5,000 rpm and 7° C.

To identify the aliquots where DR2356 eluted and to check presence and purity of the protein, samples were analyzed by a 30 % SDS-PAGE after each chromatography

Table 1. Recipe for 1l 100x *E. coli* Trace Metals and 1l 100x Vitamin Mix (adapted from Basal medium: Eagle vitamin mix)

100x <i>E. coli</i> Trace Metals	
CuCl ₂	0.01 g
CoCl ₂ · 6 H ₂ O	0.01 g
EDTA	5.00 g
in 800 ml ddH ₂ O (pH 7.0)	
FeCl ₃	0.50 g
ZnCl ₃	0.05 g
pH 7.0	
H ₃ BO ₃	0.10 g
MnCl ₂ · 6 H ₂ O	1.60 g
ddH ₂ O	200 ml
100x Vitamin Mix	
D-Biotin	10 mg
Folic acid	10 mg
Nicotinamide	10 mg
D-Pantotheine acid	10 mg
Pyridoxal-HCl	10 mg
Riboflavin	1 mg
Thiamine-HCl	10 mg
Lipoic acid	10 mg
Pyridoxamine-diHCl	10 mg
Pyridoxine-HCl	10 mg
4-Aminobenzoic acid	10 mg

step.

Purity was confirmed by mass spectrometry conducted by Dr. David King with the calculated molecular weight of 16,295.3 Da.

NMR Experiments

UV absorbance at 260 nm and 280 nm was used for protein quantification. The both NMR samples (sample 1 and sample 2) consisted of ≈ 2.21 mM protein, 10 mM NaP_i, 50 mM NaCl, 1 mM DTT and 10 % D₂O at pH 6.5.

Two protein titration series were monitored by HSQC experiments. All spectra were collected at 298 K, with sample 1 data collected on an 800 MHz DRX spectrometer with 256 scans and 256 experiments to

obtain a sufficient signal despite the low protein concentration, and sample 2 data collected on Bruker 500 MHz DRX spectrometer with 32 scans and 128 experiments and processed and analyzed with NMRPipe, NMRView, and CARA. The peaklist generated by Tuan Ngyuen [11] was applied and adapted to the obtained spectra. Spectra were taken with DR2356 and Mn^{2+} concentrations of 0.00 and 1.00 mM in the first sample, and 0.00, 0.01, 0.02, 0.05, 0.10, 0.50, and 1.00 mM Mn^{2+} in the second sample. The concentration of Mn^{2+} ions was increased by titrating $MnSO_4$ into the protein sample.

Results

Expression and Purification

Presence and purity of DR2356 was confirmed by SDS-PAGEs (see fig. 1). Sample 1 had a protein concentration of ≈ 0.16 mM, whereas in sample 2 a concentration of ≈ 2.21 mM was measured.

Mass spectrometry provided a molecular weight of 16,371.2 Da, consistent with complete ^{15}N labeling of a 16,160.2 Da protein.

Solution NMR at 800 MHz

Fig. 2 (blue) shows the 1H - ^{15}N -HSQC (Heteronuclear Single Quantum Coherence) spectrum of sample 1, which has a very high resolution and shows all peaks for the backbone amino groups that had been assigned by Tuan Ngyuen (see [11]). The peaks for all amino acids except the first three (M1, S2, A3) and the ten prolines (P5, P6, P9, P38, P48, P81, P102, P115, P130, P144), which cannot be detected by HSQC, were assigned. The HSQC of sample 1 with 1 mM Mn^{2+} showed significant resonance broadening and shifting. Additionally, 25 assigned peaks disappeared (R10, A13, H20, H28, N30, G39, G40, G41, I42, E43, A51, C52, V56, E58, N61, Q65, H77, G78, N80, E103, G104, S108, D110, N111, and Y113). Fig. 2 shows the overlaid spectra and a graph with the differences between the observed chemical shifts of the assignment without

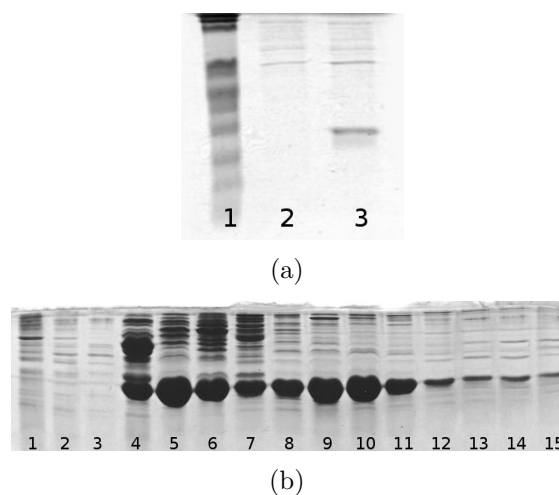


Fig. 1. Expression and purification of DR2356. (a) Protein was expressed by *E. coli* in minimal medium enriched with $^{15}NH_4Cl$ and glucose. In the 30% SDS-PAGE (1) is the marker, (2) is a sample of the medium before induction with IPTG, (3) is a sample taken 4.5 h after induction and before lysing the cells, which shows that DR2356 was expressed. (b) After purifying the protein using size-exclusion chromatography (second preparation), this 30% SDS-PAGE was run with the following aliquots: (1) Wash I, (2) Wash II, (3) aliquot 2, (4) aliquot 4, (5) aliquot 6, ..., (15) aliquot 26. Finally aliquots 5–20 were concentrated as they contained much of DR2356 and little impurity.

manganese and the assignment with 1 mM Mn^{2+} .

Solution NMR at 500 MHz

Contrary to the assignments on the 800 MHz spectrometer, there are several peaks assigned by Tuan Ngyuen missing in the spectrum of sample 2 (see fig. 3 (blue)). Altogether the peaks for the backbone amino groups of the following 23 amino acids are missing (including the ones not assigned): M1, S2, A3, N4, P5, P6, P9, R10, D18, P38, G39, P48, N61, P81, H83, C89, P102, C114, P115, P130, T139, V142 and P144.

In the spectrum of sample 2 containing 0.01 mM Mn^{2+} (see fig. 3 (red)) the peaks labeled Y16, D17, G40, G41, E59, N111, and N143 disappeared and the peaks labeled E58, L98, G104, and C132 shifted up to 0.375 ppm compared to the first 500 MHz

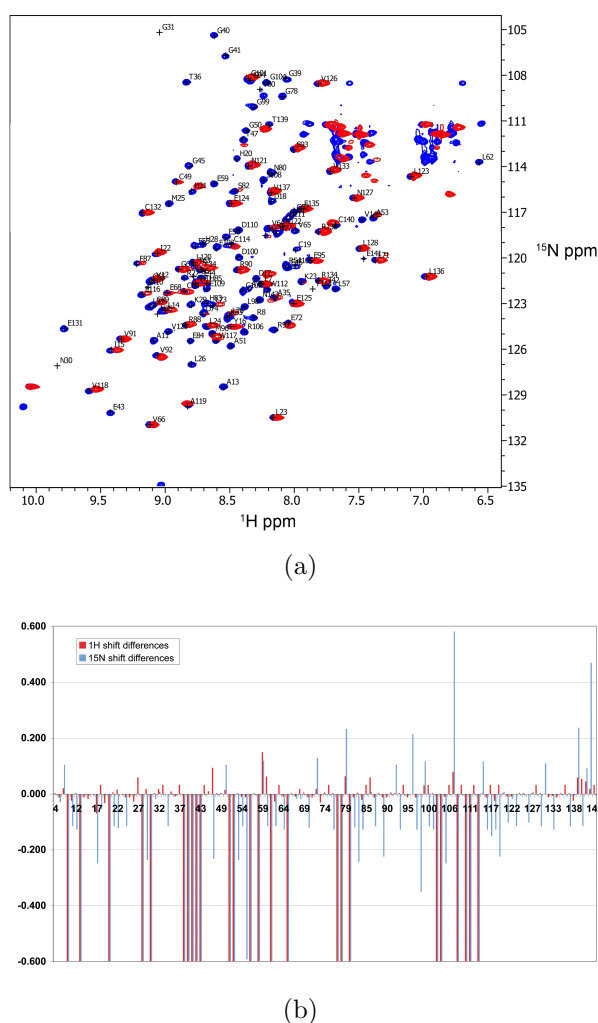


Fig. 2. (a) ^1H - ^{15}N -HSQC spectrum of DR2356 on Bruker 800 MHz DRX spectrometer processed by CARA. The blue peaks belong to sample 1 without manganese, the overlaid red peaks to sample 1 containing 1.00 mM Mn^{2+} . The peaks labeled N30, G31, and Y113 are not visible, since they can only be seen with very low contour parameters. The graph (b) shows the chemical shift differences between these two assignments. A peak disappeared in a spectrum when the bar for both the ^1H - and the ^{15}N -dimension reached the bottom of the graph.

assignment, whereas the other peaks only underwent minor shifts in the spectrum and little broadening.

Comparing the HSQC spectra of sample 2 with a Mn^{2+} concentration of 0.01 mM and 0.02 mM (data not shown), peaks for the amino acids I42, E55, E58, and W112 disappear and the peak for Y113 shifts

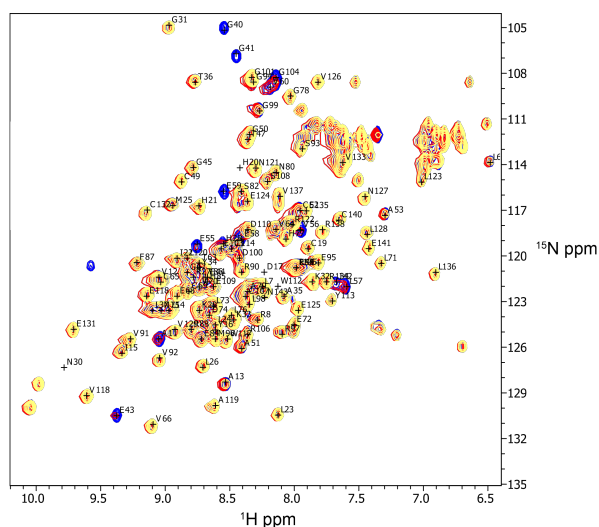
0.79 ppm in the ^1H -dimension and 3.40 ppm in the ^{15}N -dimension. The spectrum (not shown) taken after the next titration (total manganese concentration of 0.05 mM) does not show any differences apart from the fact that the peak for the backbone amino group belonging to the amino acid L98 disappeared, the peak labeled V133 shifted 0.28 ppm in the ^{15}N -dimension and minor broadening occurred.

In fig. 3 the NMR assignment of sample 2 containing 0.10 mM Mn^{2+} is shown in yellow. The only difference between the spectra with 0.05 mM and 0.10 mM Mn^{2+} is that the peaks labeled A11 and V56 disappeared and the peaks of the residues E44, Y86, and E103 experienced great shifts within the spectrum of ≈ 0.30 ppm in each case compared with minor broadening of most of the peaks.

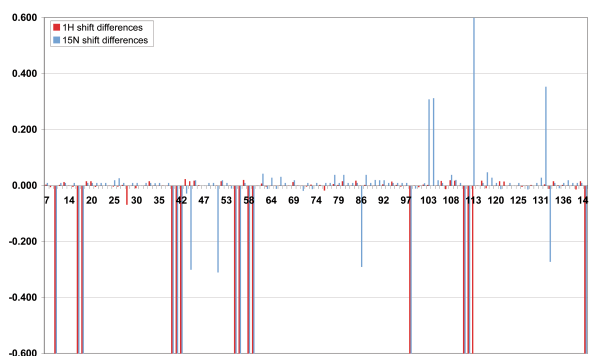
By comparing the spectrum of sample 2 containing 0.10 mM with the one of sample 2 with 0.50 mM Mn^{2+} (data not shown), huge differences (apart from minor shifts and broadening) are seen as eleven more peaks (I15, L37, E43, E46, A51, A53, R54, L57, V60, G104, and I105) disappeared, the peaks representing the amino acids A13 and L14 shifted in both the ^1H -dimension (0.43 ppm and 0.36 ppm respectively) and the ^{15}N -dimension (4.71 ppm and 2.82 ppm respectively) and the peak labeled N30 shifted 0.30 ppm in the ^{15}N -dimension.

Although the manganese concentration was doubled to 1.00 mM Mn^{2+} by the last titration, only two more peaks (C52 and D100) vanished what makes it a total of 27 disappeared peaks (out of a total of 121 peaks) and the peaks for amino acid E68 and L123 shifted 0.30 ppm and 0.63 ppm respectively in the ^{15}N -dimension. The outcome of the last assignment is shown in fig. 4 with the overlaid spectrum and a graph showing the differences of all the chemical shifts.

To summarize, it can be said that the peaks A11, I15, Y16, D17, L37, G40, G41, I42, E43, E46, A51, C52, A53, R54, E55, V56, L57, E58, E59, V60, L98, D100, G104,



(a)



(b)

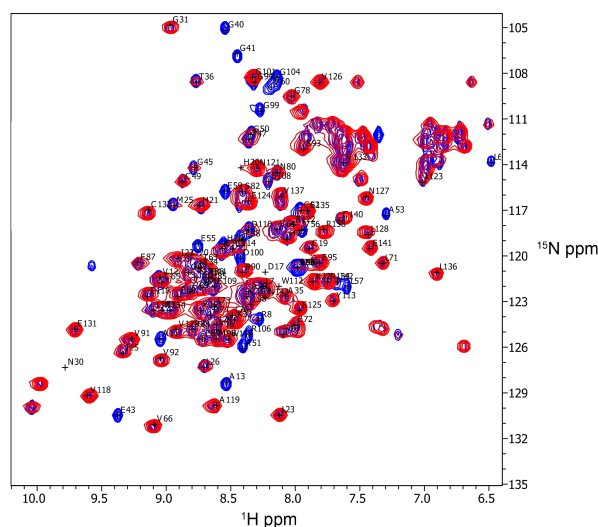
Fig. 3. (a) HSQC spectrum of the first assignment of sample 2 without manganese (blue) on Bruker 500 MHz DRX spectrometer being overlaid with the assignment of sample 2 containing a manganese concentration of 0.01 mM (red) and 0.10 mM (yellow). The graph (b) displays the shiftings of the sample containing 0.10 mM Mn^{2+} as in fig. 2.

I105, N111, W112, and N143 disappeared, some peaks shifted very much and all peaks underwent (partially extreme) broadening upon addition of a stoichiometric amount of manganese.

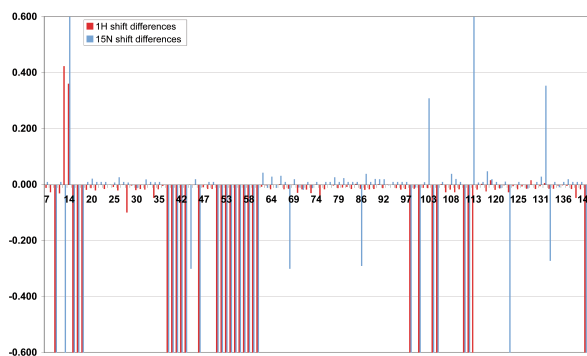
Discussion

Expression and Purification

The difference between the calculated molecular weight of 16,295.3 Da or rather 16,506.3 Da due to ^{15}N -labeling and the weight measured by mass spectrometry is



(a)



(b)

Fig. 4. (a) Final HSQC spectrum of sample 2 containing 1.00 mM Mn^{2+} is shown in red and overlaid over the spectrum of sample 2 without manganese (see fig. 3 (blue)). The chemical shift differences of each peak between the spectra are shown in the graph (b) as in fig. 2

135.1 Da. The difference in the molecular weight could result from the missing first residue (methionin), but there remains a difference of 3.9 Da. As measurement inaccuracies usually are not that huge, there could be little impurity, however, it is not perceivable in the spectra.

Solution NMR at 800 MHz

The assignments on Bruker 800 MHz DRX spectrometer suggest that we got the right protein as our spectra match pretty well with T. N. Nguyen's (published: [10], p. 96). Moreover, the data shows that manganese

ions interact with and bind to DR2356 as it has previously been stated by Cartwright et al. [6] since a conformational change can be observed.

Because of broadening due to the paramagnetic behavior of Mn^{2+} , it is possible that some peaks are declared disappeared although they are not. The chance of extreme broadening increases with the manganese concentration in the sample. Furthermore, the high manganese concentration causes non-specific binding of the metal to the protein. That is why we cannot draw any conclusions on the manganese binding site of DR2356 from the 800 MHz data.

Solution NMR at 500 MHz

The likely first binding site of DR2356 with the highest affinity to manganese ions can be deduced from the assignments on Bruker 500 MHz DRX spectrometer. Concluded from the assignments up to the one of sample 2 with 0.10 mM Mn^{2+} (see fig. 4 (yellow)), it is likely that the region around the amino acids G40, G41, I42, E55, E58, and E59 forms the binding site. As they are located near each other in the sequence, there is the possibility, though, that they effect each other, when some experience a change due to the binding of manganese.

Looking at the structure of the protein (see fig. 5), it can be noticed that the above mentioned amino acids form a pocket, in which the manganese can bind. Further evidence is given by the secondary structure (see fig. 6) as the pocket is formed by an α -helix and β -sheets. Another indication is that glutamic acids are partly negatively-charged amino acids.

The fact that eleven peaks disappeared when increasing the manganese concentration from 0.10 mM to 0.50 mM leads to the consideration that due to this titration there is too much manganese in the sample leading to non-specific binding, however, this may also reveal more manganese binding sites.

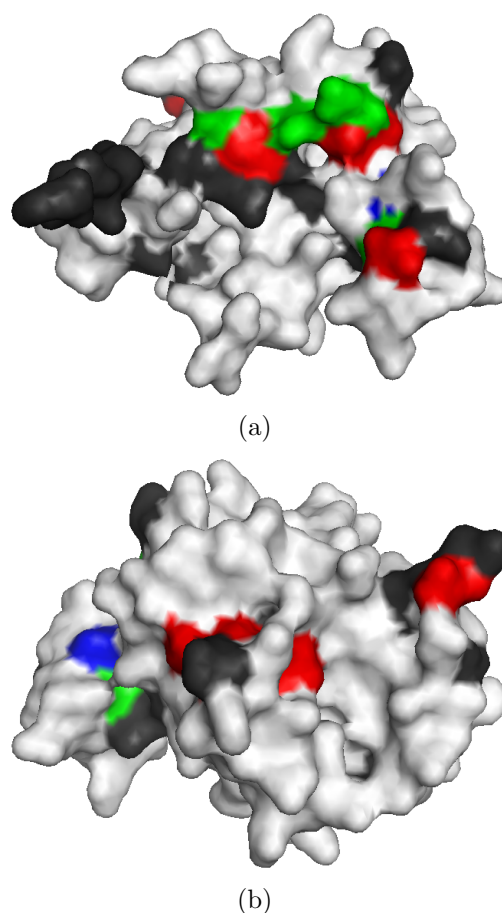


Fig. 5. Two views of the surface structure of DR2356 generated with PyMOL with (b) being rotated by 180° compared to (a). The peaks not being visible in the first assignment on Bruker 500 MHz DRX spectrometer are marked dark-gray, the ones that disappeared after the first manganese titration are colored red, the vanished peaks after the titration to 0.02 mM Mn^{2+} concentration are shown in green. In blue are the peaks that disappeared in the assignment of sample 2 containing 0.05 mM Mn^{2+} and in yellow the ones that vanished in the spectrum conducted with a manganese concentration of 0.10 mM (see also fig. 3).

Comparison of sample 1 and 2

When comparing the assignments of samples 1 and 2 both containing a manganese concentration of 1.00 mM, it can be seen that only the peaks labeled G40, G41, I42, E43, A51, C52, V56, and E58 are missing in both spectra which makes the location of the first binding site even more likely. Indeed, it has to be considered that the proportion

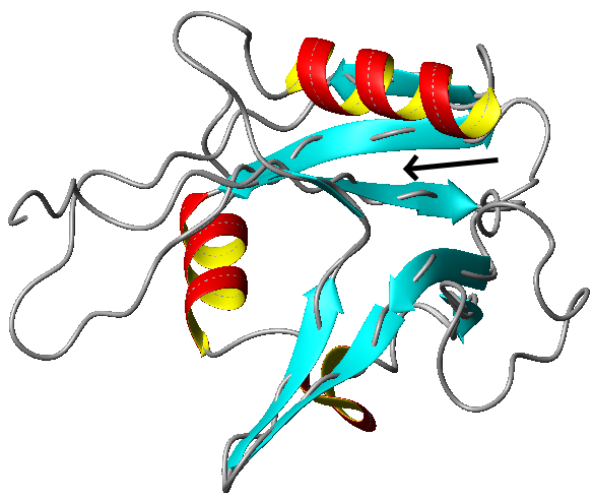


Fig. 6. Secondary and tertiary structure of the inactive DR2356 solved by T.N. Nguyen. The position of the newly found likely first binding site for manganese is marked. The figure was generated with MOLMOL.

of protein to metal concentration is different in the two samples.

Previous Work

As has been recently suggested [6], manganese binds to DR2356 and thus its activity is higher than with magnesium. As already mentioned above, we conclude from our data that there is a binding site for Mn^{2+} , even though we used manganese sulfate instead of manganese chloride. This supports the thesis that manganese is the activating cofactor for DR2356.

T. N. Nguyen suggested in [10] that R54, E55, E58 and E59 are expected to be involved in cation binding. This consideration is confirmed as E55, E58 and E59 bind manganese as their peaks already disappeared after the second titration to a manganese concentration of 0.02 mM. However, it is questionable if R54 is involved in the first binding site since the assigned peak disappeared not until the concentration of 0.50 mM in the 500 MHz assignments, at which point non-specific binding seems to be more likely, and even did not disappear in the 800 MHz assignments (see fig. 2).

Outlook

The next step is to solve the structure of the activated DR2356 to verify the location of the binding site. Another task would be to find the active center by finding and adding a substrate mimic of Ap_4A that reacts more slowly as it hardly hydrolyzes so that it gets possible to use NMR techniques. Another interesting question is why Mg^{2+} instead of Mn^{2+} is used by most of the other nudix hydrolases and how comparable the binding sites for manganese and magnesium are in this protein class. Furthermore, the correlation of the structure and the function of the protein should be investigated by studying the signal cascades and processes manganese is involved.

Acknowledgements

We want to thank Prof. David E. Wemmer for giving us the opportunity to visit his great lab and get an insight in this fascinating field of science. Moreover, we like to thank all members of the Wemmer Lab for their friendliness, their support and their acceptance. Our sincere thanks are especially expressed to our supervisors Natasha Keith and Aaron Phillips who gave us a lot of support and were always patient, encouraging and good humored. Special thanks also to Kaya Erbil for the day he supervised us and his magnet time at the Bruker 800 MHz DRX spectrometer.

Further thanks go to Prof. Libby Holbrook (Lawrence Berkeley National Laboratory) who kindly supplied *E. coli* containing the gene for DR2356, to Prof. Volker Dötsch (Department of Biophysical Chemistry, Johann Wolfgang Goethe-Universität, Frankfurt am Main, Germany) for his aid before and after the academy and to Dr. David King (Barker Hall, University of California, Berkeley) for the mass spectrometry.

We would also like to mention our parents who have always supported us and made the trip possible at all by covering all our costs.

We very much appreciate the effort of our mentors Christian Stoy and Christoph Fischer as well.

Last but not least, we would like to thank all participants of the International Science Academy San Francisco 2007 for this incredible stay in the Bay Area.

References

- [1] Anderson A, Nordan H, Cain R, Parrish G and Duggan D. (1956) Studies on a radioresistant micrococcus. I. Isolation, morphology, cultural characteristics, and resistance to gamma radiation. *Food Technol.* 10: 575-578
- [2] Battista JR. (1997) Against all odds: the survival strategies of *Deinococcus radiodurans*. *Annu. Rev. Microbiol.* 51: 203-224
- [3] Battista JR, Earl AM and Park MJ. (1999) Why is *Deinococcus radiodurans* so resistant to ionizing radiation?. *Trends Microbiol.* 7(9): 362-365
- [4] Bessman MJ, Frick DN and O'Handley SF. (1996) The MutT proteins or "nudix" hydrolases, a family of versatile, widely distributed, "housecleaning" enzymes. *J. Biol. Chem.* 271(40): 25059-25062
- [5] Edwards AJ and Reid D. (2000) Unit 17.5 Introduction to NMR of Proteins. *Current Protocols in Protein Science*: 17.5.1-39
- [6] Fisher DI, Cartwright JL and McLennan AG. (2006) Characterization of the Mn²⁺-stimulated (di)adenosine polyphosphate hydrolase encoded by the *Deinococcus radiodurans* DR2356 nudix gene. *Arch Microbiol* 186: 415-424
- [7] Lee PC, Bochner BR and Ames BN. (1983) Diadenosine 5',5"-P₁P₄-tetrphosphate and related adenylylated nucleotides in *Salmonella typhimurium*. *J. Biol. Chem.* 258: 6827-6834
- [8] Leibowitz PJ, Schwartzberg LS and Bruce AK. (1976) The in vivo association of manganese with the chromosome of *Micrococcus radiodurans*. *Photochem. Photobiol.* 23:4550
- [9] Moseley BEB. (1983) Photobiology and radiobiology of *Micrococcus (Deinococcus) radiodurans*. *Photochem. Photo-biol. Rev.* 7: 223275
- [10] Nguyen TN. (2003) Solid State NMR of Amyloidogenic Biomolecules and Solution State NMR of DR2356, a Nudix Hydrolase in *Deinococcus radiodurans*. PhD-Thesis, Chapter 5, Chemistry, University of California, Berkeley
- [11] Nguyen TN and Wemmer DE. (2003) Letter to the Editor: Complete resonance assignments for the nudix hydrolase DR2356 of *Deinococcus radiodurans*. *Journal of Biomolecular NMR* 27: 181-182
- [12] White O, Eisen JA, Heidelberg JF, Hickey EK, Peterson JD, Dodson RJ et al. (1999) Genome sequence of the radioresistant bacterium *Deinococcus radiodurans* r1. *Science* 286: 1571-1577
- [13] Xu WL, Shen JY, Dunn CA, Desai S and Bessman MJ. (2001) The Nudix hydrolases of *Deinococcus radiodurans*. *Molecular Microbiology* 39: 286-290
- [14] Software used: NMRPipe, NMRView, CARA, MOLMOL, and PyMOL

Development of *hSSTR2* Promoter to Target ON Retinal Ganglion Cells via Adeno-Associated Viral Vectors

Clemens Scherer

Laboratory of John G. Flannery

Helen Wills Neuroscience Institute

Department of Molecular and Cell Biology, University of California at Berkeley

Abstract

The human somatostatin receptor type 2 (hSSTR2) is highly expressed in retinal ganglion cells (RGC). Former studies have shown that channelrhodopsin-2 (ChR2) can add light sensitivity to ON ganglion cells. The combination of the *hSSTR2* promoter with the cDNA of *ChR2* delivered by adeno-associated viruses should be expressed constantly in diseased ON ganglion cells and thereby countervail retinal diseases. Our aim has been to prove that ON ganglion cells can be specifically targeted by adeno-associated viruses containing the *hSSTR2* promoter driving eGFP expression. The verification of our vector showed that its DNA sequence is correct. Up to now there have been no results about the expression rate of eGFP in the ganglion cells.

Introduction

The eye is an ideal object for gene therapy since it has a combination of feasible features such as the highly compartmentalised anatomy and the outstanding immune environment. By now, around 150 retinal disease loci and 90 disease causing genes have been identified. Likewise, non-invasive imaging *in vivo* is facilitated by the eye's optical transparency. Visual function can be measured by psychophysical and electrophysiological methods. Moreover, the treated eye can be compared with the contralateral nontreated eye [1].

In general, two types of viruses are used for gene therapy in the eye: Lentivirus-based vectors have the ability to steadily transduce nondividing cells. Normally, they are used to deliver gene material into the corneal endothelium and trabecular meshwork. New investigations have indicated that other cell tissues can also be targeted by the correct choice of promoter and capsid [2].

By contrast, recombinant adeno-associated viral (rAAV) vectors have turned out to be gene transfer tools for the retinal pigmented epithelium, photoreceptor and ganglion cells. The use of high titers will ensure that most postmitotic cells are transduced [3].

Up to now, there have been two possibilities to treat retinal degenerative diseases. On the one hand investigators have been seeking to slow degeneration by neuroprotection with neurotrophic factors. Virus delivery of wild-type genes for recessive null mutations have reached the point of a Phase I/II clinical trial [4].

On the other hand patients with a total loss of photoreceptor cells have few options like the transplantation of isolated photoreceptors or the differentiation of embryonic stem cells into photoreceptors, but these methods are still under development [5]. Bi et al. found a new way to regain visual response in mice by introducing a genetically encoded light-sensitive ion channel,

channelrhodopsin-2 (ChR2), into all retinal ganglion cells (RGC) using AAV vectors. ChR2 was able to depolarize ganglion cells when activated by light signals around 460 nm. Furthermore, the authors demonstrated that light signals can be transmitted to the visual cortex in mice with photoreceptor degeneration when ChR2 has been expressed [6].

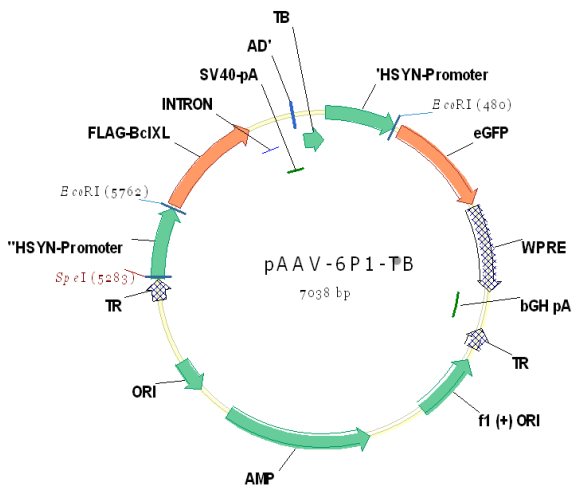


Fig. 1. *pAAV-6P1-TB* (a gift from Dr. Sebastian Kügler) was used to develop AAV vectors.

Ganglion cells are coarsely divided into ON and OFF subpopulations depending on their polarization response to light. Our aim has been to engineer AAV vectors which would only transduce depolarizing ON bipolar cells to improve the specificity of perception. Therefore, we wanted to test the expression rate of eGFP in combination with different promoters [7]. Only the *hSSTR2* promoter has successfully been cloned into AAV vectors so far. As transfer vector we used *pAAV-6P1-TB* (a gift from Dr. Sebastian Kügler, University of Göttingen Medical School, Germany, see figure 1). The primers for the isolation of the *hSSTR2* promoter (total length: 2798 bp) were recommended by Kenneth P. Greenberg and will soon be published.

Materials and Methods

PCR amplification of *hSSTR2* promoter

To isolate the *hSSTR2* promoter polymerase chain reaction was performed on human 293T cells using Platinum[®] Taq DNA Polymerase (Invitrogen #11304-029). The forward primer includes a *Spe*I restriction site in 5', the reverse primer an *Eco*RI restriction site in 3'. 35 extension cycles were conducted for 2:30 minutes each at 58° C.

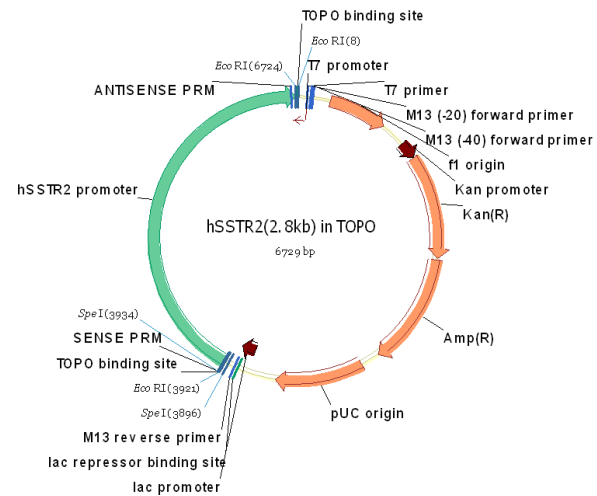


Fig. 2. *hSSTR2.TOPO* vector with used restriction sites *Eco*RI and *Spe*I.

Cloning *hSSTR2* into TOPO vector

The TOPO TA Cloning[®] system (Invitrogen #K4550-40) was used to amplify the *hSSTR2* DNA by cloning it into the *pCR2.1-Topo* vector. We incubated 2 μ l of the PCR product with 1 μ l salt solution, 1 μ l water and 1 μ l *pCR2.1-Topo* vector at 25° C for 5 min and then put it on ice. The resulting vector was called *hSSTR.TOPO* (see figure 2).

Transformation

2 μ l of the ligation product were given to One Shot[®] TOP10F' Competent Cells (Invitrogen #C3030-03) and incubated for five minutes on ice. Afterwards the cells were heat-shocked for 30 sec at 42° C, transferred on ice for two minutes each and 250 μ l of prewarmed SOC medium was

added afterwards. The cells were incubated for one hour at 37° C under agitation at 200 rpm. 50 µl of bacteria were spread on prewarmed LB medium plates containing ampicillin (100 µg/ml) and X-Gal/IPTG for blue-white screening.

After one day white colonies were picked and transferred in 50 µl LB/Amp and 10 µl water respectively. To check which clones have the right insert polymerase chain reaction was performed on the 10 µl water sample of each colony with *hSSTR2* promoter primers. Positive clones were grown up overnight at 37° C in 4 ml LB/Amp.

Cloning *hSSTR2* into *pAAV*

Plasmids of positive colonies were isolated by using the QIAprep® Spin Miniprep Kit (Qiagen #27106). *hSSTR2.TOPO* and *pAAV-6P1-TB* were cut by *Spe*I and *Eco*RI in NEBuffer *Eco*RI + BSA (New England Biolabs®, Inc.) for one hour at 37° C and run on 1% agarose gel. The 2790 bp long *hSSTR2.TOPO* and the 4803 bp long *pAAV-6P1-TB* fragments were purified. Both were ligated together with Rapid DNA Ligation Kit (Roche #11-635-379-001): First we dissolved the vector and inserted it in 1x DNA Dilution Buffer to a final volume of 10 µl and then added 10 µl T4 DNA Ligation Buffer and 1 µl T4 DNA Ligase. The ligation was performed for 30 min at 25° C.

Transformation

The ligation products (*pTR.hSSTR2.GW*) were transformed into SURE® 2 Supercompetent Cells (Stratagene #200152). Bacteria were grown on plates overnight in LB/Amp. Next day, colonies were picked and again grown in 4 ml LB/Amp.

Miniprep

After isolating *pTR.hSSTR2.GW* plasmids with QIAprep® Spin Miniprep Kit, we performed a digest with *Sma*I in NEBuffer 4 + BSA for one hour at 25° C to check whether we had the right plasmids. To visualize the fragments we used a 1% agarose gel. The

UV picture showed the expected results (see figure 3). We chose lane 3 for further investigation and let the bacteria grow for 12 h in 500 ml LB/Amp.

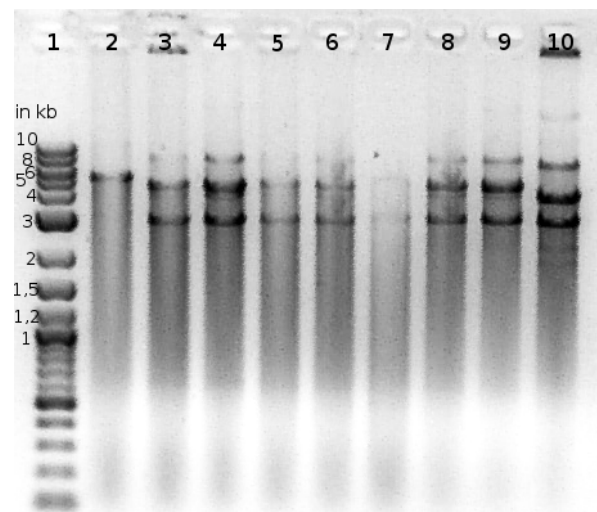


Fig. 3. Control digest of *pTR.hSSTR2.GW* with *Sma*I. (1) 2-Log DNA Ladder (Invitrogen), (2)-(10) colonies 1-9.

Maxiprep

The plasmids were isolated with the EndoFree® Plasmid Mega Kit (Qiagen #27106) and dissolved in 500 µl TE buffer. The concentration of DNA (A_{260}) was measured to 1694 ng/µl. We cut the plasmids with different restriction enzymes (see table 1) and electrophoresed results on 1% agarose gel.

Table 1. Restriction enzymes used to test orientation in *pTR.hSSTR2.GW*

Restr. Enzymes	lane	fragments
–	2	–
<i>Eco</i> RI + <i>Cla</i> I	3	6221, 774, 598
<i>Eco</i> RI	4	7593
<i>Cla</i> I + <i>Blp</i> I	5	5632, 1363, 598
<i>Sma</i> I	6	4558, 3013, 11, 11

Transfection

For transfection nine plates (DMEM, 10% FBS and 4 mM L-Glutamin Cells P4) were

used. 41.54 μ l *pTR.hSSTR2.GW* plasmids were mixed with 33.599 ml OptiMEM Reduced Serum Medium (Invitrogen #31985), 59.08 μ l XX2 and 50.23 μ l P-Helpers. In another tube 32.94 ml OptiMEM Reduced Serum Medium and 810 μ l Lipofectamine 2000 (Invitrogen #11668019) were gently mixed. Both reagents were allowed to incubate for 5 min at 25° C. Afterwards, they were combined and incubated for 20 min at the same temperature. 7.5 ml of the reagents were added to each plate.

Further investigation (purification of viruses and infection into rat retinas) has been performed by Meike Visel and Kenneth P. Greenberg.

Results and Discussion

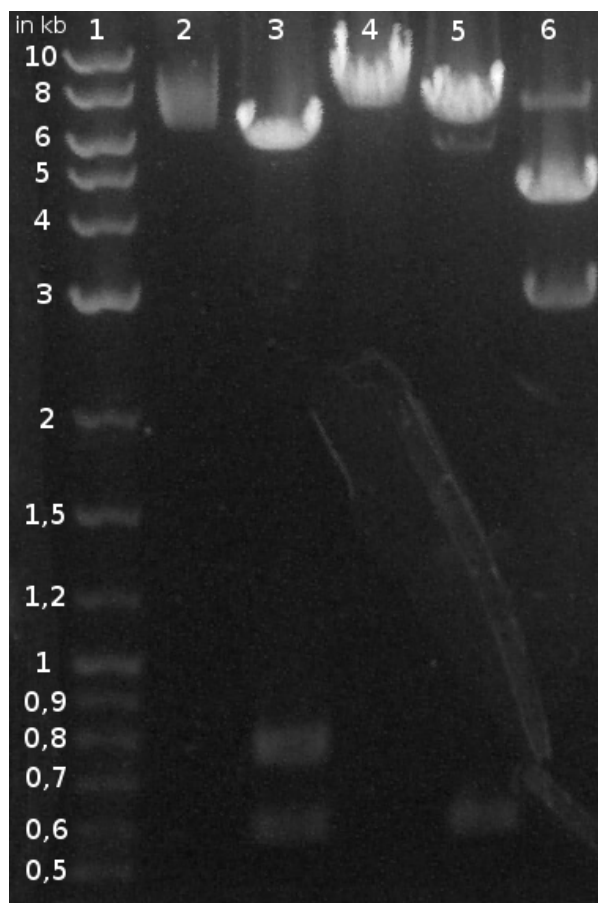


Fig. 4. Control digest of *pTR.hSSTR2.GW* with different restriction enzymes (see table 1): (1) 2-Log DNA Ladder (Invitrogen), (2) no digest, (3) *EcoRI* and *ClaI*, (4) *EcoRI*, (5) *ClaI* and *BspI*, (6) *SmaI*

Gel Electrophoresis (figure 4) proved that *pTR.hSSTR2.GW* virus vectors contain the *hSSTR2* promoter and eGFP. If eGFP expression is only visible in ON bipolar cells, this will prove, that AAV vectors with the *hSSTR2* promoter target these retinal cell types specifically. Whether the virus is able to infect RGCs can only be shown by animal models which were being performed at the time when this article was written.

If the virus could infect the RGCs, the testing of new vectors with *hSSTR2* or other promoter sequences in combination with *ChR2* in animal models would be the next step. These vectors should be able to add (non)light-sensitivity to ON/OFF ganglion cells specifically and thereby give the possibility to re-engineer retinal interneurons as genetically modified prosthetic cells for vision.

Acknowledgements

I would like to thank John G. Flannery for giving me the possibility of working in his laboratory. Furthermore, I would like to express my deepest thanks to Meike Visel, my much appreciated mentor and help in every situation. She was a great supervisor and I hope more students will benefit from her teaching. I really enjoyed the time in the Flannery lab and would be glad to work there again.

Last but not least I want to thank Christian Stoy and Christoph Fischer for their selfless engagement and also the whole group for this unforgettable month.

References

- [1] Bainbridge JWB, Tan MH, Ali RR: Gene Therapy progress and prospects: the eye, *Gene Therapy* 13, 1191-1197, 2006.
- [2] Greenberg KP, Geller SF, Schaffer DV, Flannery JG: Targeted transgene expression in muller glia of normal and diseased retinas using lentiviral vectors, *Invest Ophthalmol Vis Sci.* 2007 Apr;48(4):1844-52.
- [3] Dinculescu A, Glushakova L, Min SH, Hauswirth WW: Adeno-Associated Virus-Vectorized Gene Therapy for Retinal Disease, *Human Gene Therapy* 16:649-663, June 2005.

- [4] Hauswirth WW: The consortium project to treat RPE65 deficiency in humans. *Retina*. 2005 Dec;25(8 Suppl):S60.
- [5] Seiler MJ, Sagdullaev BT, Woch G, Thomas BB, Aramant RB: Transsynaptic virus tracing from host brain to subretinal transplants. *Eur J Neurosci*. 2005 Jan;21(1):161-72.
- [6] Bi A, Cui J, Ma YP, Olshevskaya E, Pu M, Dizhoor AM, Pan ZH: Ectopic expression of a microbial-type rhodopsin restores visual responses in mice with photoreceptor degeneration. *Neuron*. 2006 Apr 6;50(1):23-33.
- [7] Flannery JG, Greenberg KP: Looking within for vision. *Neuron*. 2006 Apr 6;50(1):1-3.

Influence and moderating role of lipids in endocytosis

Hans Urban

Laboratory of David Drubin

Department of Molecular and Cell Biology, University of California at Berkeley

Abstract

A variety of studies have described that endocytosis is the movement of solutions and solids from the outside of the cell into the cytoplasm and towards the nucleus. In further studies the importance of the lipid phosphatidylinositol-(4,5)-bisphosphate (PtdIns_(4,5)P₂) for endocytosis was identified. However, it has not yet been determined which mediating roll lipids could play. In the present study we tried to find out more about the mapping and function of lipids in endocytosis. Therefore yeast cells were labeled with the markers for the proteins YLR064w, YHL044w, YBR220c and YBR042c and the effects of lipids on the endocytosis of budding yeast were examined.

Introduction

Endocytosis is a very important activity in every eucaryotic cell and is handled as one of the basic reactions of life.

The last twenty years of endocytosis research have brought a spate of new insights on the function and mode of endocytosis. Meanwhile, it is normal to discern three different forms of endocytosis: (1) Phagocytosis is known as the process by which cells ingest huge objects, such as cells which have undergone apoptosis, bacteria, or viruses. (2) Pinocytosis (literally: cell-drinking) is normally a synonym for endocytosis. This process is concerned with the uptake of solutes and single molecules such as proteins. (3) Receptor-mediated endocytosis is a more specific active event where

the plasma membrane folds inward to form coated pits. In the following article only pinocytosis is meant when the term endocytosis appears.

Cells transfer different kinds of substances in and out of their soma via endocytosis. It regulates the pH-value of the environment, the contact with other cells by messengers, the secretion of proteins like enzymes, peptides, and hormones from cells or the defaecation of the cell by emptying the vacuole. The process of endocytosis is divided into five different steps: vesicle trafficking, vesicle tethering, vesicle docking, vesicle priming and vesicle fusion. Actin is associated with each of the five steps of endocytosis and acts as one of the initiating proteins of endocytotic processes.

In budding yeast, many proteins, adapters, actin cytoskeleton proteins and lipids are involved in endocytosis. Prior studies (Engqvist-Goldstein and Drubin, 2003; Munn, 2001; Geli and Riezmann, 1998; Qualmann et al., 2000) have found out more about the importance of actin in the process of endocytosis, but there are also references that lipids are involved in this basic reaction of life.

During the internship in the Barnes/Drubin Lab, I tried to find out more about which actins and lipids occur during endocytosis, because these reactions are not thoroughly explored at the moment.

Materials and Methods

PCR

Polymerase Chain Reaction (PCR) 1

Used ingredients: 20 μ l 10x Opti Buffer (Mg free), 10 μ l 50 mM MgCl₂, 4 μ l 10 mM dNTPs, 4 μ l template DNA 20 ng/ μ l GFP marked, 1 μ l primer 1, 1 μ l primer 2, 1 μ l primer 3, 1 μ l primer 4, 1 μ l primer 5, 1 μ l primer 6, 1 μ l primer 7, 1 μ l primer 8, 150 μ l ddH₂O and 4 μ l BioxAct polymerase.

Temperature settings were: (1) 98° C for 30 sec, (2) 98° C for 25 sec, (3) 68° C for 1 min, (4) 72° C for 5 min, (5) 72° C for 10 min and 12° C forever. Step (2)–(4) were repeated 29 times.

Polymerase Chain Reaction (PCR) 2

Used ingredients: 20 μ l 10x Opti Buffer (Mg free), 10 μ l 50 mM MgCl₂, 4 μ l 10 mM dNTPs, 4 μ l template DNA 20 ng/ μ l RFP marked, 1 μ l primer 1, 1 μ l primer 2, 1 μ l primer 3, 1 μ l primer 4, 1 μ l primer 5, 1 μ l primer 6, 1 μ l primer 7, 1 μ l primer 8, 150 μ l ddH₂O and 4 μ l BioxAct polymerase.

Temperature settings were: (1) 98° C for 30 sec, (2) 98° C for 25 sec, (3) 68° C for 2 min, (4) 72° C for 8 min, (5) 72° C for 10 min and 12° C forever. Step (2)–(4) were repeated 39 times.

Agarose gel electrophoresis

All experiments were controlled with a 1 %, 1x TAE buffer agarose gel electrophoresis which was run at 100 V.

Purification of DNA

The PCR-amplified DNA was separated by gel electrophoresis (1 % agarose gel, 1x TAE buffer) and then eluted from the gel with QIAquick PCR Purification Kit (50) by Qiaagen (Catalog No. 28104)

Cultivation of yeast

Budding yeast *Saccharomyces cerevisiae* was cultivated in a standard yeast peptone dextrose (YPD) medium at 30° C over night until it reached the exponential growth phase, which was suitable for the further

steps. The ideal growth rate, which was necessary for subsequent experiments, was at 8 % per hour

Lithium Acetate Yeast Transformation

For transformation, yeast DNA and PCR product were melted. The PCR DNA was marked either with GFP (in the first PCR) or RFP (in the second PCR).

Cells were inoculated from an o/n culture in 100 ml liquid YPD at OD₆₀₀ of 0.125 and were grown to an OD₆₀₀ of 0.5–0.7 at 30° C. After spinning at 2500 rpm for 3 min at RT and washing with 10 ml H₂O, the cells were resuspended in 1 ml H₂O and transferred to a microfuge tube. The cells were pelleted briefly at 3000 rpm for 2 min and all the H₂O was removed. The cells were resuspended in 1.5 ml 1x TE (10 ml 1 M Tris-HCl and 400 μ l 0.25 M EDTA in 990 ml ddH₂O) containing 1 % LiAc. 10 μ l of transforming DNA were mixed with 20 μ l herring sperm DNA (re-boiled before use) and 200 μ l yeast suspension were added. 1.2 ml sterile 40 % PEG 4000 solution (40 % PEG 4000, 1x TE containing 1 % LiAc), were incubated for 30 min at 30° C and heat shocked for 15 min in a 42° C water bath. The tubes were spinned for 10 sec, washed with 1 ml H₂O, resuspended in YPD, plated out and incubated at 30° C.

Fluorescence Microscopy

Fluorescence microscopy was performed by using an IX81 Olympus equipped with 100X/NA 1,4 objectives and an ORCA II camera by Hamamatsu. The wavelength of the light was 395 nm for GFP and 425 nm for the RFP. Live cells were grown in YPD medium to the log phase at 30° C over night and fixed on a normal microscope slide.

Image Analysis

Patch lifetime analysis was done by visually identifying every single appearance and disappearance in the pictures. ImageJ (<http://rsb.info.nih.gov/ij/download.html>)

software was used for the postprocessing of the single pictures.

Results

To investigate differential *in vivo* functions of lipids during endocytosis of budding yeast, the eight recently developed primers for YLR064w, YHL044w, YBR220c and YBR042c proteins were used. The DNA bands in the agarose gel, which was run before the transformation (to check if the primers marked in the proper condition) were unequivocally distinguishable.

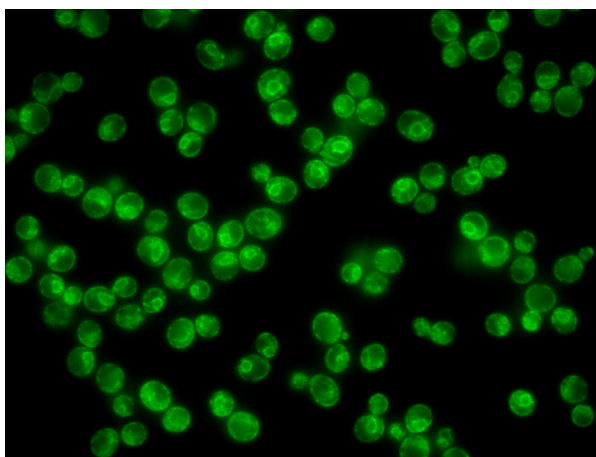


Fig. 1. YLR064w (green) activation during the beginning of endocytosis.

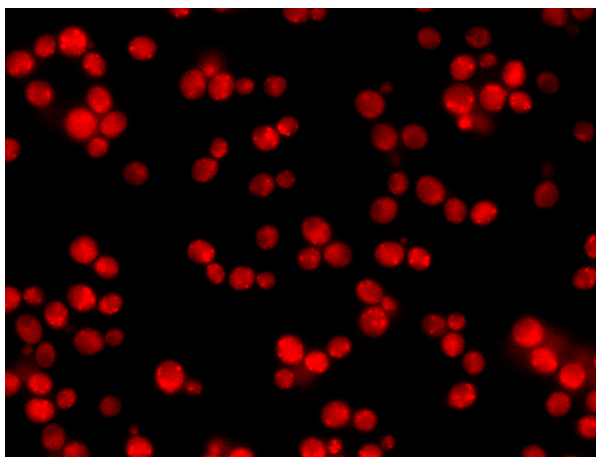


Fig. 2. The strong background signal indicates that YBR042c (red) interacts with PtdIns_(4,5)P₂.

After the lithium acetate yeast transformation the cells showed a large amount of

green and red fluorescence, which shows the different proteins in the differing states of endocytosis. It was necessary to use not only a GFP (green fluorescence protein) but also an RFP (red fluorescence protein) fusion protein since YBR220c and YBR042c did not show results when fused to GFP.

The proteins can be split up in two groups, which were calculated by their influence during endocytosis. Whereas YLR064w plays a rather important role at the beginning of endocytosis (fig. 1), YBR042c has its optimum activity just before the end of endocytosis and very near to the plasmosome (fig. 2).

Fluorescence microscopy shows a specifically high activity for YLR064w near the membrane at the beginning of the process and it disappears when the proteins approximate the cell nucleus.

Only YHL044w has a noticeable activity over the whole process of endocytosis and it seems to interact also with PtdIns_(4,5)P₂ during its way to the nucleus (fig. 3).

It seems interesting that only YBR220c shows a strange amount of fluorescence during the whole process of endocytosis and not only near the membrane but also very close to the nucleus.

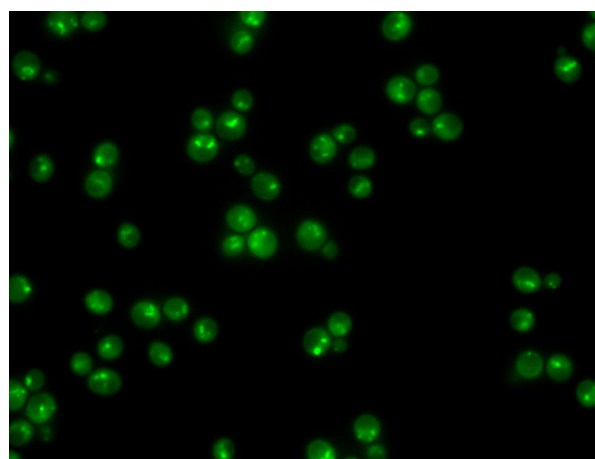


Fig. 3. Signal intensity of YHL044w (green) decreases at the nucleus.

Discussion

The results suggest that all of the examined proteins play important roles in endocytosis. YLR064w and YHL044w have their highest activity near the membrane and immune fluorescence signals decrease in the nucleus. Further experiments can be used to study the interaction of $\text{PtdIns}_{(4,5)}\text{P}_2$ with YLR064w and YHL044w since our findings suggest that YLR064w and YHL044w may interact with membrane lipids. It might be possible that these two proteins interact exceptionally with coated pits. Although it is now generally accepted that $\text{PtdIns}_{(4,5)}\text{P}_2$ powers late endocytosis and is strongly related to YBR042c, which can be clearly seen in the results, it can not be explained yet. It will be necessary to further investigate these interactions in the future.

Another interesting aspect seems to be which cargos are transported by YBR220c, because it is the only protein during the process of endocytosis which has a strong activity just at the nucleus (fig. 4). The resulting question is why it does not show such activity fluctuations as the other proteins and in what kinds of cargo transports it is involved. Further experiments will have to give answers of these questions.

Acknowledgements

I want to thank David Drubin for giving me the opportunity to visit his great lab and get a deeper insight in that fascinating field of life science. Otherwise warmest thanks to my supervisor Yidi Sun who answered me every question I asked and for her lovely welcome to me. Last but not least I want also thank all people who took care of me, particularly Prof. Dr. Heeg who hosted me in his lab and all members and mentors of the International Science Academy San Francisco 2007.

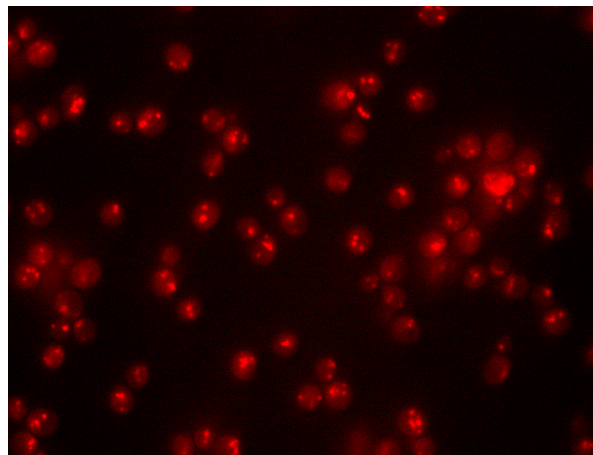


Fig. 4. YBR220c (red) has its highest activity at the nucleus

References

- [1] Yidi Sun, Sunsheelia Carroll, Marko Kaksonen, Junko Y. Toshima, and David G. Drubin, 2007 $\text{PtdIns}_{(4,5)}\text{P}_2$ turnover is required for multiple stages during clathring and actin-dependent endocytic internalization.
- [2] Yidi Sun, Marko Kaksonen, David T. Madden, Randy Schekman and David G. Drubin, 2005 Interaction of Sla2p's ANTH domain with $\text{PtdIns}_{(4,5)}\text{P}_2$ is Important for Actin-dependent endocytic.
- [3] Marko Kaksonen, Yidi Sun and David G. Drubin, 2003 Cell A Pathway of Association of Receptors, Adaptors and Actin during Endocytic Internalization.

Structural Similarities of Small Hairpin RNA Structure to the Inverted Terminal Repeat T-shape correlate with unsteadiness in packaging of Adeno-Associated Virus vectors for RNA interference gene therapy

Philipp Bayer and Daniela Paunescu

Laboratory of Mark A. Kay

Institute of Pediatrics and Genetics, Stanford University School of Medicine

Introduction

Gene therapy vectors derived from the single-stranded DNA (ssDNA) virus Adeno-associated virus (AAV) possess features that offer the leap from the laboratory bench to the clinic bedside for promises and hopes gene therapy raises. AAV has several characteristics that make it an appealing human gene therapy vector:

1. AAV requires the help of a co-infecting virus, usually adeno-virus (Ad), to efficiently complete its life cycle. Therefore it is naturally defective.
2. AAV establishes a lysogenic state in the absence of helper virus infection, mostly in a site-specific locus on chromosome 19.
3. Although AAV seroprevalence usually approaches 80% the virus has not been implicated as the causative agent for any known disease [1].
4. The 4680 nucleotide AAV genome allows for easy manipulation by standard recombinant DNA methodology.

There are several significant challenges currently preventing AAV from vaulting to the forefront of viral gene delivery systems, two of which refer to the development of accurate viral packaging methods. The

widespread development and use of AAV vectors will advance due to the development of an efficient packaging system that enables cost-effective production of high titer recombinant vectors. The second challenge arises out of the cumbersome vector production and purification procedures that are currently in use. Especially development of new packaging systems towards improvement of vector purity is crucial for successful medical appliance of gene therapy with AAV – particularly referring to existent public and professional scepticism towards gene-therapeutic approaches in medicine.

Unsteadiness in the length of packed viral DNA occasionally occurs during transfection with vectors containing cassettes for intracellular expression of small hairpin RNA (shRNA) for RNA interference (RNAi). The fusion of new RNAi – sequence-specific post-transcriptional silencing of gene expression mediated by small double-stranded RNAs – methodology with established gene transfer by viral vectors for efficient and tissue-specific RNAi delivery to patients is particularly promising from a medical point of view.

The 145 inverted terminal repeat sequences (itr) at each end of the 4680 nucleotide virus genome are the only known cis-acting elements that are required for packaging of AAV DNA. Therefore vectors containing heterologous genes flanked

by only the terminal 145 bases of AAV DNA are packaged into infectious particles. In the single-stranded form, the trs snaps back on itself to form a T-shaped three-way junction. This structure serves as the viral origin of DNA replication from which a large pool of replicative, double-stranded DNA (dsDNA) arises during AAV and Ad co-infection. The trs also contains elements that function as a transcription promoter [2]. The unsteadiness in packaging of shRNA containing vectors is suspected to occur due to an ability of shRNA to undertake several mentioned functions of the viral itr based on similarities in structuring of the T-shaped itr and the shRNA hairpin.

This hypothesis has never been proven as a fact in appropriate experiments and is subject of this work. To prove correlations the shRNA gene hairpin structure was dislocated by recombinant cloning of existing *psdsAAV-H25* vector [3]. Three constructs were tested for existing unsteadiness and length of extracted viral DNA after transfection in Human embryonic kidney cells.

Material and Methods

Generation of Vector D

A 582 bp fragment spanning the human U6 promoter driving a 25mer shRNA directed against human alpha-1-antitrypsin (hAAT) was PCR-amplified, using plasmid *psdsAAV-H25* (Grimm et al., Nature, 2006) as template, and as primers 5'-CT GACTGCGGCCGCGAGTCCAACAC C-3' and 5'-GCCTAGGGCGCGCCAAA AAAGAAGCGTTTAGGCATGTTTAAACA TC-3'. The primers contained a *Not* I (bold) or *Asc* I (bold/underlined) site for subsequent straight-forward cloning into the *Asc* I/*Not* I digested plasmid *psdsAAV-U6* (Grimm et al., manuscript in preparation). The PCR was carried out in a PTC-200 Thermal gradient cyler (MJ Research, Waltham, MA, USA), using Platinum Pfx Polymerase (Carlsbad, CA, USA) and supplied reagents according to manufacturer's

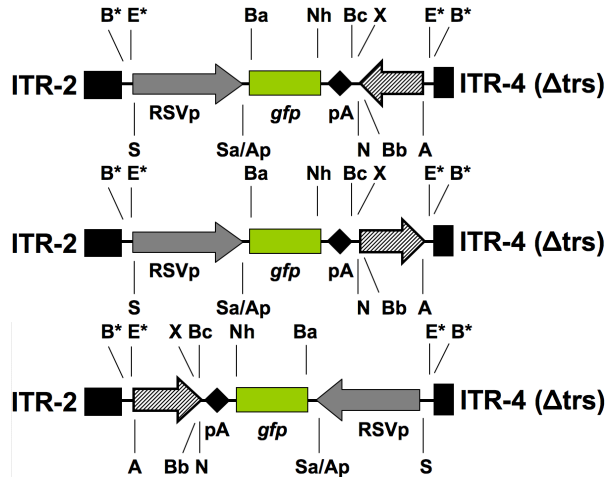


Fig. 1. Map of AAV Vectors designed by Grimm

Table 1. The important cleavage sites and the actual restriction enzymes

cut surface	restriction enzyme
A	<i>Asc</i> I
B	<i>Bgl</i> II
E	<i>Fro</i> RV
N	<i>Not</i> I
S	<i>Sal</i> I
X	<i>Tho</i> I

instructions (annealing temperature was 60° C, extension time was 1 min).

Generation of Vector C

Plasmid *psdsAAV-H25* was digested with *Bgl* II, in order to release a ~2.2 kb band representing the bi-cistronic insert (RSV promoter driving the *gfp* gene, as well as human U6 promoter driving an *anti-hAAT* shRNA). This band was separated from the ~3.3 kb plasmid rest via DNA gel electrophoresis (1% agarose gel). Both fragments were isolated from the gel (using the Gel extraction kit from QIAGEN, Valencia, CA, USA). To prevent religation of the 3.3 kb plasmid backbone, this fragment was dephosphorylated using Shrimp Alkaline phosphatase according to manufacturer's instructions (Promega, Madison, WI, USA). The reaction was terminated after one hour by heating the sample for 15 min at 68° C.

DNA gel purification

DNA fragments were extracted from agarose gels after electrophoresis (1% agarose gel, 1xTAE as running buffer) using the QIAquick Gel Extraction Kit (QIAGEN, Valencia, CA, USA).

Ligation of DNA fragments

Ligations of purified (see above) DNA fragments were carried out using T4 DNA ligase (NEB, Beverly, MA, USA). Therefore, plasmid and insert were mixed in a 1:5 ratio in a total volume of 20 μ l (containing DNA ligase and supplied buffer) and incubated for at least 1 h at room temperature (or overnight at 16°C).

Cell Transformation

For transformation of ligated DNA into *E. coli* K12, 2 μ l from a ligation reaction were added to 40 μ l of chemically competent DH10B *E. coli* (Max Efficiency, Invitrogen), incubated on ice for 30 min and heat shocked for 60 sec at 42°C. 400 μ l of SOC medium were then added followed by incubation in a 37°C shaker for 30 to 60 min. 100 μ l from the transformation reaction were plated out on LB-Agar with Ampicillin (100 μ g/ml) and incubated overnight at 37°C. Individual colonies were picked from the plates and grown in 4 ml of LB/Amp medium for 12-16 h.

Mini Prep and Mega Prep

For preparation of "Mini Prep" plasmid DNA, 1.5 ml of transformed *E. coli* cells (see above) were collected by spinning at 14,000 rpm for 3 min at room temperature. Plasmid DNA was then purified using the QIAprep Spin Miniprep Kit (QIAGEN, Catalog No. 27104), according to provided instructions. For preparation of "Mega Prep" plasmid DNA, 500 ml of transformed *E. coli* cells were collected by spinning at 6,000 rpm for 15 min at 4°C. Plasmid DNA was then purified using the Mega Prep Kit from Invitrogen, according to provided instructions.

Production of rAAV

Human embryonic kidney 293 cells were grown in DMEM with 10% fetal bovine serum (FBS), penicillin/streptomycin and antibiotics/antimycotics (all Gibco BRL) for 3 days. For each AAV virus stock, 20x 225 cm² flasks were plated at a density of $\sim 3 \cdot 10^6$ cells per flask (in 40 ml DMEM). Per flask, 25 μ g of an AAV vector plasmid (four different plasmids were used: *TTR-hfIX*, *lacZ1.6*, *sAg25*, *luc29*) were aliquoted, along with 25 μ g of an AAV-2 helper plasmid (*pHLP19*) and 25 μ g of an adenoviral helper construct (*plAdeno5*). (The four different plasmids have different positions of shRNA and they have different types of ITRs.)

The transfection was carried out using calcium phosphate methodology. Therefore, per flask, 4 ml of 300 mM calcium chloride solution and 4 ml of 2x HBS were mixed with the three plasmids (AAV vector, AAV helper, adenoviral helper). Following a media change on the plated flasks (20 ml of old DMEM were replaced with fresh DMEM), 8 ml of the DNA/calcium/HBS mix were added to each flask. The media was changed again (this time entirely, and leaving out FBS) after a 5 hour incubation, and the cells were then further incubated for 3 days at 37°C and 5% CO₂. After this period, the cells containing the recombinant AAVs were harvested by adding 0.5 ml of 0.5 M EDTA to each flask and incubating for 5-10 min. The cells were then collected (by tapping the flasks and pipetting up and down) and pelleted at 3,000 rpm for 15 min. The cell pellet was finally resuspended in Benzonase buffer (~ 1 ml per flask).

Purification:

To digest and eliminate cellular or non-packaged viral DNA, Benzonase endonuclease was added (0.8 μ l/ml of virus solution) and incubated for 1 h at 37°C. Following a 15 min centrifugation at 4,000 rpm, the supernatant was transferred into a new tube, 1/39 volumes of 1 M calcium chloride were added and the reaction was again incubated

Table 2. Standard table for cesium chloride precipitation (Nakai et al., 1998) with RI average values compared to the actually measured RIs.

Fraction	Volume	Average RI
11	0.5 ml	1.3781
12	0.5 ml	1.3760
13	0.5 ml	1.3755
14	0.5 ml	1.3737
15	0.5 ml	1.3720
16	0.5 ml	1.3710
17	0.5 ml	1.3700
18	0.5 ml	1.3698

for 1 h, this time on ice. After a 15 min centrifugation at 4,000 rpm, the supernatant was transferred into a new tube and mixed with 1/4 volumes of 40 % PEG8000/2.5 M NaCl, followed by overnight incubation on ice. The next morning, AAV particles were precipitated by centrifugation at 4,000 rpm for 30 min. The viral pellet was resuspended in Na-HEPES/EDTA buffer (20 ml) under vigorous pipetting. Cesium chloride was then added (13.2 g per stock) and the refractive index (RI) of the suspension was adjusted to 1.3710 with NA-HEPES/EDTA buffer using a refractometer. The solution was centrifuged for 23 h at 45,000 rpm and 21° C in a Beckman Ultracentrifuge, using a 70 Ti rotor. Fractions of 0.5 to 3 ml were then collected from the bottom of each tube and analysed further. The fractions were collected according to table 2.

Viral DNA preparation

To extract DNA genomes from viral particles, 5 µl of each AAV stock were mixed with 20 µl of 10x ProtK buffer, 13 µl Proteinase K (Invitrogen) and 162 µl H₂O, and incubated for 1 h at 55° C. The DNA was then purified using the DNA extraction kit from Wako, according to manufacturer's instructions.

Southern Blotting

Extracted viral DNAs were separated on 1 % agarose gels and then transferred onto nitro-

cellulose membranes via overnight capillary transfer.

The membranes were then cross-linked and pre-hybridized at 66° C for 1 hour in PerfectHyb buffer (SIGMA). Radioactive (³²P) probes were generated using *Bgl* II fragments of the respective AAV vector plasmid as templates, and using the Random Priming II Kit from Stratagene according to provided instructions. The membranes were incubated overnight with the appropriate radioactive probe in a rotation oven set at 66° C, and next day washed with low and high stringency buffers (2x SSC/0.1 % SDS or 0.1x SSC/0.1 % SDS respectively) for 2 times, 20 min each. Bands corresponding to AAV vector DNA were detected and quantitated using a Biorad Phosphoimager and provided software.

Results and Discussion

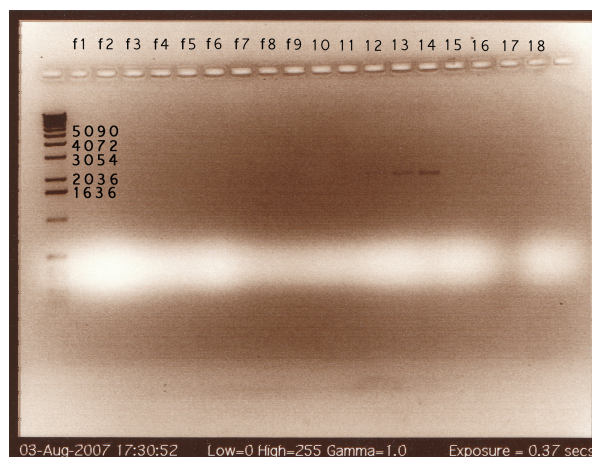


Fig. 2. Gel electrophoresis of extracted viral DNA (Vector E), ordered by number of collected fractions (f1-f18, see table 2)

Gel electrophoresis could not prove existence of viral genomes shorter than the expected length of 4680 nt occurring during rescue neither for the original vector *psdsAAV-H25* (data not shown) nor for the created vectors Vector E (fig. 2) and Vector D (data not shown). Conclusive evidence was expected from the blotting results due to superior sensitivity of the radioactive

method but results appeared rather defective. A reason could be the late fixation and analysis of the data caused by the untimely departure of the investigating scientific team.

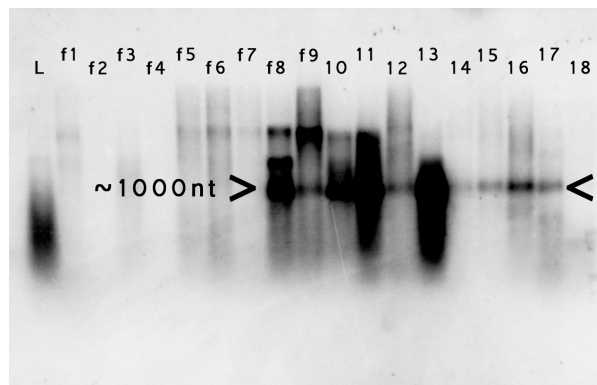


Fig. 3. Defective radioactive blots: *psdsAAV-H25* blot shows marked DNA material containing 1000 nt-fragments (est.)

Predictions can be derived from the *psdsAAV-H25* vector results (fig. 3). Though blurred, the blot shows aggregation of DNA around 1000nt on lanes 8 to 17. For *psdsAAV-H25* the length matches the distance in nucleotides between the shRNA hairpin and the ITR-4 (Δ trs). Then it is speculated that the hairpin and the ITR frame the finally packaged DNA fragment during virus rescue and thereby define the length of the viral genome. The present results are not adequate to prove unsteadiness in packaging of AAV or further on a certain connection to the shRNA hairpin's localization. Experiments should be repeated and more vector constructs

should be designed for investigation of specific interactions between the hairpin and different ITRs (serotype 1-11).

Acknowledgements

At first we like to thank Prof. Marc A. Kay for his kind hospitality and the greatest liberties one may concede to interning high school students. Special thanks go to Jeffery Giering, Neil Phillips, Lora Wang and especially Yul Yang for scientific support, perfectly wonderful talks and shared daily lab-experiences. Finally our special thanks go to Dr. Dirk Grimm who kindly and patiently introduced us first to the thrilling fields of viral gene therapy and RNAi, then to the viands offered by Peete's Coffee, Cold Stone and Jamba Juice.

Last but not least there is a special thanks referring to all preparations, hints and encouragements unseen to the reader of this documentation provided by mentors and alumni of the Heidelberg Life-Science Lab in which the founders of both the unique Lab program and this brilliant academy should be mentioned in the first place.

References

- [1] Flotte TR, Afione SA, Conrad C, McGrath SA, Solow R, Oka H, Zeitlin PL, Guggino WB, Carter BJ. Stable *in vivo* expression of the cystic fibrosis transmembrane conductance regulator with an adeno-associated virus vector. *Proc Natl Acad Sci USA* 90(22):10613-7. 1993
- [2] Parks WP, Boucher DW, Melnick JL, Taber LH, Yow MD. Seroepidemiological and Ecological Studies of the Adenovirus-Associated Satellite Viruses. *Infect Immun* 2(6):716-722. 1970
- [3] Grimm D, Kay MA. RNAi and Gene Therapy: A Mutual Attraction. *Hematology Am Soc Hematol Educ Program* 2007:473-81. 2007

The Rab9 effector GCC185 interacts with several other Rab family proteins

Leonie Kastner and Dustin Klinger

Laboratory of Suzanne R. Pfeffer

Department of Biochemistry, Stanford University School of Medicine

Abstract

During intracellular transport processes proteins are delivered to their specific destination by membrane-bound vesicles. Accuracy and precision of these transport processes are provided by Rab GTPases, enzymes that catalyze many of the necessary reactions required for proper transport. The correct function of several pathways, e.g. the mannose 6-phosphate receptor (MPR) pathway, depends upon Rab GTPases. It is known that the MPR pathway is also dependent upon the Rab9 effector protein GCC185. While the role of Rab9 within the MPR pathway has been studied more extensively, the role of GCC185 has yet to be fully characterized. There are likely other unidentified proteins that GCC185 interacts with in addition to Rab9 and they also play crucial roles within the MPR pathway. To gain further information about how GCC185 contributes to the MPR pathway, the interaction with 56 other human Rab proteins was tested by using a yeast-two-hybrid screen.

It has been confirmed that GCC185 binds to Rab6 and Rab9 and a new and previously unknown interaction between GCC185 and few other Rabs (1A, 1B, 30, 33B, 35) was shown. It will now be important to confirm these interactions *in vitro* with purified proteins and to carry out subsequent experiments to identify the significance of these interactions within the MPR pathway.

Introduction

Rab proteins are monomeric GTPases that are vital for regulating diverse vesicular transport processes within cells. Vesicles that contain proteins destined either for the plasma membrane, the Golgi apparatus or secretory vesicles must be directed to their specific target subcellular compartment. Rab GTPases mediate and control the target oriented transportation of vesicles from one cell compartment to another through binding to effector proteins. These effectors catalyze many vesicular transport processes such as vesicle formation, vesicle motility, vesicle docking and vesicle fusion with the target membrane.

Rab proteins regulate the activity of effector proteins by facilitating their proper localization inside the cell and act as molecular switches as they are able to change between an active GTP-bound and an inactive GDP-bound state. When active and bound to GTP, Rab proteins are able to bind to effector proteins. However, when Rabs are bound to GDP their binding to effector proteins is inhibited. Thus, Rabs can only localize effector proteins and allow for the catalysis of vesicular transport when bound to GTP.

Suzanne Pfeffer's lab has focused on the mannose 6-phosphate receptor (MPR) and its circle pathway between the trans-Golgi network (TGN) and the early endosomes. When localized in the Golgi, MPR binds to newly synthesized lysosomal enzymes and carries them to the early endosomes where the lysosomal hydrolases are released due to

the acidic environment. MPR is then recycled back to the trans-Golgi network for reuse through a Rab9 GTPase dependent step (Ghosh et al. 2003).

One previously identified Rab9 effector, GCC185, has been proved to be necessary in the MPR recycling pathway (Reddy et al. 2006). GCC185 is a Golgi-localized putative tether of the Golgin protein family, which are generally large coiled-coil proteins, important for Golgi organization, vesicle tethering, and secretory protein transport. To further understand the role of GCC185 in the MPR pathway, the ability of GCC185 to bind to other human Rab protein family members was investigated. The identification of other Rabs binding to the effector will offer further insight into the function of GCC185 within the MRP pathway by providing additional clues to the mechanism of its action. Specifically, the interaction of 57 different human Rab proteins with the C-terminus and full length of GCC185 was tested through the use of a yeast-two-hybrid screen.

Material and Methods

Cloning the Full-length Gene of GCC185 into a Vector

The gene for the GCC185 full-length protein was cloned into the *pACT2* vector by incorporating the gene into the multiple cloning site (MCS) between the restriction sites of *NcoI* and *BamHI*. After cloning, the *pACT2* vector was transformed into XL-1 Blue cells in media containing ampicillin (Amp).

The *pACT2* vector encoded for an Amp resistance. Cells that were growing on the ampicillin plates were then put into a liquid Amp media over night, and DNA from the cells was subsequently purified using the QIAprep Spin Miniprep Protocol. The vector encoding the C-terminus of GCC185 and the vectors encoding the 57 different Rabs had been previously created by the Pfeffer Lab and were kindly provided for this work. The gene of the C-terminus of GCC185 had been inserted into *pACT2*, the Rab proteins were cloned into the *pGBT9* vector between the restriction sites of *EcoRI* and *BamHI*.

Vector Digestion

To verify if the cloning had been successful and the vector included the insert encoding for the full-length *GCC185*, the samples were digested with *NcoI* and *BamHI*.

2 μ l of the purified DNA sample were added to 2 μ l 10x Buffer 3, 2 μ l 10x BSA, 12 μ l of double distilled water, 1 μ l of *BamHI* and 1 μ l of *NcoI*.

Additionally, the vector *pACT2* was digested with *EcoRI* to ensure it was correct, by using 6 μ l of the purified vector, 2 μ l *EcoRI* buffer, 2 μ l 10x BSA, 1 μ l *EcoRI* and 9 μ l double distilled water. Both samples with a total volume of 20 μ l were incubated at 37° C for 3 h.

If *pACT2* includes the insert with a length of about 5 kb, this gene can be excised by using *NcoI* and *BamHI*. After digesting the vector, two bands are expected, one with the size of the vector (8.1 kb) and one representing the insert with a length of 5 kb.

pACT2 has a length of 8.1 kb and one restriction site for *EcoRI* at the MCS. Therefore it was expected to yield one linear piece of DNA with a length of 8.1 kb for the second digestion.

Agarose Gel Electrophoresis

To evaluate the digestion, an agarose gel electrophoresis was performed by using a 3% agarose gel (3 g agarose, 300 ml buffer [20 ml 50x TAE (242 g Tris; 57.1 ml 100% acetic acid; 100 ml 0.5 M EDTA; pH 8.0), 980 ml distilled water]).

5 μ l of DNA-Ladder were added to Lane 1. 4 μ l of 6x loading dye were added to the full amount (20 μ l in total) of the two digestion samples before putting the samples to their respective lanes. The vector digested with *EcoRI* was put into Lane 1 and the vector including the inserted *GCC185* gene and digested with *NcoI* and *BamHI* into Lane 2.

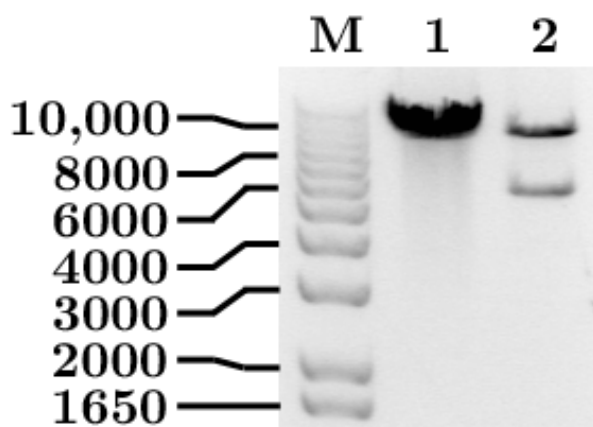


Fig. 1. Agarose gel electrophoresis to check the vector and the insertion of the full-length *GCC185* gene. M: DNA-Ladder – 1: *pACT2* vector digested with *EcoRI* – 2: *pACT2* vector with inserted *GCC185* digested with *NcoI* and *BamHI*.

Lane 1 of fig. 1 clearly shows one band with a length of about 10 kb. The plasmid has been cleaved by the restriction enzyme once as it has been expected. It has therefore been shown that *pACT2* has one restriction site for *EcoRI*.

Lane 2 contains the vector, including the full-length gene of *GCC185* that has been

digested with *BamHI* and *NcoI*. Two bands are recognizable, one has a length of about 6 kb, the other one of about 10 kb. The larger one is identified as the plasmid, the smaller one is the inserted *GCC185* gene.

PJ69-4A component yeast cells

PJ69-4A yeast cells were taken from overnight culture and diluted to an OD_{600} of 0.15 in YPDA media. The cells were incubated at 30° C until they showed an OD_{600} of 0.5–0.6. 100 ml of the culture volume was centrifuged at 3,300 rpm for 5 min. After discarding the supernatant the cells were resuspended in 50 ml of sterile H₂O and centrifuged as before. The pellet was resuspended in 12.5 ml LiSorb (100 mM LiOAc, 10 mM Tris-HCl, pH 8.0, 1 mM EDTA, pH 8.0, 1 M Sorbitol, filter sterilized). Then the solution was centrifuged again and the pellet resuspended as before. 10 μ l of Gibcon Salmon Sperm DNA were added to the yeast solution (that had been 100 ml in the beginning) and the sample was immediately gently mixed. The cells were then frozen at -80° C.

Transform *GCC185* (full-length and C-terminus) and several Rab-genes into yeast cells

Before starting the transformation, the cells were thawed at room temperature. 57 different samples were made, each started with 25 μ l of the PJ69-4A yeast cells. 1 μ l of the *pACT2* vector which included the gene for the C-terminus of *GCC185* or the full-length *GCC185*-gene was added to each sample. Additionally 1 μ l of *pGBT9* that contained one of the 57 Rab GTPases was added to the respective sample. 150 μ l LiPEG (100 mM LioPC, 10 mM Tris, 1 mM EDTA, 4000 mg/ml PEG-3350) were put into each test-tube, the samples were vortexed and then incubated for 15 min at RT. After adding 17.5 μ l dimethylsulfoxide (DMSO) and vortexing again, the cells were heat-shocked at 42° C for 15 min.

Afterwards, all samples were centrifuged at less than 2,000 rpm for two minutes. Af-

ter discarding the supernatant, the cells were resuspended in 200 μ l of sterile water and 100 μ l of each sample were placed and spread onto Petri dishes with media lacking leucine and tryptophan and a limiting concentration of adenine. The media was formulated using the following protocol:

6.7 g yeast base (Sigma) and 2.0 g amino-acid mix (all amino acids except tryptophan and leucine) were added to 500 ml water, pH was adjusted to 6.5, then 20 g agar were added. 20 g of glucose were added to another 500 ml of water and both solutions were autoclaved. Afterwards, the solutions were combined and 20 ml adenine (2 mg/ml) were given to the mixture. 25 ml of this solution were allocated to each Petri dish and allowed to solidify overnight.

After placing the cells onto the media, they were incubated at 30° C for 5 days.

Streaking out the colonies on Leu⁻, Trp⁻, and His⁻ plates

Five different colonies from the Petri dishes, grown from the Rab/GCC185 transformed cells were streaked out on a Petri dish, yielding five streaks for each Rab/GCC185 combination. First they were streaked on non selective plates (Trp⁻, Leu⁻, low adenine) again, as a control of viability. Subsequently, the colonies were streaked likewise on plates additionally lacking histidine (Trp⁻, Leu⁻, His⁻), this type of media being known as triple-knockout. The dishes were incubated at 37° C for 3 days.

Yeast-two-hybrid screen

The yeast-two-hybrid screen is used to identify protein-protein interactions. To investigate the interaction of the Rab9 effector protein GCC185 with the 57 human Rab GTPases, two plasmids, *pGBT9* and *pACT2*, were transformed into PJ69-4A component yeast cells.

In addition to the Rab genes, the vector *pGBT9* included a GAL4 Binding Domain (BD) and a gene encoding for an enzyme needed in tryptophan (Trp) production. The plasmid *pACT2* included the

gene for the full-length or the C-terminus of GCC185 and a GAL4 Activation Domain (AD), a gene encoding for an enzyme that is necessary for the production of leucine (Leu). If placed on media without leucine and tryptophan (Leu⁻, Trp⁻), only cells that took up both vectors are able to grow since they have an auxotrophy for both amino acids. If one or both plasmids are missing, the cells are not able to grow. To prove an interaction between the GCC185 full-length protein or its C-terminus with the Rab GTPases, the cells are placed on media additionally lacking Histidine (Leu⁻, Trp⁻, His⁻). This method is also known as a triple-knockout. If both proteins that are encoded on the two transformed vectors and necessary for the production of leucine or tryptophan, bind to each other, the GAL4 AD and the GAL4 BD can interact as well. In this case, an enzyme required for the production of histidine (His) is expressed. If the Rab protein and the effector protein, (in this case) GCC185, do not interact, the GAL4 BD and the GAL4 AD do also not interact. Histidine can not be produced and the yeast cells are not able to grow on the triple-knockout plates. Therefore, there will only be growth on the Leu⁻, Trp⁻, His⁻ plates if there is an interaction between the effector and the Rab protein.

Results

The gene of the GCC185 C-terminus was successfully cloned into the multiple cloning site of the *pACT2* vector. Accordingly, the gene of GCC185 full-length has been cloned separately. This was verified by a restriction digestion (see Material and Methods).

The yeast-two-hybrid screen confirmed Rab9 binding to the C-terminus of GCC185 as it has been proved previously (Reddy et al. 2006 A functional role for the GCC185 Golgin in mannose 6-phosphate receptor recycling.) and showed that Rab30 and probably Rab33b are also interacting with the last 110 residues of the Golgin (fig. 2). This

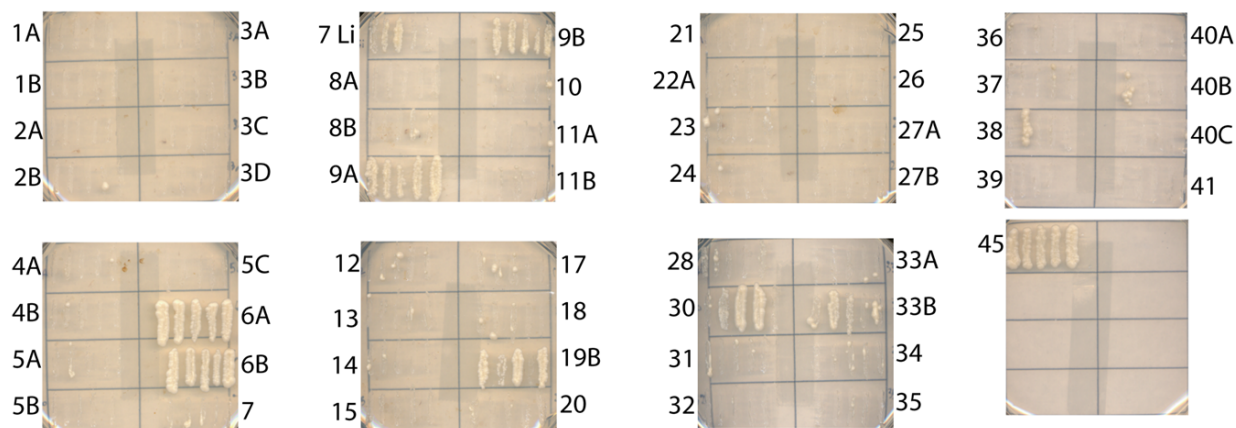


Fig. 2. Yeast-two-hybrid screen between the C-terminus of GCC185 and the different Rab GTPases showing a clear interaction between Rab6a, 6b, 9a, 9b, 19b, 30 and 45 and the effector protein. There might be also an interaction between the Rab9 effector and Rab7li and 33b.

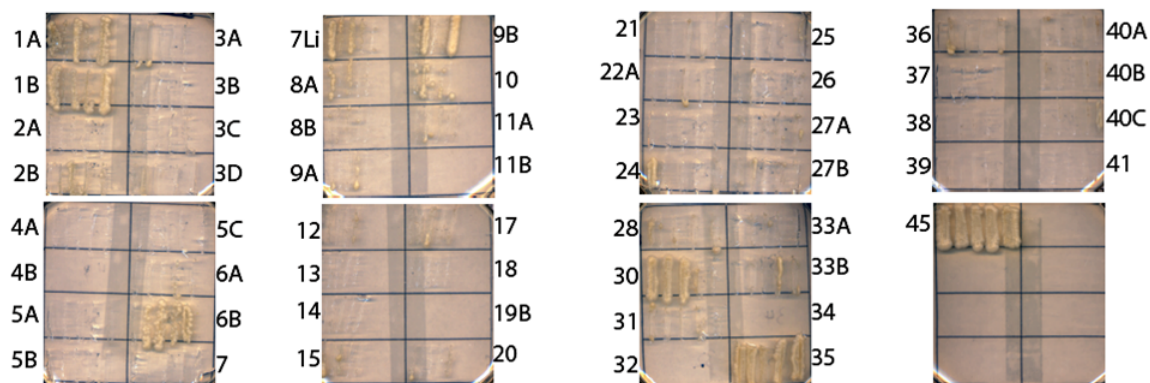


Fig. 3. Screening of the interaction of GCC185 full-length with the respective Rabs. Rab1a, 1b, 6b, 9b, 30, 35 and 45 showed an affinity to the effector.

an exiting result as there have been no previous studies concluding an interaction between GCC185 and Rab30 or Rab33b. Also other Rab proteins (7Li, 19b and 45) showed a positive interaction with the C-terminus of GCC185. However, these Rabs have provided many false positives in previous yeast-two-hybrid experiments conducted by members of the Pfeffer lab and are not thought to represent actual interactions.

Screening the interaction of full-length GCC185 with the 57 Rab GTPases, it has been shown that Rab1a, Rab1b and Rab35 bind to the effector protein elsewhere than at the C-terminus (fig. 3).

Corresponding to the results of the in-

vestigation with the C-terminus, Rab6b, Rab9b, and Rab30 bind to the full-length protein. Interestingly, Rab6a and Rab9a both interacted with the C-terminus, but did not show an affinity to full-length GCC185.

A reason for the missing interaction with the full-length protein might be that GCC185 is a large coiled-coil protein and the constitution in full-length is different than the one in C-terminus. Therefore the binding domain of Rab6a and Rab9a might be masked in the constitution of the whole protein or the recognition-area is too far away from the binding domain.

It will now be important to verify the results of the yeast-two-hybrid screen with

purified proteins to confirm the tested interactions and exclude any wrong conclusion. Future experiments will seek the significance of these interactions between Rabs and the effector protein GCC185 within the MPR pathway. Moreover, the binding site for each Rab GTPase at GCC185 will be localized by using truncations of the protein.

Acknowledgements

Our sincere thanks are expressed to Professor Suzanne R. Pfeffer who kindly hosted us in her lab and gave us the chance to actively participate in her research. We also like to thank James K. Godfrey who guided our first and following working steps in the lab and kindly let us partake in his work. Special thanks go to Garret Hayes for mentoring all three of us and being open for questions at any time. We also express our gratitude to Benedikt B. Brommer. He spent three months in the Pfeffer

Lab and made our time pleasant and helped us to understand everything.

Moreover, we want to thank all other members of the Pfeffer Lab: Leo Serrano, Eric Espinosa, Ryan Nottingham, Melissa Laughery and Shirley Sutton for making our stay at Stanford an unforgettable and magnificent experience.

References

- [1] Reddy et al.. A Functional Role for the GCC185 Golgin in Mannose 6-Phosphate Receptor Recycling. *Mol Biol Cell* 17(10):4353–4363. 2006
- [2] Ghosh et al.. Mannose 6-phosphate receptors: New Twists in the tale. *Nat Rev Mol Cell Biol* 4(3), 202–212. 2003
- [3] Derby et al.. The trans-Golgi Network Golgin, GCC185, is Required for Endosome-to-Golgi Transport and Maintenance of Golgi Structure. *Traffic* 8(6):758–773. 2007

Invasion of a two-deme population by an imprinting allele

Tina Schmidt

Laboratory of Marcus W. Feldman
Department of Biological Science, Stanford University

Abstract

Unlike most genes, imprinted genes function differently depending on whether they come from mother or father, often resulting in the expression of those genes from only one of the two parental chromosomes. In order to study the evolution of genetic imprinting, Spencer and Clark mathematically constructed and analyzed a two-locus, two-allele modifier model. One locus codes for a character under viability selection and the second locus is a cis-acting modifier of imprinting. The authors study the effect of genomic imprinting in a population consisting of two demes, which are connected by male-only migration [2]. Here, the model is developed further by adding deme specific dominance parameters in order to examine the conditions in which the imprinting allele can invade a population.

Introduction

Genomic imprinting – the differential expression of mammalian genes depending on the sex of the parent from which they are inherited – was discovered in the early 1980s and is subject of a significant research effort today. Epigenetic instructions, such as DNA methylation are crucial for the function of genomic imprinting. Depending on whether the allele is paternally or maternally inherited, it exhibits different patterns of DNA methylation. These imprints are established during the development of germ cells into sperm or eggs [4].

Over 80 transcriptional units are known

to be imprinted in mammals, located in 27 chromosomal regions [1]. About 80% of all imprinted genes are linked in clusters with other imprinted genes [4].

Imprints can suppress, attenuate or activate the expression of a small number of genes in a parent-of-origin specific manner. Imprinting can reduce the expression of a gene from a default state of biallelic to monoallelic expression, but for many genes, the silencing is only partial [1].

Imprinting is thought to influence the transfer of nutrients from the mother to the fetus and the newborn, and it also tends to affect growth in the womb and behavior after birth [4]. Aberrant imprinting disrupts development and is the cause of various disease syndromes, including Prader-Willi syndrome, Beckwith-Wiedemann syndrome and several cancers [1].

Since imprinting alters the usual biallelic genetic expression to a monoallelic state in at least some tissues for some period of development, the imprinted locus is effectively hemizygous for that period. This pseudo-hemizygosity removes the effect of diploidy and consequently the organism is exposed to deleterious mutations that might otherwise not be expressed from a normal locus. Still, imprinting has evolved at many mammalian loci and therefore it is likely that imprinting has a selective advantage.

Spencer and Clark mathematically model a hypothesis that proposes that imprinting will evolve in situations in which selection favors offspring being similar to the parent of one sex, the “Chip off the old block”-

Table 1. Fitness for the gametes in deme X and Y

in deme X				
	$x_{1_m} AE$	$x_{2_m} Ae$	$x_{3_m} aE$	$x_{4_m} ae$
$x_{1_f} AE$	1	1	$1 - hs$	1
$x_{2_f} Ae$	1	1	$1 - hs$	1
$x_{3_f} aE$	$1 - hs$	$1 - s$	$1 - s$	$1 - s$
$x_{4_f} ae$	$1 - hs$	$1 - s$	$1 - s$	$1 - s$

in deme Y				
	$y_{1_m} AE$	$y_{2_m} Ae$	$y_{3_m} aE$	$y_{4_m} ae$
$y_{1_f} AE$	$1 - t$	$1 - t$	$1 - kt$	$1 - t$
$y_{2_f} Ae$	$1 - t$	$1 - t$	$1 - kt$	$1 - t$
$y_{3_f} aE$	$1 - kt$	1	1	1
$y_{4_f} ae$	$1 - kt$	1	1	1

hypothesis. The analyzed model of two demes, connected by migration, contains three parameters: The migration rate, the recombination rate and the selection pressure, which is the same in both demes [2]. Here, dominance parameters for each deme are added to the model.

The purpose of this study is to explore the conditions under which the e allele can invade a population fixed at the modifier locus for the E allele. Such invasion can be thought of as the evolution of genomic imprinting.

Model

A two-locus, two-allele modifier model is constructed. The two demes X and Y are connected by migration. It is assumed that only males migrate at a rate m . Recombination occurs in both males and females at a rate r . The effects of genetic drift and mutation are ignored. Mating is random within each deme.

In the context of this study, a modifier locus that acts late enough in gametogenesis that the imprinting status of an allele at the primary locus depends only on the identity of the modifier allele present in the gamete is called a cis-acting gametic modifier. The

modifier allele is assumed to be a cis-acting gametic modifier which inactivates the paternally inherited allele. Sperm with the imprinting allele e inactivate the allele at the A locus in the resulting offspring; sperm with the Mendelizing allele E do not. Individuals with an inactivated allele are assumed to have the same fitness as homozygotes for the activated allele. s and t are the selection coefficients for the A locus and h and k are the dominance coefficients in deme X and in deme Y , respectively. In deme X , the AA genotype is selectively favored, with Aa genotypes having a fitness $1 - hs$ and aa genotypes $1 - s$. In deme Y , the aa genotype is selectively favored, with Aa genotypes having a fitness $1 - kt$ and AA genotypes $1 - t$.

Table 1 shows the fitness matrix for the individuals in deme X and Y . Columns show the paternal allele and rows show the maternal allele.

We keep track of the haplotype frequencies in each deme instead of allele frequencies. Distinguishing between male and female frequencies is not necessary, since they are regenerated afresh each generation from the postselection, premigration haplotype frequencies. The four possible haplotypes

AE , Ae , aE and ae are numbered 1–4. Let x_i and y_i denote these frequencies in deme X and Y , respectively, where i denotes the haplotype number. Then the postmigrational frequencies, denoted by the addition of subscripts f and m for females and males, respectively, are given by

$$x_{i_f} = x_i \quad (1)$$

$$x_{i_m} = x_i(1 - m) + y_{i_m} \quad (2)$$

$$y_{i_f} = y_i \quad (3)$$

$$y_{i_m} = y_i(1 - m) + x_{i_m} \quad (4)$$

Assuming, that selection occurs after zygote formation, the required recursions, in which the prime indicates the respective frequencies in the following generation, are thus given by

$$\begin{aligned} \overline{w_x}x'_1 &= x_{1_f} \cdot (x_{1_m} + x_{2_m} + (1 - hs) \cdot x_{3_m} \\ &\quad + x_{4_m}) + x_{1_m} \cdot (x_{1_f} + x_{2_f} \\ &\quad + (1 - hs) \cdot x_{3_f} + (1 - hs) \cdot x_{4_f}) \\ &\quad - r \cdot d_x \end{aligned} \quad (5)$$

$$\begin{aligned} \overline{w_x}x'_2 &= x_{2_f} \cdot (x_{1_m} + x_{2_m} + (1 - hs) \cdot x_{3_m} \\ &\quad + x_{4_m}) + x_{2_m} \cdot (x_{1_f} + x_{2_f} \\ &\quad + (1 - s)x_{3_f} + (1 - s) \cdot x_{4_f}) \\ &\quad + r \cdot d_x \end{aligned} \quad (6)$$

$$\begin{aligned} \overline{w_x}x'_3 &= x_{3_f} \cdot ((1 - hs) \cdot x_{1_m} + (1 - s) \cdot x_{2_m} \\ &\quad + (1 - s) \cdot x_{3_m} + (1 - s) \cdot x_{4_m}) \\ &\quad + x_{3_m} \cdot ((1 - hs) \cdot x_{1_f} + (1 - hs) \\ &\quad \cdot x_{2_f} + (1 - s) \cdot x_{3_f} + (1 - s) \\ &\quad \cdot x_{4_f}) + r \cdot d_x \end{aligned} \quad (7)$$

$$\begin{aligned} \overline{w_x}x'_4 &= x_{4_f} \cdot ((1 - hs) \cdot x_{1_m} + (1 - s) \cdot x_{2_m} \\ &\quad + (1 - s) \cdot x_{3_m} + (1 - s) \cdot x_{4_m}) \\ &\quad + x_{4_m} \cdot (x_{1_f} + x_{2_f} + (1 - s) \cdot x_{3_f} \\ &\quad + (1 - s) \cdot x_{4_f}) - r \cdot d_x \end{aligned} \quad (8)$$

where

$$\begin{aligned} d_x &= x_{1_f} \cdot x_{4_m} + (1 - hs) \cdot x_{4_f} \cdot x_{1_m} - \\ &\quad (1 - hs) \cdot x_{2_f} \cdot x_{3_m} - (1 - s) \cdot x_{3_f} \cdot x_{2_m} \end{aligned} \quad (9)$$

and $\overline{w_x}$ is the sum of the right-hand side of

equations 5–8. Similarly, in deme Y

$$\begin{aligned} \overline{w_y}y'_1 &= y_{1_f} \cdot ((1 - t) \cdot y_{1_m} + (1 - t) \cdot y_{2_m} \\ &\quad + (1 - kt) \cdot y_{3_m} + (1 - t) \cdot y_{4_m}) \\ &\quad + y_{1_m} \cdot ((1 - t) \cdot y_{1_f} + (1 - t) \cdot y_{2_f} \\ &\quad + (1 - kt) \cdot y_{3_f} + (1 - kt) \cdot y_{4_f}) \\ &\quad - r \cdot d_y \end{aligned} \quad (10)$$

$$\begin{aligned} \overline{w_y}y'_2 &= y_{2_f} \cdot ((1 - t) \cdot y_{1_m} + (1 - t) \cdot y_{2_m} \\ &\quad + (1 - kt) \cdot y_{3_m} + (1 - t) \cdot y_{4_m}) \\ &\quad + y_{2_m} \cdot ((1 - t) \cdot y_{1_f} + (1 - t) \cdot y_{2_f} \\ &\quad + y_{3_f} + y_{4_f}) + r \cdot d_y \end{aligned} \quad (11)$$

$$\begin{aligned} \overline{w_y}y'_3 &= y_{3_f} \cdot ((1 - kt) \cdot y_{1_m} + y_{2_m} + y_{3_m} \\ &\quad + y_{4_m}) + y_{3_m} \cdot ((1 - kt) \cdot y_{1_f} \\ &\quad + (1 - kt) \cdot y_{2_f} + y_{3_f} + y_{4_f}) \\ &\quad + r \cdot d_y \end{aligned} \quad (12)$$

$$\begin{aligned} \overline{w_y}y'_4 &= y_{4_f} \cdot ((1 - kt) \cdot y_{1_m} + y_{2_m} + y_{3_m} \\ &\quad + y_{4_m}) + y_{4_m} \cdot ((1 - t) \cdot y_{1_f} \\ &\quad + (1 - t) \cdot y_{2_f} + y_{3_f} + y_{4_f}) \\ &\quad - r \cdot d_y \end{aligned} \quad (13)$$

where

$$\begin{aligned} d_y &= (1 - t) \cdot y_{1_f} \cdot y_{4_m} + (1 - kt) \cdot y_{4_f} \cdot y_{1_m} \\ &\quad - (1 - kt) \cdot y_{2_f} \cdot y_{3_m} - y_{3_f} \cdot y_{2_m} \end{aligned} \quad (14)$$

and $\overline{w_y}$ is the sum of the right-hand side of equations 10–13.

The purpose of this model is to determine when the e allele can invade a population fixed at the modifier locus for the E allele.

The simulation has been run under certain conditions until an equilibrium state was reached at the A locus. Then this equilibrium state was perturbed by a change in the gamete frequencies, caused by adding $\Delta x_2 = \Delta x_4 = \Delta y_2 = \Delta y_4 = 10^{-3}$. Before the perturbation, no e allele was present in either deme and therefore $x_2 = x_4 = y_2 = y_4 = 0$.

Analysis

A C-program was used to simulate the equations described in the Model section. The code is available upon request¹.

¹contact: tinaschmidt@onlinehome.de

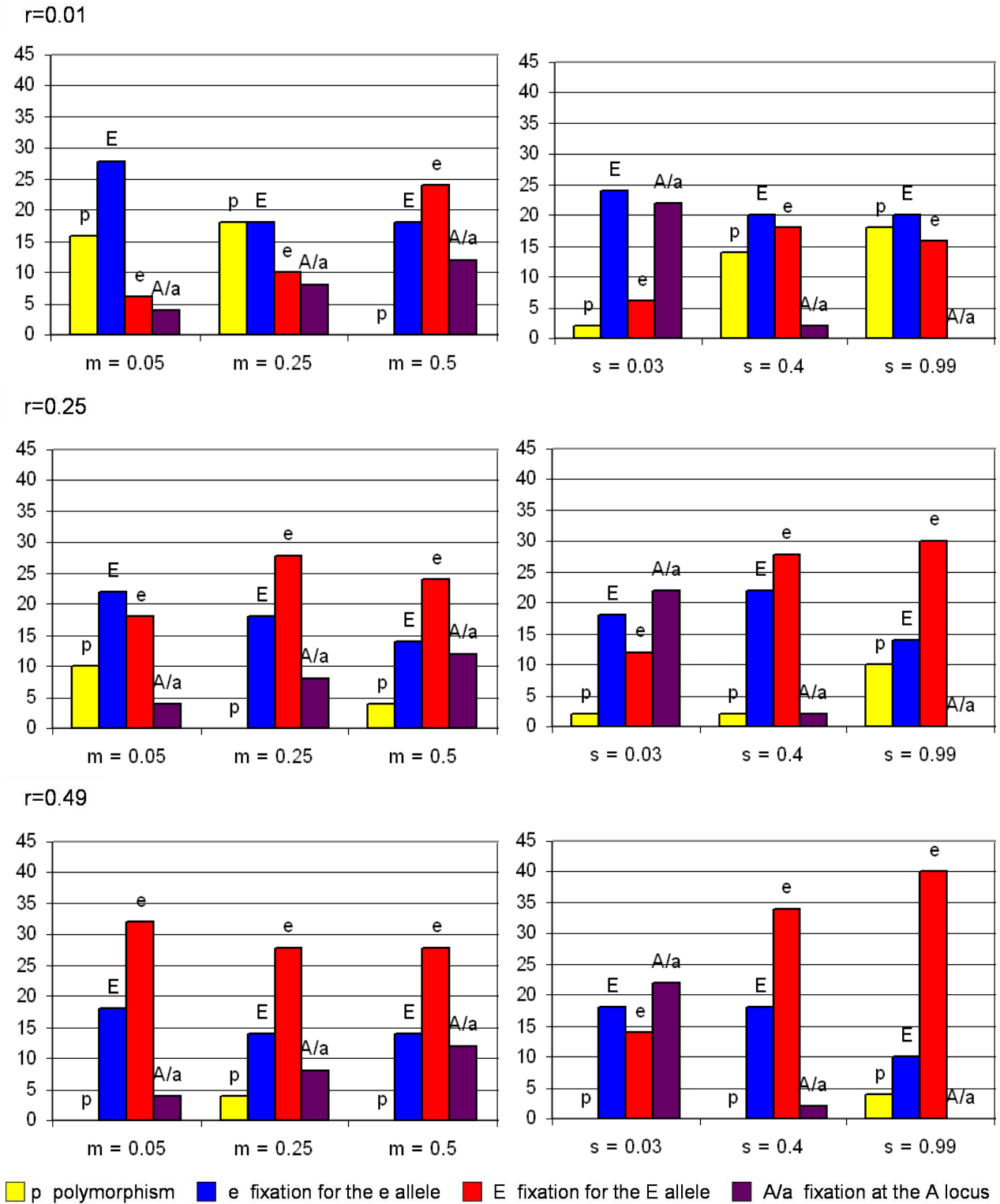


Fig. 1. Analysis of the model, grouped for the same recombination rate and the migration rate (left) as well as the selection pressure (right), showing what state is reached as a post-perturbation equilibrium.

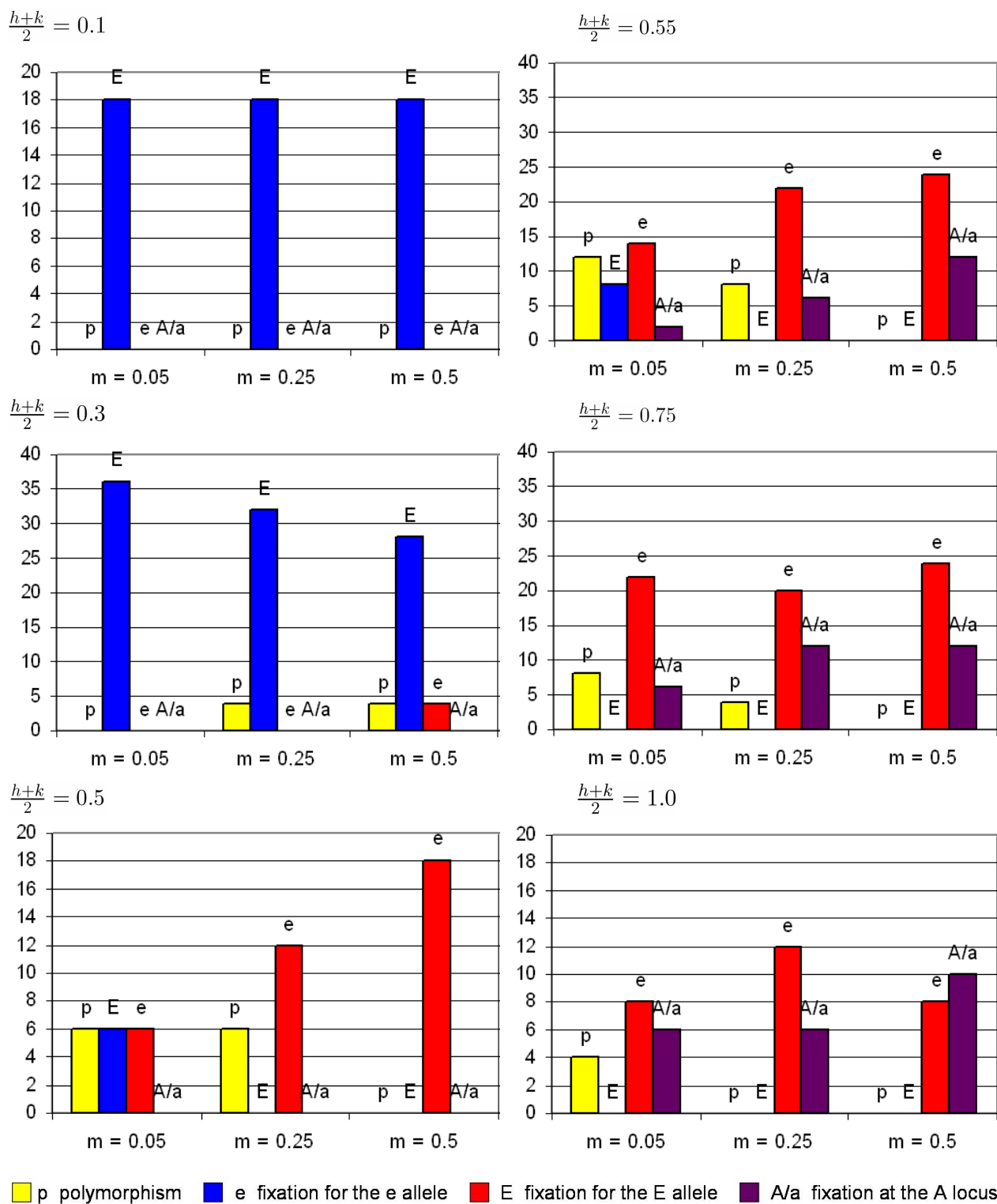


Fig. 2. Analysis of the model, grouped for different average values of the dominance coefficients, showing what state is reached as a post-perturbation equilibrium.

Note that the total number of cases studied varies between the diagrams, since there were 54 cases studied with $\frac{h+k}{2} = 0.1$, $\frac{h+k}{2} = 0.5$ and $\frac{h+k}{2} = 1.0$ and 108 cases studied with $\frac{h+k}{2} = 0.3$, $\frac{h+k}{2} = 0.55$ and $\frac{h+k}{2} = 0.75$

As initial frequencies, all simulations were run with $x_1 = 0.4$, $x_2 = 0$, $x_3 = 0.6$, $x_4 = 0$ and $y_1 = 0.2$, $y_2 = 0$, $y_3 = 0.8$, $y_4 = 0$ as well as $x_1 = 0.6$, $x_2 = 0$, $x_3 = 0.4$, $x_4 = 0$ and $y_1 = 0.8$, $y_2 = 0$, $y_3 = 0.2$, $y_4 = 0$ until an equilibrium was reached. Since there was no mutation included, no e appears before the perturbation.

As for recombination and migration rate, three values $r = \{0.01, 0.25, 0.49\}$ and $m = \{0.05, 0.25, 0.5\}$ were used. Assuming, that the selection pressure is equal in both demes, we used $s = t = \{0.03, 0.04, 0.99\}$. The dominance coefficients were varied between the following three values $h = \{0.1, 0.5, 0.4\}$ and $k = \{0.1, 0.5, 0.4\}$.

In the simulation, the genotype frequencies are considered to have reached equilibrium values when the Euclidean difference between genotype frequencies in successive generations is less than 10^{-12} .

If an allele's frequency was smaller than 10^{-12} , it was considered lost and the population was fixed for the other allele. When no equilibrium was reached after 5,000,000 generations and no allele frequency was smaller than 10^{-3} , the state was considered to be polymorphic. The cases, when an allele frequency was between 10^{-3} and 10^{-12} , the simulation was run again, using 500,000 and 50,000,000 iterations, so that it was possible to determine whether the reached state was polymorphic or an allele was on the way to getting lost.

Simulating the two-locus, two allele model with the above recursions, all starting conditions reached a pre-perturbation equilibrium. Every time x_i approached zero also y_i approached zero, so the same gametes are getting lost in deme X and Y . All post-perturbation equilibriums were either polymorphisms with all chromosomes present or a fixation at either the E locus or the A locus with two of the four chromosomes present. There was no case, where three chromosomes were left at the post-perturbation equilibrium, which is explained by r being unequal to 0 and there-

fore a single lost chromosome would be created again by recombination. Under no researched conditions, a population got fixed for one chromosome.

There were four different outcomes of the post-perturbation equilibrium distinguished: First, a polymorphism at the E locus (p); second and third the fixation of the E allele (E) and the e allele (e) and last but not least the fixation at the A locus (A/a).

Polymorphism

Under 10.7% of the studied starting conditions, no allele was lost and a polymorphism was obtained. As the selection pressure s increases, it is more likely to obtain a polymorphism (see fig. 1 and fig. 3). The higher the recombination rate, the less likely it is to obtain a polymorphism. According to the average of the dominance coefficients h and k , it is most likely to obtain a polymorphism, when $\frac{h+k}{2} = 0.5$.

Fixation at the e locus

Before the perturbation, there was no e allele present. But still in some cases, it was possible that the e allele could invade the population. As for selection pressure s and migration rate m , none of the figures shows a clear pattern. As the recombination rate r increases, a fixation for the e allele becomes more likely. For $\frac{h+k}{2} \geq 0.5$ an invasion of the e allele is most likely.

In other cases, the perturbation did not affect the population and the E allele became fixed. As shown in fig. 1 as well as fig. 2 and 3, the fixation for the E allele is more likely with a small migration rate. As the recombination rate r decreases, a fixation for E becomes more likely.

As shown in fig. 2 and 3, a fixation for the E allele is impossible, when the average of the dominance coefficients h and k is greater than 0.55. For $\frac{h+k}{2}$ decreasing, a fixation at the E locus becomes more likely. For $\frac{h+k}{2} = 0.1$ in every studied case, the population became fixed for the E allele, meaning that the perturbation

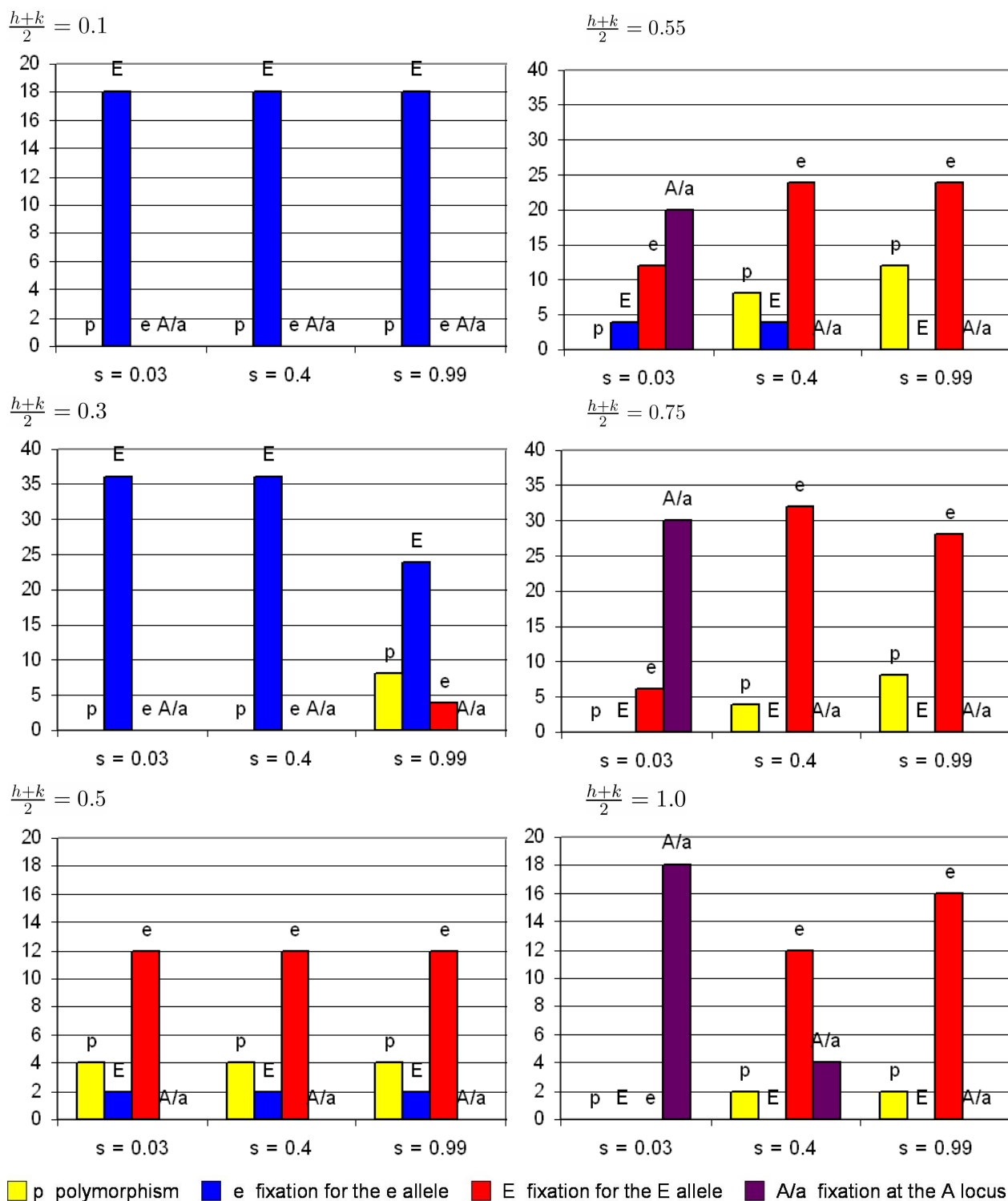


Fig. 3. Analysis of the model, grouped for different average values of the dominance coefficients, showing what state is reached as a post-perturbation equilibrium. Note that the total number of cases studied varies as in fig. 2.

did not have any effect on the population.

In 33.7% of all studied cases, the *E* allele became fixed, meaning that the *e* allele

got lost when the post-perturbation equilibrium was reached. Therefore, in 33.7% of all studied cases, the perturbation

does not affect the population. In 66.3% of all studied cases, the newly introduced e allele survives in a polymorphism, its fixation or a fixation at the A locus. The imprinting allele e invades in 40.7%.

Fixation of A and a

Under some starting conditions, either x_1 and y_1 or x_3 and y_3 became very close to zero at the pre-perturbation equilibrium. In those cases, the A allele or the a allele is already lost before the perturbation resulting in a post-perturbation equilibrium which is fixed for the a or the A allele. Fixations at the A locus only occurred, when x_1 or x_3 approach zero when the pre-perturbation equilibrium was reached.

As shown in fig. 1, the fixation for the A allele or the a allele depends on the migration rate as well as the selection pressure in the two demes. As the migration rate increases, a fixation at the A locus becomes more likely and as the selection pressure decreases, a fixation at the A locus becomes more likely. Furthermore, the recombination rate r has no effect on the probability of a fixation at the A locus: For each recombination rate, 24 fixations at the A locus were obtained.

The average of the dominance parameters h and k influences the probability of a fixation at the A locus. As fig. 2 shows, there is no fixation at the A locus, for $\frac{h+k}{2} \leq 0.5$ and as $\frac{h+k}{2}$ increases, a fixation at the A locus becomes more likely.

Discussion

For $h = k = 0.5$, this simulation yields the same results as predicted by Spencer and Clark. Note, that the values for the selection pressure in Spencer and Clark are different to this paper's values; to convert, dividing this paper's s by 2 results in Spencer and Clark's s [2].

This model's results for the invasion of the e allele, depending on the average of the dominance coefficients, are consistent with the ones of Van Cleve and Feldman [3].

There were also simulations run with $s < t$. Therefore, only fixation for the a allele occurred and never fixation for the A allele. Generally, the results maintained with $s \neq t$ also support the thesis above. Nevertheless, there are also cases, that do not match the above patterns: Some populations become fixed at the A locus at post-perturbation equilibrium, but they were not fixed at the A locus at pre-perturbation equilibrium. With $s = t$, the results for the second set of initial frequencies was always the same as with the first set of initial frequencies for the dominance parameters h and k switched around. However, with $s \neq t$ different initial frequencies sometimes reach different equilibrium states. For example for $r = \{0.01, 0.25, 0.49\}$, $m = 0.25$, $s = 0.4$, $t = 0.99$, and $h = k = 1.0$ the population becomes fixed for the a allele under the first set of initial frequencies and a polymorphism occurs after the perturbation with the second set of initial frequencies.

Another way of investigating the model further is to run the simulation for different allele frequencies, also including initial frequencies where no $x_i = 0$ and no $y_i = 0$. Then, the population is not fixed for the E allele at pre-perturbation equilibrium, so also the perturbation by adding some E alleles would have to be examined.

Acknowledgements

Warmest thanks to Prof. Marcus W. Feldman for inviting me to his lab in Stanford. I want to thank every member of the Feldman Lab for giving me this wonderful research opportunity. Special thanks to Jeremy van Cleve for providing the programming code for this simulation and patiently answering all my questions. Within the short three weeks, I have learned about many things and I am sure that this special experience will influence my further career and will remain an unforgettable time.

References

- [1] Morison, Ian M., Ramsay, Joshua P. and Spencer, Hamish G. A census of mammalian imprinting. *Trends Gen.* 21: 457 - 465

- [2] Spencer, Hamish G. and Clark, Andrew G. A Chip off the Old Block: A Model for the Evolution of Genomic Imprinting via Selection for Parental Similarity, *Genetics* October 2006.
- [3] Van Cleve, Jeremy and Feldman, Marcus W. Sex-Specific Viability, Sex Linkage and Dominance in Genomic Imprinting, *Genetics* April 2007.
- [4] Reik, Wolf and Walter, Jörn 2001. Genomic Imprinting: Parental Influence on the Genome, *Nat. Rev. Gene.* 2: 21-32.

The role of Bmi-1 in maintaining self-renewal of cancer stem cells

Miriam Wiestler

Laboratory of Michael F. Clake

Institute for Stem Cell Biology and Regenerative Medicine

Stanford University School of Medicine

Abstract

Dr. Michael Clarke and the members of his laboratory are working on the recently introduced topic of cancer stem cells. They focus on two areas of research: the regulation of self-renewal between normal stem cells and their malignant counterparts and the identification and characterization of cancer stem cells. Since it has been suggested that cancer stem cells may be responsible for initiating cancer, it is necessary to study these cells and their transformation in terms of therapeutic strategies to better treat cancer. Recently, it was found that the proto-oncogene Bmi-1 participates in the Polycomb Repression Complex 1 (PRC1) in mammals, which has been found to repress many transcriptional target genes by recognizing methylation marks embedded in genomic DNA. The actual mechanism (epigenetic or otherwise) has yet to be determined. Dr. Clarke's laboratory and others found that Bmi-1 is necessary but not sufficient for self-renewal of murine hematopoietic stem cells. By investigating the pathways upstream and downstream of Bmi-1, the laboratory is actively investigating the molecular pathways that regulate self-renewal.

Introduction

The proto-oncogene Bmi-1 is known to have several protein binding domains, none of which allow for direct binding of Bmi-1 to DNA. Since Bmi-1 does not appear to bind DNA directly, it was hypothesized that

Bmi-1 must localize to specific genomic sequences through protein intermediate(s), as it participates in the PRC1. Moreover Bmi-1 is said to repress the Ink4a/ARF locus, which codes for two alternate transcripts: p16 and p19, thus reducing transcription of both p16 and p19. Three genes that are activated by the p19 transcription factor, which functions upstream of p53, were identified through literature search. These genes were p21, Wig1, and Bax. The first two genes participate in cell cycle regulation, whereas Bax plays a role in promoting apoptosis. Taken together with the p19/Bmi-1 interaction, these data suggest a scenario in which repression of p19 by Bmi-1 may lead to altered expression of p21, Wig1, and Bax which may have an effect on self-renewal as these three genes play a crucial role in this process. To test this hypothesis a chromatin immunoprecipitation (ChIP) assay, used to study the genomic binding sites of both transcription factors and the location of histone modifications, was designed to assess localization of Bmi-1 in murine mammary stem cells.

During my internship I worked out the protocol for amplification of genomic DNA that covered the promoter regions of the genes p21, Wig1, and Bax. These experiments were crucial as they serve as readout for the entire ChIP procedure. Prior to my arrival, primers were designed and then synthesized. This was the point at which my contribution began.

Material and Methods

Extraction and Purification of genomic DNA

Chemical Extraction of genomic DNA

Immortalized mouse epithelial tissue culture cells (CRL1616) were spun out of their serum-containing media. Adherent cells were trypsinized and collected from the flask. Afterwards they were centrifuged at 500 *g* and the supernatant discarded. To remove the serum containing media, these cells were resuspended with 1 to 10 ml ice-cold PBS, centrifuged for 5 min at 500 *g* and the supernatant was discarded. This resuspension and centrifugation step was repeated one more time. The cells were then resuspended in 1 vol digestion buffer to lyse them. Afterwards the samples were incubated with proteinase K, and left shaking at 50° C for 12 h to digest proteins bound to the genomic DNA. The samples were then cleaned by mixing with an equal volume of phenol/chloroform/isoamyl alcohol which denatured the proteins and retained them in the organic phase of the extraction, followed by centrifugation for 10 min at 1,700 *g* in a swinging bucket rotor. The aqueous top layer was transferred to a new tube and 0.5 vol of 7.5 M ammonium acetate and 2 vol of 100 % ethanol were added to precipitate the cleaned DNA from solution. The DNA was recovered by centrifugation at 1,700 *g* for 10 min. The DNA pellet was rinsed with 70 % ethanol and spun at 500 *g* for 10 min. Afterwards the ethanol was decanted and the pellet was air dried for a few minutes. Then the DNA was resuspend in TE buffer (10 mM Tris and 1mMEDTA, brought to pH 7.5 with HCl) and was gently shaken at room temperature until it was dissolved. Finally, the sample was stored at 4° C.

DNA Extraction with Qiagen DNeasy Kit

As it was thought that the DNA samples were contaminated (see Fig. 1(a)), they were

re-extracted with Qiagen DNeasy tissue kit (cat. No. 69506). Of this re-extraction, four different samples were obtained: two first elutions and two second elutions with different amounts of DNA. All the four samples were tested with DNA spectrophotometry and run on a 1.5 % agarose gel to verify their amounts of DNA and their status of purification.

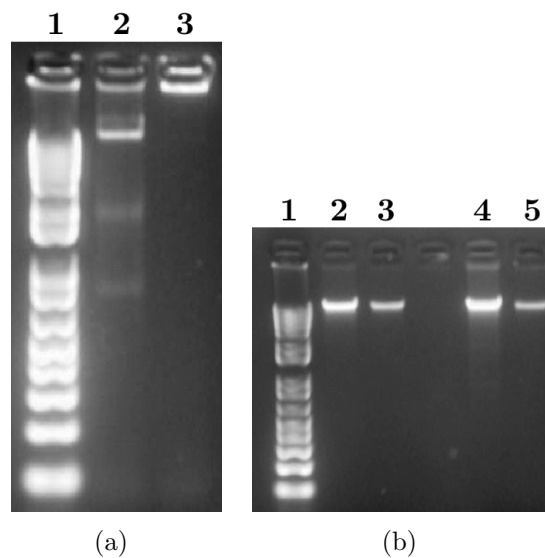


Fig. 1. (a)(1) 1 kb DNA ladder; (2) and (3) contaminated DNA samples (out of chemical genomic DNA extraction). The smears seen in bands 2 and 3 indicated that the DNA was contaminated.

(b) (1) 1 kb DNA ladder; (2) first elution of CRL1616 extracted DNA sample A; (3) second elution of CRL1616 extracted DNA sample A; (4) first elution of CRL1616 extracted DNA sample B; (5) second elution of CRL1616 extracted DNA sample B

Gradient PCR with advanced Polymerase

A gradient PCR was performed to determine the optimal primer annealing temperature. A designer Taq polymerase variant (Advantage cDNA Polymerase Mix (50x) (Clontech 50595)) with increased polymerization activity was used. With all the three different primer-sets (Wig; p21; Bax), this specialized PCR was performed, starting at an annealing temperature of 55.1° C

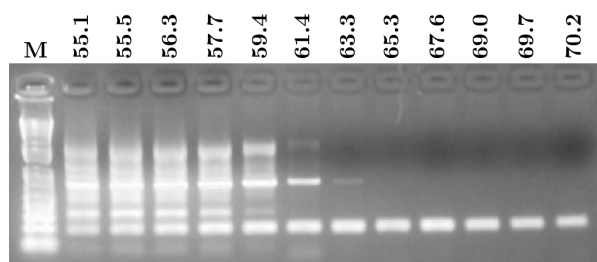


Fig. 2. PCR products of primer-set 1 p21. The different annealing temperatures are shown by the numbers on top of the picture. Out of this data it was thought, that 65.3° C was the optimal annealing temperature.

and ending at an annealing temperature of 70.2° C. Afterwards the PCR-products were run on an 1.5 % agarose gel (1X TAE-buffer).

Gradient PCR with a new template

Once again a gradient PCR was performed. DNA was extracted from murine mammary cells (by Qiagen DNeasy tissue kit) to obtain a new template to test the primer-sets for the Bax and Wig1 promoter regions.

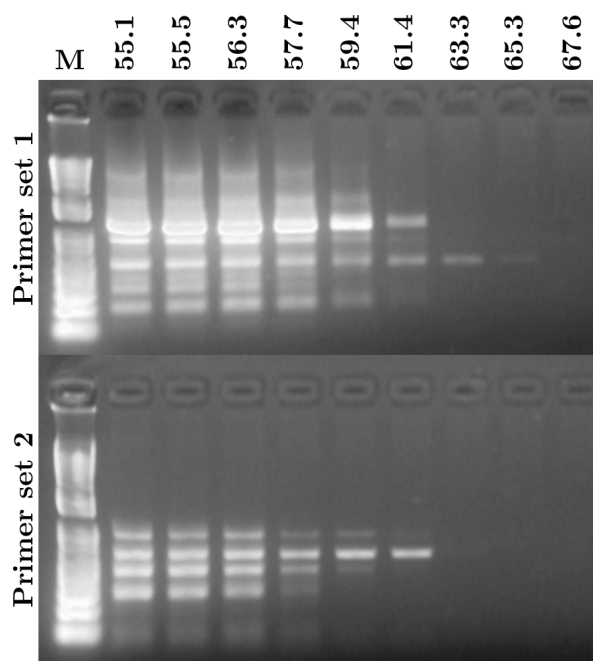


Fig. 3. PCR Products of a gradient PCR with primer-sets 1 and 2 from Bax and new template. This data illustrates, that Bax (as Wig1) has a different annealing temperature than p21. Its perfect annealing temperature is at 61.4° C.

Table 1. sonication conditions for all the four DNA samples

Sample	Power [V]	Seconds	Cycles
1.1	1	10	1
1.2	2	5	2
2.1	2	10	1
2.2	3	10	2

DNA Sonication

DNA was fragmented by sonication to test the primers on DNA fragments as the primers did not bind specifically enough to the genomic DNA. Sonication facilitates specific binding of the primers on DNA by shearing the genomic DNA in smaller fragments, consisting of 100–2,000 bp. This was performed by placing a microcentrifuge tube containing the buffered DNA sample into an ice-water bath and sonicating for a varying number of 10 second bursts using maximum output and continuous power in order to fragment the DNA via ultrasonic waves. To test conditions that lead to the best results of fragmented DNA, a different sonication condition was used for each of the four DNA samples. After sonication all four samples were analyzed with DNA spectrophotometry and run on 1.5 % agarose gels to verify their amounts.

Discussion

Unfortunately, in the end of my internship it became clear, that all the three primer sets (p21, Baxm and Wig1) did not work properly. Although the conclusion that some primer sets would not work in a practical setting, all primer sets were designed by prediction software using algorithms proven extremely effective in other PCR applications. Therefore, one main conclusion from my work was the outcome that the theoretical design of the amplification primers was different than the application.

Since I did not find a notable difference between genomic DNA and fragmented

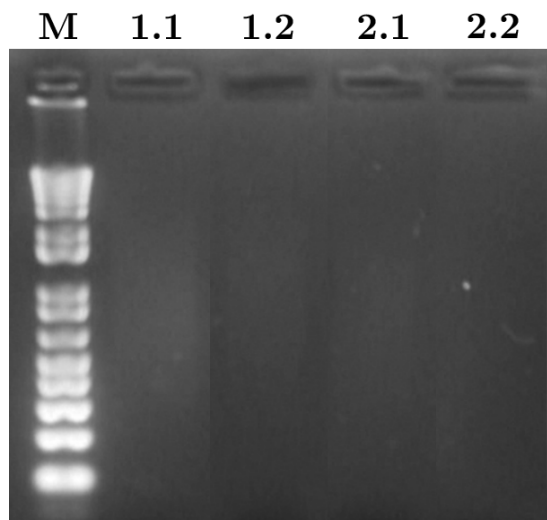


Fig. 4. The four differently treated sonicated DNA samples. (M) 1 kb DNA ladder. The faint smear observed in all four lanes indicates a successful sonication of genomic DNA into fragments. At least it was thought that sample 1.1 was best to use for PCR.

DNA in one of my results, one would assume that the difficulties with the PCR were not due to size of DNA template but rather to inherent sequence structure (like long strings of As and Ts) which made it hard to get specific products.

Personal Remarks

I have learned at least three important things from my internship. First of all, I have learned the relation between empirical determination of optimal primer melting temperature and amplicon specificity. Throughout my work it became clear, that one should not take the prefabricated annealing temperature for granted as it is shown through the different annealing temperatures of the three different primers. Secondly, I have learned that generic Taq polymerase is somewhat limited in its polymerization potential. There was a huge difference between the PCR products of standard Taq-Polymerase and the advanced one. It can be said that the standard Taq-Polymerase synthesizes in a very stringent way, which can lead to false-negative outcomes of an experiment. And last but not least I have learned that intrinsic genomic sequence characteristics may affect PCR as much as the protocol or reagents used. Therefore it is all important to examine ones outcomes very closely. A troubleshooting and following advancement of the PCR protocol

should never be missed, as my experiments illustrated.

Therefore one of my conclusions is that the PCR protocol should be adjusted to get better product amplification. For instance the initial denaturation step could be increased to allow better melting of the genomic DNA.

My last and final conclusion would be the modification of primer design which would lead to more successful amplification.

Acknowledgements

I would like to sincerely thank Dr. Michael F. Clarke for giving me the unique opportunity to work in his highly interesting laboratory for four weeks and for his friendly support during my stay. I am very thankful for the knowledge I have gained as well as the experiences I have made within my internship. Furthermore, I hold Neethan Lobo in high regards, due to his support in supervising me as well as his enthusiasm and patience while teaching me important basics of molecular biology. In addition to this, I would like to thank all members of the laboratory for being so kind and helpful. I had a great time during my internship and I have learned a lot of amazing things which will help me with my future studies.

References

- [1] Lobo NA, Shimono Y, Qian D, Clarke MF. The Biology of Cancer Stem Cells. *Annu Rev Cell Dev Biol.* 2007 Jul 23
- [2] Huntly BJ, Gilliland DG. Leukaemia stem cells and the evolution of cancer-stem-cell research. *Nat Rev Cancer.* 2005 Apr;5(4)
- [3] Dalerba P, Cho RW, Clarke MF. Cancer stem cells: models and concepts. *Annu Rev Med.* 2007
- [4] Clarke MF, Becker MW. Stem cells: the real culprits in cancer? *Sci Am.* 2006 Jul
- [5] Clarke MF, Fuller M. Stem cells and cancer: two faces of eve. *Cell.* 2006 Mar 24;124(6)
- [6] Clarke MF. A self-renewal assay for cancer stem cells. *Cancer Chemother Pharmacol.* 2005 Nov
- [7] Takahashi K, Yamanaka S. Induction of pluripotent stem cells from mouse embryonic and adult fibroblast cultures by defined factors. *Cell.* 2006 Aug 25;126(4)



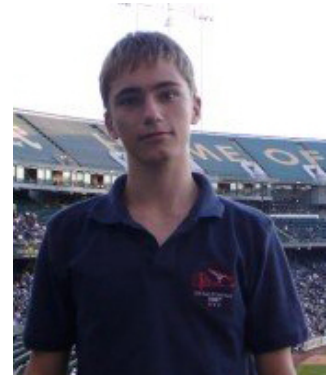
The academy participants at Main Quad, Stanford University

The Academy Participants

Philipp Bayer

was born on April 23rd, 1988 in Karlsruhe.

During the National Science Academy in 2003 – where I was sent to in 9th grade by my biology teacher Stefan Klär – my scientific interests focused on molecular biology, microbiology and biochemistry which finally culminated in my internship at Prof. Mark A. Kay's Lab in this summer 2007. In the last four years the Life-Science Lab lifted the word "Science" up on top of my list of favourite activities now ranking above "Sports" and "Music". Accomplishing my first bacterial transformation in 2003, meeting wild life and social drawbacks in Kenya 2004, giving my first talk as a student tutor in 2005 and the intense preparations for the International Science Academy San Francisco beginning in 2006 were pivotal experiences I shared with members of the Life-Science Lab. The 2007 Academy to the Bay Area was finally crowning my activities in the Life-Science Lab. The internship features the uncommon opportunity to experience the fascinating facets of authentic international research in a foreign country. In addition, I visited one of the most beautiful and interesting cities I have ever seen.



Enjoying the opportunities and the unique learning environment of the Life-Science Lab I found myself increasingly interested in figuring out crucial prerequisites for effective learning processes. In 2006, I decided to join the team of tutors providing the framework for the success of the Lab's members and became student tutor of the molecular biology study group – a highly motivating responsibility that led to further tutorial activities like the mentoring and support of seminars, workshops and academies in- and outside the Life-Science Lab. I would be over the moon joining preparations for the 2009 academy to San Francisco!

Tim Bleul

born on July 4th, 1987. I graduated with honours from the Carl-Friedrich-Gauß-Gymnasium in Hockenheim near Heidelberg in 2007. Presently, I am enrolled in medical studies at the University of Heidelberg. I joined the Heidelberg Life-Science Lab in 2004 attending workgroups in molecular biology, medicine and scientific English. Besides science my passion is music. I like to play the piano, guitar and to sing. As I am also very interested in politics, I worked as the leader of the local council for young people in Hockenheim.



I will never forget the three weeks at the laboratory of Kristin Scott, giving me the ability to work in a world-class biology laboratory and to feel the fascination of basic research. It encouraged me in my plans to study medicine and to focus on implementing basic research into practical medical progress. I would like to thank all those who have worked hard to make this great academy possible.

Janina Bucher

was born on August 31st, 1987, in Schwetzingen. In 11th grade (2004), I joined the Heidelberg Life-Science Lab as a member of the molecular biology study group. A year later, I became part of the chemistry group of which I will become tutor after returning from the academy.

During my time at school I also attended the “Schülerzirkel Mathematik” of the University of Mannheim as well as the “Naturwissenschaftliche Sommerakademie” of the BASF.

After graduating from Carl-Friedrich-Gauß Gymnasium in Hockenheim, I enrolled in chemistry at the University of Heidelberg. Besides science, my hobbies are focused around all kinds of endurance sports such as biking, walking or aerobic courses at our local fitness facility.

The San Francisco Academy was a most significant experience in my life and encouraged my decision to become a scientist. The atmosphere, creativity and enthusiasm of the participants and lab members left me deeply impressed.



Steffen Bübecker

I was born in Heidelberg on October 19th, 1988. I am still graduating at the Gymnasium Bammental, near Heidelberg, and currently my last year at high school is coming to an end. Besides reading and doing several kinds of sports I care for some rodents and exotic insects let in terraria at home. Since the age of 15 I investigated the behaviour and environmental interactions of stick insects (*Carausius morosus*, *Extatosoma tiaratum*) by breeding many generations. I focused on the question how modification and phenotypical adaption occurred.

After my participation in the Heidelberg Life-Science Lab had started in grade 8 (2003), I worked in the molecular biological as well as in the zoological study group and continuously gained experience in different lab techniques. We went on excursions to observe and to learn more about the domestic fauna. Furthermore, the pre-historical species of the Grube Messel was a central issue this year. I also contributed to the Science Academy Dresden 2006 and in the context of a high school program I visited the institute for theoretical astrophysics (ITA) in Heidelberg for one week, which gave me an insight into current working projects. Thus, my interests are scattered to multiple scientific fields, such as zoology, biochemistry and astronomy.

The ISA San Francisco 2007 was a meaningful experience, concerning both my autonomy in life and the knowledge about authentic research. It was great to evolve experiments day after day, gradually learning more about the organisms we concentrated on. Surely, I can well imagine to do similar research in the future and I wish to be able to combine my interests. The opportunities given today are highly motivating and the ISA 2007 made me confident.



Ralph Falk

was born on May 11th, 1987 in Baden-Baden. Physics and geography have been my main interests since I learned to read. Out of this reason I focused on these two sciences in High School. In 2005, I joined the physics study group at the Heidelberg Life-Science Lab and worked as a mentor in this group during my second year. After graduating from High School in summer 2007, I intended to study physics. However, I first had to do my social service at the International Youth Hostel in Heidelberg.

As a participant of the International Science Academy San Francisco 2007 I learned much about the work in a Lab and how I would like to work in my future. Due to all these experiences, I decided to study physics. Besides, I will follow my interest of inventing new solutions for companies to make their work easier and more profitable.

The whole journey was an incredible experience for me. So I thank everybody who made it possible for me to get there, spending the best time of my life.



Christoph Fischer

was born on July 25th, 1984 in Heidelberg. Having graduated from the St. Raphael Gymnasium in 2003, I performed my civilian service at a school for disabled children with speech disorders. After that I studied law in Heidelberg and Boston. While my special interest lies in criminology and international criminal law, I enjoyed the chance of spending an enriching internship with the Electronic Frontier Foundation during this academy.

After participating in the first International Science Academy San Francisco in 2003, I decided to stay involved in the Heidelberg Life-Science Lab and promote the successful San Francisco program. Also, I have initiated a new International Science Academy to Estonia that took place in 2007 for the first time. I believe there is no experience as precious for young people as getting in touch with other cultures. Having lived in Belgium for seven years, I experienced such enriching exchange myself and try my best to pass on this appreciation to the academy participants.

Being involved with the San Francisco Academy for more than 5 years now, I would like to thank everyone who put their efforts into making this project so successful and wish all the best to the new group of academy participants in 2009!



Julia Flanjak

was born on August 30th, 1988 in Mannheim. I graduated from High School in 2007. After returning from the ISA San Francisco I enrolled in Medical Studies at the University of Heidelberg.

Since 2003 I have been a member of the Heidelberg Life-Science Lab. I attended in molecular biology, neurobiology and philosophy and absolved a lot of internships.

The San Francisco Academy 2007 was a great, but challenging experience. I went to San Francisco within the hope to learn a lot more about neurobiology and chemistry. Because of internal problems at the Department of Chemistry I was forced to find a new lab in a short period of time. Kindly I was hosted by Kevin Mayeda at the Department of Seismology. I had to become quickly acquainted with the topic, but I was really motivated, because we witnessed an earthquake in our first night in Berkeley.

I hope that the academy will be carried on, because it is a great way to release students from the Life-Science Lab and to start an academic career.



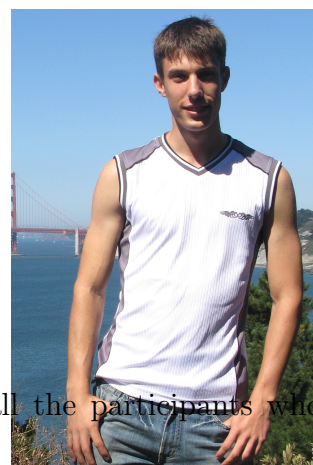
Jan Freudenberg

was born on March 16th, 1988; graduated from high school in Schifferstadt in 2007 with profile courses in English, physics and chemistry.

After returning from the ISA 2007, I enrolled in chemistry at the Ruprecht-Karls-University of Heidelberg.

Within the Heidelberg Life-Science Lab I attended workshops in the math simulation as well as the chemistry study group, in which I am one of the student tutors by now.

As the academy was a really great experience regarding scientific, social as well as cultural aspects, I would like to thank all the people who made the ISA SF 2007 possible and, of course, all the participants who contributed to our great time in San Francisco.



Jan Gotthardt

was born on January 26th, 1988 in Speyer. I joined the Life-Science Lab in 2005 as a member of the chemistry and English study group. After I graduated from Carl-Friedrich-Gauß Gymnasium Hockenheim in 2007 the International Science Academy San Francisco was an unforgettable experience and it made me even more determined to study chemistry. Besides the scientific work and the warm and motivating atmosphere in Prof. Long's laboratory I was deeply impressed by university life in Berkeley and the city of San Francisco itself. Staying at UC Berkeley and traveling around California for a few weeks taught me a lot about cultural diversity and enriched my experience tremendously.



Returning from San Francisco I was happy to enroll in chemistry at Heidelberg University in September 2007. Since fall 2007 I have been a tutor for the chemistry study group of the Life-Science Lab, sharing my enthusiasm for sciences, especially chemistry, with high school students.

When I am not studying or working for the Life-Science Lab I enjoy playing the viola da gamba, listening to music, reading or meeting up with friends.

Maximilian Heeg

was born on August 22nd, 1988 in Ulm. I attended Highschool at the Bunsen-Gymnasium in Heidelberg, graduating in June 2007 (Abitur). Currently, I am studying medicine at the University of Freiburg in my first year. Besides reading and climbing, science has always fascinated me.



My participation in the Heidelberg Life-Science Lab started in my 12th grade (2005). I have been participating in the study groups on microbiology, molecular biology and mathematics. I am very glad that I had the chance to take part in the International Science Academy to San Francisco. My stay at the Drubin-Barnes-Lab together with Hans Urban was a marvelous experience, which will certainly have an enormous influence on my career. But not only the laboratory but also the other participants, the atmosphere and the Californian way of life left a deep impression on me.

I would like to thank all the people, who made this Academy an unforgettable experience, especially Professor Drubin, Christoph Fischer and Christian Stoy. Hopefully, the next generations will have the same opportunity to take part in this unique program.

Leonie Kastner

was born on January 18th, 1989 in Wiesbaden. In June 2007, I graduated from the Martin-Niemöller-Gymnasium Wiesbaden with profile courses in biology and chemistry. Presently, I am enrolled in molecular cell biology at the University of Heidelberg.

I joined the Heidelberg Life-Science Lab in 2005. I participated in the molecular biology and the philosophy working group and since 2006 I have been mentoring the microbiology working group. Beside my interest in sciences I love swimming, reading and traveling. The International Science Academy has been my first stay in the United States and I was truly fascinated by the landscapes and areas surrounding San Francisco. Working in the laboratory of Professor Pfeffer, living on Stanford Campus and exploring the area around, have been significant and unique experiences I really enjoyed and that will influence my further career. I want to thank everyone who put a lot of work and enthusiasm into the academy and especially Professor Suzanne R. Pfeffer for giving us the chance to work independently on a true research project and making our time at Stanford unforgettable.



Jonas Kiefer

was born on February 13th, 1989 in Heidelberg. I attend high school at the Friedrich-Ebert-Gymnasium in Sandhausen and will graduate in 2008. After graduating from high school I would like to start studying medicine. In summer 2004 I became a member of the Heidelberg Life-Science Lab. In my first year I attended the neurobiology and zoology group. From 2006–2008 I participated in the microbiology group. Beside science I am interested in sports, especially soccer, in photography and in fantasy books. The International Science Academy San Francisco was a great experience. I learned a lot, not only referring to science, and I believe that the ISA will have a lasting influence on my personality. I spent four wonderful weeks in San Francisco and enjoyed every day at Kristin Scott's Lab at Berkeley University where I worked together with Tim Bleul. I would like to thank all persons who worked hard to make the San Francisco Academy possible.



Dustin Klinger

was born on January 30th, 1989 in Munich, Germany. In 2004 I moved from Max-Born-Gymnasium Germering to the boarding school “Schule Schloss Salem” at Lake Constance to continue my secondary education. One year later I became a member of the Heidelberg Life-Science-Lab enrolling in molecular biology.

In boarding school rather involved in the social sciences like politics (class representative in 2006/07), philosophy and philology and music I looked for experiences in the domain of natural sciences. The ISA SF 2007 seemed the right place to experience applied sciences hands on.

The internship was most enriching and proved how important interdisciplinary thinking is for both natural and social sciences. I would like to thank the Pfeffer lab and especially Garret Hayes who was willing to help us out at any time.

After the ISA SF 2007 I have one year to go for my Abitur in Salem; next year I will have to do my military or civil service. After that I hope to study Ancient Greek, philosophy or political sciences abroad.



Alexandra Nothnagel

was born on August 18th, 1987. I joined the Heidelberg Life-Science Lab in 2005. I was involved in the Biochemistry and in the molecular biology study groups. The work in these groups and the ISA encouraged me in what I wanted to major in. To prepare myself for my stay at UCB I have done an 8-week internship at the Kinematic Cell Research Group of Frankfurt’s Goethe-University to gain some experience in scientific research work at university and to get some basic skills. After graduating from high school in Frankfurt am Main in June 2007 I participated in the ISA San Francisco. Together with Benjamin I was in the Wemmer Lab and discovered my interest in protein biochemistry, biophysical chemistry and NMR experiments. It was my first visit to the US and I hope it was not the last.

One day after my return I had my successful interview at the Johann-Wolfgang-Goethe-University at Frankfurt where I am studying biochemistry now. This academy changed my life fundamentally and opened up many new possibilities – since the beginning of my studies I am e. g. member of the Dötsch group and work on my own little project.

Next to science my interests are digital photography, architecture, arts, medieval times, rock and medieval music, detective stories, dancing and sports, e. g. working out at a gym and inline-skating.



Daniela Paunescu

was born on March 24th, 1988 in Timisoara (Romania). After graduating from secondary school at the Otto-Hahn-Gymnasium in Landau I began my studies in chemistry at the Ruprecht-Karls-University of Heidelberg. In 2005, I became a member of the Heidelberg Life-Science Lab and participated in the chemistry study group. I am impressed and eagerly interested in sciences particularly in chemistry and biology. Due to my participation in several exchange programs (USA/Great Britain/Croatia) I know that visiting other countries is helpful in expanding my scientific and cultural horizons. This insights together with the opportunity to perform my own scientific work were the reasons why I gladly joined the International Science Academy San Francisco 2007.



Philipp Bayer and I were fortunate to spend three weeks at the laboratory of Mark Kay at the Stanford Medical School. This program gave me the chance to study, research and socialize with internationally well-known scientists. The stay in San Francisco has become a big step to a career in chemistry.

Clemens Scherer

was born in Heidelberg on July 2nd, 1988. In 2003, I joined the Heidelberg Life-Science Lab where I have attended different study groups for chemistry, molecular biology and computer science. After graduating from school in July 2008, I would like to enrol in the Medical School in Heidelberg. Next to science, my interests are reading, playing the piano, sailing and dancing. Moreover, I have been trying to optimize algorithms for 3D rendering (displaying three dimensional objects at the computer).

America is the centre of the modern world and the focus of scientific development and new inventions – and the everlasting attraction for people who want to broaden their horizons. In my opinion the San Francisco Academy 2007 was a great success for all participants. Following the old path of immigrants, scores of people have been attracted by American academic institutions. The wonderful work in the laboratory has encouraged my decision to aspire a career in life sciences. I want to thank all those persons who have made the academy possible.



Tina Schmidt

was born on the June 25th, 1988. In 2007 I graduated from the Ernst-Sigle-Gymnasium Kornwestheim. Presently I am enrolled in mathematics at the “Technische Universität” of Munich.

After joining the Heidelberg Life-Science Lab in 2003, I attended the mathematics workgroup. In my free time, I enjoy doing sports such as swimming, running, skiing, biking or hiking as well as the participation in math competitions, such as the “Bundeswettbewerb Mathematik”. Currently, I am also involved in the Science Academy Baden Württemberg as a mentor for mathematics courses.

After attending an U.S. High School for one year in Turpin, Oklahoma, this was my first time to visit a university in the US. This International Science Academy is a very special experience for me, which will positively influence my future career. Therefore, I want to thank Prof. Marcus W. Feldman for hosting me and everyone else for putting his efforts into this program. Hopefully, the next generation of high school students attending activities of the Heidelberg Life-Science Lab will have the same opportunity to travel to the U. S. and experience its culture beyond a tourist’s view.



Christian Stoy

was born on December 2nd, 1983. I became a member of the Heidelberg Life-Science Lab in its founding year, 2000, participating in several study groups – molecular biology, internet, biochemistry, and chemistry; in spring 2003, I became a tutor for the molecular biology group which later on became the microbiology group. In 2004, I began studying biology at the University of Heidelberg.

My first stay at Stanford University with the ISA San Francisco 2005 was a unique and challenging experience. Therefore, I was very glad when I got the opportunity to supervise the ISA 2007 and to return to this wonderful place. Preparing the academy together with all the participants was a strenuous but more than worthwhile task and I want to thank everybody involved for the great time we had.



Hans Urban

was born in Heidelberg on October 3rd, 1987. After graduating (Abitur) from the St.-Raphael-Gymnasium in Heidelberg in 2007, I performed my civil service at a research laboratory of the university hospital. After that, I enrolled in medicine at the Goethe-University of Frankfurt.

In 2002, I became a member of the Heidelberg Life-Science-Lab and during my years I participated in the study groups for medicine, molecular biology, pharmacy and philosophy. Due to my membership in the Life-Science Lab I attended several internships at the European Molecular Biology Laboratory and the Heidelberg Exploratorium. I am happy to support the Heidelberg Life Science Lab now as a mentor of the medical science study group.

My particular science interests are in the biological aspects of medicine. Besides, I enjoy playing the tube (for myself or in different orchestras), reading, swimming and climbing.

As a participant of the third San Francisco Academy I want to thank all the people who accompanied me during my preparation time and during the academy.

The San Francisco Academy 2007 was a key event in my life and working with the American professors and their lab members has not only given me a wonderful experience but also encouraged me in my studies for becoming a scientist.

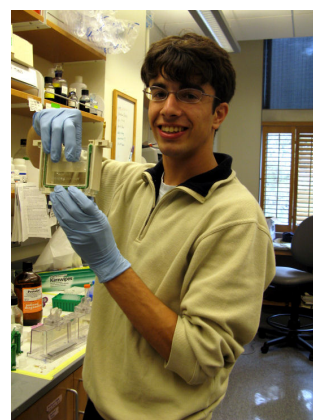


Benjamin Wallisch

was born on November 24th, 1988, in Tübingen. In 2008, I will be graduating (Abitur) from the Quenstedt-Gymnasium in Mössingen with profile courses Mathematics and Physics. After my social civilian service I intend to study physics, since science has always been one of my passions ever since I attended the Science Academy Baden-Württemberg 2003 in Adelsheim.

I joined the Heidelberg Life-Science Lab as a member of the study groups of pharmacy as well as philosophy in 2003. Since 2007 I have been a student tutor for the pharmacy study group. Apart from science, my hobbies are hiking, traveling, and computers.

As I participated in several exchange programs (France/Poland) and have stayed for three month in a High School program in Washington State, US, I knew from experience that it is quite different to visit a foreign country as a non-tourist, which additionally gives you a closer look. This knowledge, the chance to work in a scientific laboratory for four weeks and the possibility to travel to the United States again were reasons why I was curious about my participation in the third International Science Academy to San Francisco. The work in the lab of David Wemmer in Berkeley together with Alexandra Nothnagel and the whole academy itself was a great opportunity to broaden my scientific and cultural horizons. All together it was an experience I do not want to miss. I am grateful for this magnificent experience and want to thank everyone participating in the academy, especially Christian Stoy and Christoph Fischer.



Miriam Wiestler

was born on August 14th, 1987 in Freiburg, Germany. Currently, I am a medical student at the University of Heidelberg. Life sciences have always played an important role in my life. During my whole school career I have been interested in science and research. I chose biology and chemistry as my main subjects in school. In my spare time, next to horse riding and meeting friends, I always spent considerable time with life sciences. I joined the Heidelberg Life-Science Lab in 2005 as a member of the medicine study group as well as the molecular biology study group and became a participant of the International Science Academy San Francisco. In August 2006 I had the opportunity to spend four weeks at the German Cancer Research Center (DKFZ) in Heidelberg in the Department of Molecular Epidemiology, headed by Dr. Barbara Burwinkel. This project was so successful that I could participate in several publications on breast cancer risk factors. In 2007, I graduated from St. Raphael Gymnasium in Heidelberg. During the summer term in 2007, I spent four weeks in Dr. Clarke's laboratory at Stanford University. This was a wonderful experience and a unique opportunity to work with exceptional scientists. I have learned a lot about scientific work as well as about the American way of life. This experience will be of major importance for my future career and I would like to thank everybody who made this possible for me.

